

A Microscopic Model of Black Hole Evaporation in Two Dimensions

Adwait Gaikwad^{a,b12}, Anurag Kaushal^{b,c3}, Gautam Mandal^{b4}, and Spenta R. Wadia^{c5}

a. School of Physics and Astronomy,

Tel Aviv University, Ramat Aviv 69978, Israel

b. Department of Theoretical Physics

Tata Institute of Fundamental Research, Mumbai 400005, India.

c. International Centre for Theoretical Sciences

Tata Institute of Fundamental Research, Shivakote, Bengaluru 560089, India.

Abstract

We present a microscopic model of black hole (BH) ‘evaporation’ in asymptotically AdS_2 spacetimes dual to the low energy sector of the SYK model. To describe evaporation, the SYK model is coupled to a bath comprising of N_f free scalar fields Φ_i . We consider a linear combination of couplings of the form $O_{SYK}(t) \sum_i \Phi_i(0, t)$, where O_{SYK} involves products of the Kourkoulou-Maldacena operator $iJ/N \sum_{k=1}^{N/2} s'_k \psi_{2k-1}(t) \psi_{2k}(t)$ specified by a spin vector s' . We discuss the time evolution of a product of (i) a pure state of the SYK system, namely a BH microstate characterized by a spin vector s and an effective BH temperature T_{BH} , and (ii) a Calabrese-Cardy state of the bath characterized by an effective temperature T_{bath} . We take $T_{bath} \ll T_{BH}$, and T_{BH} much lower than the characteristic UV scale J of the SYK model, allowing a description in terms of the time reparameterization mode. Tracing over the bath degrees of freedom leads to a Feynman-Vernon type effective action for the SYK model, which we study in the low energy limit. The leading large N behaviour of the time reparameterization mode is found, as well as the $O(1/\sqrt{N})$ fluctuations. The latter are characterized by a non-Markovian non-linear stochastic differential equation with non-local Gaussian noise. In a restricted range of couplings, we find two classes of solutions which asymptotically approach (a) a BH at a lower temperature, and (b) a horizonless geometry. We identify these with partial and complete BH evaporation, respectively. Importantly, the asymptotic solution in both cases involves the scalar product of the spin vectors $s \cdot s'$, which carries some information about the initial state. By repeating the dynamical process $O(N^2)$ times with different choices of the spin vector s' , one can in principle reconstruct the initial BH microstate.

¹Part of the work was completed when the author was at *b*.

²adwaitgaikwad@gmail.com

³anuragkaushal314@gmail.com

⁴mandal@theory.tifr.res.in

⁵spenta.wadia@icts.res.in

Contents

1	Introduction and Summary	1
2	Review : Thermal microstates and off-diagonal operators	5
3	The model	9
3.1	Schwinger-Keldysh Formalism and the Effective Action	11
3.2	Fluctuations and a Langevin equation	15
3.3	Solving the Langevin equation in a perturbative expansion in $1/\sqrt{N}$	17
4	Schwarzian + bath dynamics to leading order in large N: description and results	17
4.1	Model (a): Interaction with just the relevant operator ($\Delta = 1/2$)	19
4.1.1	Numerical solution	19
4.1.2	Analytic solution	21
4.1.3	Comparison of numerical and analytical solutions	22
4.1.4	Unphysical solutions in Model (a)	23
4.2	Model (b): Complete Evaporation: Relevant + marginal interaction	23
4.2.1	Analytic solution at large times in terms of Airy functions	25
4.2.2	Quench and stabilizing the effective potential	26
4.3	Nature of solutions and admissible domain of the g - g' plane	29
5	Information recovery	31
5.1	Model (a): partial evaporation	31
5.2	Model (b): complete evaporation	32
5.3	Choice of s'	33
6	Two-point function of fluctuations	33
6.1	Model (a)	34
6.2	Model (b)	34
7	Diagnostics of black hole evaporation	36
7.1	Energy loss	37
7.2	Existence and location of the horizon	37
7.3	Radiation into the bath	38
8	Discussion	39
8.1	Comments on thermalization and comparison with other works	39
8.2	Some comments on black hole entropy	40
8.3	The final state	42
8.3.1	Model (b): the evaporation model	42

8.3.2 Model (a): incomplete evaporation	43
Appendix A SYK Operators in the IR	43
Appendix B Effective Action and Feynman-Vernon phase	44
B.1 Euclidean evolution and the initial bath wavefunctional	45
B.2 Real time evolution	46
B.3 The Feynman-Vernon influence functional	49
B.4 Bath at a finite cutoff Λ	50
B.5 Thermal bath	51
Appendix C Initial conditions (61)	52
Appendix D Other bath couplings	52
D.1 Interaction with just the marginal operator ($\Delta = 1$)	52
D.1.1 Numerical solution	52
D.1.2 Analytic solution	53
D.2 Relevant Interaction + KM term	54
Appendix E Finding spin of the initial state in Model (a)	55
Appendix F Two-point function in Model (a)	56
Appendix G A geometrical appendix	56
G.1 Condition for existence of a horizon and how to locate it	58

1 Introduction and Summary

In the past few years the Sachdev-Ye-Kitaev (SYK) model [1–3] has emerged as a soluble model at large N that is dual to two-dimensional gravity [4, 5] (see, e.g., [6, 7] for reviews). At low energies compared to a characteristic scale J that occurs in the SYK Hamiltonian, this model is near an infrared fixed point which is characterized by the group of time reparameterizations. The corresponding action functional is the Schwarzian of these one dimensional maps. The SYK model has important positivity properties; the 4-point function can be described in terms of a discrete spectrum that is positive and bounded from below, together with a pseudo-continuum with level spacings $O(e^{-N})$. In the large N limit, this pseudo-continuum is described by the Schwarzian action and leads to a density of states $e^{Ns_0} \sinh\left(2\pi\sqrt{2NE/J}\right)$ [8, 9]. For many reasons the character of the low lying spectrum mentioned above is perhaps one of the most important lessons of the SYK model for black hole physics.

Historically the work of Bekenstein and Hawking [10–13] described black holes as thermodynamic objects. The work of Strominger and Vafa [14] that constructed and counted black hole micro-states from D-branes enabled a statistical treatment of black hole thermodynamics and Hawking radiation for a class of

near extremal supersymmetric black holes [15]. Maldacena’s AdS/CFT correspondence gave an in-principle framework for quantum gravity including black holes [16–19], but the characteristics of the black hole spectrum remained unanswered till one learned to solve the SYK model. Whether such characteristics persist for higher dimensional black holes is a fundamental question to answer in the future. The other related problem is the bulk description of a general non-extremal black hole state in terms of elementary degrees of freedom of string theory similar to the brane construction of Strominger and Vafa for supersymmetric extremal black holes which avoided dealing with the strong coupling problem.

Recently there has been a lot of progress in our understanding of the information loss problem, especially in the context of the semiclassical treatment of the generalized entanglement entropy of an evaporating black hole in contact with a large reservoir [20, 21] (see also [22–28]). Some other relevant papers discussing this are [29–37]. Most of these developments involve (proposed modifications of) semiclassical gravity calculations. The subtlety and novelty of these ideas underline the need of a dual QFT calculation. Some progress in such calculations has been made in the context of the SYK model coupled to a bath (see, e.g. [38–40]). A common feature of these references is that the SYK model is treated in the bilocal G - Σ formulation and is outside the scope of the Schwarzian description⁶ for part of the time development, so that a gravity description of the entire dynamics is not possible.

The motivation of our work is two-fold:

- (i) Can we have a model of black hole evaporation entirely within the Schwarzian description (which can, therefore, be equivalently interpreted in terms of JT gravity [41, 42])?
- (ii) Can we retrieve, at the end of the evaporation process, some information about the initial pure state?

At the outset we must specify what we mean by ‘evaporation’ in the boundary setup considered in this paper. The bath is coupled directly to the reparameterization mode whose dynamics determines the bulk geometry. An observer in the bath would see an influx of energy coming from its boundary at $x = 0$ where the SYK model sits. This loss of energy of the SYK model is interpreted as evaporation of the black hole in the dual theory as the horizon vanishes.⁷ (See below and Section 7 for more details.)

⁶As a reminder, the Schwarzian mode of the SYK model, with a $2p > 2$ -body interaction, is the pseudo Nambu-Goldstone mode which describes the spontaneously broken time-reparameterization symmetry $f(\tau) : G(\tau_1, \tau_2) \rightarrow G^f(\tau_1, \tau_2) = G(f(\tau_1), f(\tau_2)) f'(\tau_1)^{1/2p} f'(\tau_2)^{1/2p}$. The symmetry is also explicitly broken slightly at finite but large J , which defines the range of energies $\ll J$ at which the system is essentially described by the dynamics of $f(\tau)$. The time reparameterization symmetry can be directly identified in a dual bulk gravity model, namely JT gravity, for which $f(\tau)$ can be identified by a large diffeomorphism at the boundary or alternatively as the shape deformation of the UV boundary curve defined by a constant dilaton.

⁷In the bulk picture of [21], demanding energy conservation between the AdS_2 and the bath leads to the equation: $\frac{d}{dt} E_{sch}(t) = f'(t)^2 (T_{\hat{x}^-\hat{x}^-} - T_{\hat{x}^+\hat{x}^+}) = T_{tx}^{bdy}$. Here $\hat{x}^\pm = \hat{t} \pm \hat{z}$ are AdS_2 Poincare coordinates (209). A decrease of the Schwarzian can happen through a negative $T_{\hat{x}^-\hat{x}^-}$ [43] or a positive $T_{\hat{x}^+\hat{x}^+}$ [44]. In either case the horizon shrinks and we interpret this as black hole evaporation.

Our model is described in Section 3. It consists of an SYK model (characterized by N , the number of fermions) and a bath consisting of N_F massless scalar fields $\Phi_i(x)$ on a half-line $x > 0$. In the large N limit, N_F/N is held fixed. The bath is coupled to the SYK model at $x = 0$, through a coupling of the form $\mathcal{O} \sum_i \Phi_i(0)$, where \mathcal{O} is an operator of the SYK model (13). The dynamics is computed starting from a product of an SYK pure state $|B_s(l)\rangle$ (see [43], also reviewed in Section 2) and a pure state of the bath (of the Calabrese-Cardy type [45, 46]). An effective description of the SYK dynamics can be obtained by integrating out the bath. At low energies such dynamics can be entirely written in terms of the time reparameterization mode $f(t)$ ⁸ (which we will equivalently parameterize in terms of the Liouville mode $\phi(t)$ defined by $\dot{f}(t) = e^{\phi(t)}$). In the low-energy limit the coupling essentially becomes $\sum_i \Phi_i(0) [ge^{\phi(t)/2} - g'e^{\phi(t)}]$. We look at two models (which we call (a) and (b)), depending on the type of SYK operator used to couple to the bath. In Model (a), $g' = 0$ and in Model (b), both g and g' are non-zero. We find that the $g - g'$ parameter space is restricted to a subregion, outside which the large N equations of motion do not have well-behaved solutions (see section 4.3 for more details). *Since the time reparameterization mode $f(t)$ equally well describes JT gravity, our low energy model is equivalently described in terms of JT gravity coupled to a bath.* We compute the classical solution $\phi(t)$ of the Liouville mode in the large N limit as well as the mean-square fluctuation $\langle \delta\phi(t)\delta\phi(t') \rangle$. The results of these computations are detailed in Sections 4 and 6, while the JT interpretation in terms of black hole evaporation is described in Section 7.

Our results (see Sections 4, 5 and 6) are summarized below:

1. Long time dynamics

As indicated above, in this paper we focus on two main models of coupling to the bath:

- (a) In the first model, which we call Model (a) (Section 4.1), we couple the SYK system to the bath by an operator that is closely similar to the operator $g\mathcal{O}_{KM}$ introduced by Kourkoulou and Maldacena [43]. In this case, the dynamics reaches a well-defined equilibrium when the coupling g is below a certain critical value. The classical solution $\phi(t)$ asymptotically reaches a form which can be identified with a black hole solution with lower ADM energy $E_\infty < E_{\text{ini}}$ where E_{ini} is original energy of the SYK before coupling to the bath (*i.e.* the initial ADM energy of the black hole microstate). The fluctuation $\sqrt{\langle \delta\phi(t)^2 \rangle}$ in equilibrium is characterized by Brownian-type fluctuations at the bath temperature around the classical motion $\phi(t)$.
- (b) In the second model which we call Model (b) (Section 4.2), the bath is coupled to a linear combination of a relevant and a marginal SYK operator. After a characteristic time, the coupling is slowly switched off to prevent the low energy approximation from breaking down. Here, the final form of the solution $\phi(t)$ has a bounded oscillatory behaviour which can be identified in terms of a horizonless geometry. Such a solution represents a process of complete evaporation, in the sense we mentioned above. The fluctuation $\sqrt{\langle \delta\phi(t)^2 \rangle}$ also exhibits oscillatory behavior characteristic of a Brownian particle in a bounded potential.

⁸Sometimes this is also called the ‘Schwarzian mode’.

In both models, coupling to the bath, in effect, dynamically changes the KM deformation parameter (recall that this parameter was changed externally in [43, 47]). Other couplings to the bath are described in Appendix D.

2. Black hole evaporation

In Section 7 we interpret some of the above results in terms of JT gravity. While Model (a) can be interpreted as incomplete black hole evaporation, Model (b), with a horizonless asymptotic geometry, can be interpreted as complete black hole evaporation. The horizon structure is described in detail in Section 7.2 and Appendix G. The final state in both models is described in Section 8.3.

3. Retention of memory of the initial state through the evaporation

The initial pure state $|B_s(l)\rangle$ can be regarded as a black hole ‘microstate’, where different microstates are distinguished from each other by the spin vector s . In [43] the SYK model was deformed by an operator \mathcal{O}_{KM} carrying a spin vector which was chosen to be identical to that of the pure state, similar to the idea of [48, 49]. In [47] the computation was generalized to the case where the spin vector s' of the operator \mathcal{O}_{KM} and the spin vector s of the pure state are different; the resulting dynamics carried information about the scalar product $s' \cdot s$. In the present work too, the SYK operators coupling to the bath carry a particular spin vector s' ; the dynamics carries information about the scalar product which, in fact, survives at asymptotic times as well, both in models (a) and (b). If we regard the coupling to the bath as a probe, and *if* we are able to repeat the experiment with various choices of the spin vector s' , every choice of s' gives us additional information about the spin s which characterizes initial $|B_s(l)\rangle$ state. A step by step algorithm of how to do this is described in Section 5, where we show that if we repeat these experiments $O(N^2)$ times, we can have an in principle reconstruction of the spin s and consequently the initial state. Note that the $O(N^2)$ repetitions are consistent with the polynomial form of unrestricted complexity [50], since our protocol involves the couplings which act both on the SYK and the bath⁹.

The discussion above is similar to the extraction of information about a black hole microstate from polarization tensors of the probe graviton in [51] (see equations (2.5), (2.6); the scattering amplitude in equation (2.4) depends on the inner product of polarization tensor of the probe particle and that of the black hole microstate – hence by repeating the scattering experiment one can extract more and more information about the polarization tensor of the microstate). Similar remarks apply to the analysis of [52] where the decay amplitude of a near-BPS state depends on the specific microstate (see equation (8) of [52]).¹⁰

We note that even the two-point correlators of the models discussed in this paper retain the information about the initial state. This is rather non-trivial since one normally associates the asymptotic

⁹We thank Onkar Parrikar for a discussion on this point.

¹⁰Note that while in these papers the properties of the probes can be tuned at low energies, in our current work, the specific coupling to the bath, and in particular, the information about the spin vector s' is a microscopic (UV) property. This is elaborated further in Section 5.

two-point fluctuation with equilibrium properties (e.g. for a normal Brownian particle) which does not have a memory of the initial state.

See Section 5 (also Section 8.1) for more details.

2 Review : Thermal microstates and off-diagonal operators

Thermal microstates

In this section, we briefly review the relevant properties of the pure states of [43]. We will start with the SYK Hamiltonian which is written in terms of N Majorana fermions

$$H_0 = H_{SYK} = - \sum_{1 \leq a < b < c < d \leq N} j_{abcd} \psi_a \psi_b \psi_c \psi_d \quad (1)$$

where the couplings j_{abcd} are drawn randomly from a Gaussian distribution with zero mean and variance, $\langle j_{abcd}^2 \rangle = 3!J^2/N^3$. The equal time anticommutation relation of the Majorana fermions, $\{\psi_a, \psi_b\} = \delta_{ab}$, coincides with the $O(N)$ Clifford algebra. We will call the normalized states which provide a spinorial representation of the above algebra, $|B_s\rangle$, where $s = (\pm, \pm, \dots)$ are $N/2$ dimensional ‘spin’ vectors. The total number of such vectors is $2^{N/2}$. Ref. [43] introduced a class of pure states (similar to the Calabrese-Cardy states [53] that were introduced to model quantum quench) given by ¹¹

$$|B_s(l)\rangle = \exp[-lH_0]|B_s\rangle, \quad (2)$$

which reproduce thermal properties for a large class of observables, corresponding to a temperature $T = 1/\beta$ where $\beta = 2l$. E.g.

$$\overline{\langle B_s(l)|B_s(l)\rangle} = \overline{\langle B_s|e^{-2lH_0}|B_s\rangle} = 2^{-N/2} \overline{\text{Tr}(e^{-\beta H_0})} \equiv 2^{-N/2} \overline{Z(\beta)}, \quad (3)$$

$$\frac{\overline{\langle B_s(l)|\psi_a(t)\psi_a(t')|B_s(l)\rangle}}{\overline{\langle B_s(l)|B_s(l)\rangle}} = \frac{\overline{\text{Tr}(e^{-\beta H_0}\psi_a(t)\psi_a(t'))}}{\overline{Z(\beta)}} = G_\beta(t-t'). \quad (4)$$

The ‘bar’ on these expressions indicate a disorder average. We will be discussing the low-energy sector at large N in this paper so henceforth we will drop the ‘bar’ on the expressions. All the expectation values discussed will be disorder averaged expectation values. The fermion bilinear can be replaced by any flip-symmetric¹² operator. These equations show that the basic dynamical variable of the SYK model, the bilocal variable $G(t, t') = (1/N) \sum_a \psi_a(t)\psi_a(t')$ which describes the $O(N)$ invariant sector, does not distinguish between the pure states $|B_s(l)\rangle$ and the thermal (mixed) state $\rho_\beta = \frac{1}{Z(\beta)} \exp[-\beta H_0]$, $\beta = 2l$.

Equalities like (3) can be obtained from a path-integral [43] (a detailed derivation is presented in the appendix of [47]). For large enough l ($lJ \gg 1$), both sides of the equation (3) can be expressed as follows in

¹¹Since the Hilbert states of the SYK model is a linear space, in principle one can consider low-energy properties of a linear combination of these states. In particular it will be interesting to know if all microstates are black holes. We leave this discussion for future work.

¹²a discrete subgroup of $O(N)$, for more details see [43].

terms of a path-integral over the time-reparameterization or Schwarzian mode $f(\tau) := \frac{\pi}{\beta J^2} \tan(\pi\varphi(\tau)/\beta)$

$$\int [Df] \exp[iS_0[f]], \quad S_0[f] = -\frac{N\alpha_s}{J} \int_{-l}^l d\tau \{f, \tau\} = -\frac{N\alpha_s}{J} \int_{-l}^l d\tau \left[\{\varphi(\tau), \tau\} + \frac{2\pi^2}{\beta^2} \dot{\varphi}(\tau)^2 \right]. \quad (5)$$

In the above we have used the notation for the Schwarzian of a function $f(\tau)$

$$\{f, t\} \equiv \frac{\ddot{f}}{f} - \frac{3}{2} \left(\frac{\dot{f}}{f} \right)^2, \quad (6)$$

where dot denotes derivative with respect to τ . The boundary condition for the path integral to describe the LHS of (3) is appropriate for an interval (see [43]):

$$\varphi(-l) = -l, \quad \varphi(l) = l, \quad \dot{\varphi}(-l) = \dot{\varphi}(l) = 1. \quad (7)$$

The boundary condition for the circle is given by periodic identification of $\tau = -l$ and $\tau = l$ and winding number 1. The saddle point solutions for the two boundary conditions are different; however, the classical action $S_0[f]$ evaluates to the same value in both cases (the two boundary conditions differ in the SL(2) zero modes, which are gauge modes and do not affect physical quantities). Both boundary conditions also lead to the same result for Green's functions e.g. (4) or (10), which explains why $|B_s(l)\rangle$ states reproduce thermal properties despite different boundary conditions.¹³

The saddle point solution corresponding to the boundary condition (7) is $\varphi(\tau) = \tau$. In terms of the f variable the solution is

$$f(\tau) = \frac{\pi}{\beta J^2} \tan\left(\frac{\pi}{\beta}\tau\right). \quad (8)$$

Liouville theory

The Schwarzian action is a higher derivative action. To discuss Hamiltonian formulation of such an action we can introduce auxiliary variables in terms of which the action becomes 2nd order [44]. This can be done by introducing a field ϕ defined by $\dot{f} =: e^\phi$ through a Lagrange multiplier λ . Remember that the Schwarzian mode is a reparameterization of time and should be monotonic ($\dot{f}(t) > 0$), this redefinition implicitly takes care of this. We will refer to $\phi(t)$ as a Liouville mode (the nomenclature will be clear from the form of the action). Introducing the Liouville mode, the Schwarzian action can be rewritten as¹⁴ (see, e.g. [43])

$$S_0 = \frac{N\alpha_s}{J} \int dt \left[\frac{\dot{\phi}^2}{2} - 2J^2 e^\phi \right], \quad \dot{f}(t) =: \exp[\phi]. \quad (9)$$

This is simply Liouville theory [44, 54], namely a particle moving in an exponential potential¹⁵.

¹³We acknowledge crucial discussions with Juan Maldacena regarding the issue of boundary conditions.

¹⁴In arriving at this expression, one ignored a total derivative term of the form $\int dt \dot{f}$ [43], which contributes an unimportant constant to the path integral. Further λ , which is a constant by equation of motion, is set to $\lambda = -4J$ by a gauge choice which is also made in writing the Euclidean solution (8).

¹⁵It was shown in [54] that the measure in terms of the Liouville variable is flat.

Off-diagonal operators

Equation (4) demonstrates diagonal observables which show thermal properties in the $|B_s(l)\rangle$ states. What about off-diagonal bilinears? An important relation (presented in [43]) is

$$\frac{1}{Z} \langle B_s(l) | s_k \psi_{2k-1}(t) \psi_{2k}(t') | B_s(l) \rangle = 2i G_\beta(t-il) G_\beta(t'-il) + O\left(\frac{1}{N}\right), \quad Z = \langle B_s(l) | B_s(l) \rangle, \quad (10)$$

which shows that the off-diagonal bilinears $\psi_{2k-1}(t) \psi_{2k}(t')$ by themselves do *not* have a thermal form (and depend on the spin vector s); but when they are in the combination as shown above ($s_k \psi_{2k-1}(t) \psi_{2k}(t')$), then the RHS is a product of thermal Greens functions and the memory of the spin vector s is erased on the RHS. This relation can be generalized, using similar methods as above, to the case where the spin vector in the operator and the state is not aligned, to

$$\frac{1}{Z} \langle B_s(l) | \sum_{k=1}^{N/2} s'_k \psi_{2k-1}(t) \psi_{2k}(t') | B_s(l) \rangle = 2i s \cdot s' G_\beta(t-il) G_\beta(t'-il) + O\left(\frac{1}{N}\right), \quad s \cdot s' = \sum_{k=1}^{N/2} s'_k s_k =: N/2 \cos \theta. \quad (11)$$

This shows that unlike in (10), if the spin vectors in the state and operator are not matched, some memory of both spin vectors is retained.

Modified SYK

We would like to deform the SYK theory with similar off-diagonal operators. We can write down a list of operators similar to (10) and (11) which have a large N expression in terms of fermion 2-point function G_β . Description of the UV operators in terms of bilocal variables G_β is desirable to discuss the low-energy sector of SYK and also the SYK-JT duality. Before we present the explicit form of the operators in the UV, let us write down the corresponding low energy path integral modified by such an operator in terms of the Schwarzian mode

$$\frac{1}{Z} \langle B_s(l) | e^{-i \int dt \epsilon(t) O_\Delta(t)} | B_s(l) \rangle = \int [Df] e^{i S_0[f] - i \int dt \epsilon(t) \frac{1}{2} \langle B_s(l) | O_\Delta(t) | B_s(l) \rangle^{(f)}}, \quad (12)$$

where the superscript (f) denotes the reparameterization $t \rightarrow f(t)$. Δ here is the IR mass dimension of the operator. Above equation is clearly correct in the perturbative regime of $\epsilon(t)$ but this relation can be exactly derived by expanding the exponent and resumming the pieces which are leading order in N (similar to the presentation in Appendix of [47]).

Consider the following off-diagonal operators

$$\mathcal{O}_m^{\{s^{(1)}, s^{(2)}, \dots, s^{(m)}\}}(t) = \mathcal{O}_{\Delta=2m\Delta_f}(t) = (-1)^{m+1} J \prod_{j=1}^m \left(\frac{i}{N} \sum_{k=1}^{N/2} s_k^{(j)} \psi_{2k-1}(t) \psi_{2k}(t) \right). \quad (13)$$

This operator is characterized by m different spin-vectors $s^{(j)}$. Here the factor of J is multiplied to ensure that the coupling constant is dimensionless in the UV, and Δ_f is the conformal dimension of the SYK fermion near the IR fixed point which is equal to $\frac{1}{4}$ ¹⁶. The operator is composite of $2m$ fermions and hence

¹⁶We are considering a 4 body interaction SYK Hamiltonian, in the case of q-body SYK Hamiltonian, $\Delta_f = 1/q$.

has a mass dimension $\Delta = 2m\Delta_f$. The $m = 1$ operator is the one which was originally introduced in [43]. The leading large N expectation values of these operators in a thermal microstate are (see Appendix A for the derivation)

$$\frac{1}{Z} \langle B_s(l) | \mathcal{O}_m^{\{s^{(1)}, s^{(2)}, \dots, s^{(m)}\}}(t) | B_s(l) \rangle = -J \left(\prod_{j=1}^m \cos(\theta^{(j)}) \right) G_\beta(t-il)^{2m}, \quad N \cos(\theta^{(j)})/2 = \sum_{k=1}^{N/2} s_k s_k^{(j)}. \quad (14)$$

As indicated earlier when the spin vectors in the state and operator are not matched, some information about the spin vector s of the pure state can be recovered from choices of the spin vectors $s^{(j)}$ of the probe operators. Note that, near the IR fixed point, operators \mathcal{O}_m with $m < 1/2\Delta_f$ are relevant operators and with $m = 1/2\Delta_f$ is a marginal operator. For $\Delta_f = 1/4$, we have a relevant ($m = 1$) and a marginal operator ($m = 2$) each.

The last step to get the interaction term of the action is to couple the Lorentzian Schwarzian mode $f(t) := \frac{\pi}{\beta J^2} \tanh(\pi\varphi(t)/\beta)$ to

$$G_\beta(t-il) = \frac{C_{\Delta_f}}{\left[\frac{J\beta}{\pi} \cosh\left(\frac{\pi t}{\beta}\right) \right]^{2\Delta_f}}, \quad \text{with } C_\Delta = \left[\left(\frac{1}{2} - \Delta \right) \frac{\tan \pi \Delta}{\pi} \right]^\Delta. \quad (15)$$

In order to couple the Schwarzian mode $\varphi(t)$, we reparameterize above expression with it

$$G_\beta^\varphi(t) = \dot{\varphi}(t)^{\Delta_f} G_\beta(\varphi(t) - \varphi(il)) \dot{\varphi}(il)^{\Delta_f} = \frac{C_{\Delta_f} \dot{\varphi}(t)^{\Delta_f}}{\left[\frac{J\beta}{\pi} \cosh\left(\frac{\pi\varphi(t)}{\beta}\right) \right]^{2\Delta_f}} = C_{\Delta_f} \dot{f}(t)^{\Delta_f}, \quad (16)$$

hence the interaction term in the action is

$$\hat{g}_m \int dt \epsilon(t) \frac{1}{Z} \langle B_s(l) | \mathcal{O}_m^{\{s^{(1)}, s^{(2)}, \dots, s^{(m)}\}}(t) | B_s(l) \rangle^{(f)} = -g_m J \int dt \epsilon(t) e^{m\phi(t)/2}, \quad g_m = \hat{g}_m \prod_{i=1}^m \frac{\cos(\theta^{(i)})}{\sqrt{4\pi}}. \quad (17)$$

In the equation above we have used $\Delta_f = 1/4$ and use it in all the equations hereafter. For $m = 1$, which corresponds to a relevant operator, the above equation looks like

$$\hat{g}_1 \int dt \epsilon(t) \frac{1}{Z} \langle B_s(l) | \mathcal{O}_1^{s'}(t) | B_s(l) \rangle^{(f)} = -g J \int dt \epsilon(t) e^{\phi(t)/2}, \quad g = \hat{g}_1 \frac{\cos \theta}{\sqrt{4\pi}}, \quad (18)$$

where we have written g for g_1 and θ for $\theta^{(1)}$. For $m = 2$, which corresponds to a marginal operator, we take the two spins to be the same

$$\hat{g}_2 \int dt \epsilon(t) \frac{1}{Z} \langle B_s(l) | \mathcal{O}_2^{\{s', s'\}}(t) | B_s(l) \rangle^{(f)} = g' J \int dt \epsilon(t) e^{\phi(t)}, \quad g' = -\hat{g}_2 \left(\frac{\cos \theta}{\sqrt{4\pi}} \right)^2, \quad (19)$$

where we have written g' for $-g_2$ and θ for $\theta^{(1)}$. Note that $\mathcal{O}_2^{\{s', s'\}}$ is the same as $(\mathcal{O}_1^{\{s'\}})^2$.

We can also couple multiple operators in a similar way. When operators with only $m = 1$ and $m = 2$ are used

$$\int dt \epsilon(t) \frac{1}{Z} \langle B_s(l) | \hat{g}_1 \mathcal{O}_1^{\{s'\}}(t) + \hat{g}_2 \mathcal{O}_2^{\{s', s'\}}(t) | B_s(l) \rangle^{(f)} = -g \int dt \epsilon(t) F[\phi(t)], \quad (20)$$

$$gF[\phi(t)] = J \left[g e^{\phi(t)/2} - g' e^{\phi(t)} \right], \quad (21)$$

where g, g' are given by (18) and (19). Note that the information $s \cdot s'$ from the UV stays unaltered in the IR limit.

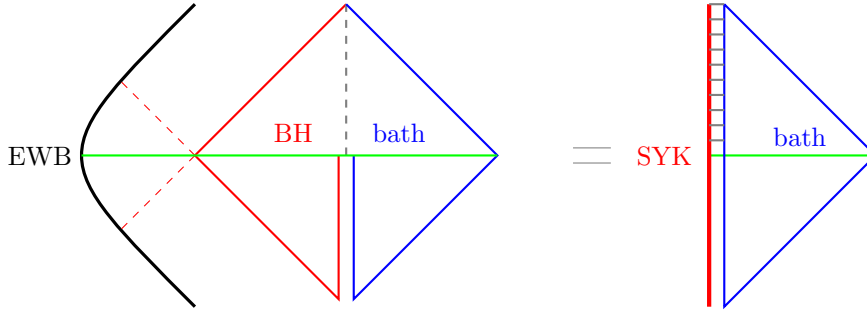


Figure 1: The field theory setup (right) is a 1-d holographic quantum mechanical system coupled at $t = 0$ to a 1+1 dimensional CFT on a half Minkowski plane. The horizontal gray lines indicates interaction. The green line is the $t = 0$ slice and where the theory is prepared in a pure state given in (22). In the dual bulk theory (left), we simply replace the 1-d holographic system by its dual, as we have prepared it in a thermal microstate the dual geometry is a black hole containing an end of the world brane in the interior [43]. The black holes is coupled to flat space at $t = 0$ (green slice).

3 The model

In this section, we will describe the coupled system consisting of N_f free scalars on a half line ($x \in [0, \infty)$), modeling the bath, and the SYK theory at the boundary ($x = 0$), modeling the quantum system dual to a black-hole (see Figure 1). As mentioned in the introduction, we will focus on the IR regime of the SYK theory where it is described by a pseudo Nambu-Goldstone (NG) mode and the dynamics of this mode is governed by the Schwarzian action (5),(9)

At $t = 0$, the SYK and bath are prepared in a pure state of the form

$$|B_s(l)\rangle \otimes |\Psi_0(L)\rangle. \quad (22)$$

The geometry dual to the state $|B_s(l)\rangle$ is a black hole with inverse temperature $\beta = 2l$, containing an end of the world brane (EWB) in the interior [43] (see also [55]). Further, the averaged expectation values of flip-symmetric operators in these pure states are the same as their averaged thermal expectation values with $\beta = 2l$. The bath state $|\Psi_0(L)\rangle$ is a Calabrese-Cardy (CC) state [53].

$$|\Psi_0(L)\rangle = e^{-LH_{bath}} |Bd\rangle, \quad \text{with } \Phi |Bd\rangle = 0. \quad (23)$$

The CC states have a similar thermal character as $|B_s(l)\rangle$, to be precise, the expectation values of a string of local operators (confined to a subregion) are thermal at large times with an effective inverse temperature $\beta_b = 4L$ [53, 56–58]. Hence, the rationale for preparing the coupled system in the (22) is to have an interpretation of coupling two systems with effective inverse temperature $2l$ (black-hole) and $4L$ (bath) respectively.

In the bulk dual description, Hawking radiation from a black hole in an asymptotically AdS (AAdS) spacetime cannot escape and falls back in due to the effective AdS potential. As a result large black holes in AAdS spacetimes do not evaporate. One way to extract the radiation from the AdS region is to couple the AAdS geometry to an auxiliary non-gravitational system with a large number of degrees of

freedom [20–23, 59]. In such a treatment of the evaporation process, the black hole is treated as an open system in both the bulk and boundary descriptions.

The action for the coupled system in the boundary description can be obtained as follows – the interaction term S_{int} is the same as (20) with the external parameter $\epsilon(t)$ now replaced by the dynamical bath fields, i.e. $\epsilon(t) \rightarrow \sum_i \Phi_i(t, 0)$

$$S_{int}^{UV} = \int dt \sum_i \Phi_i(t, 0) \left(\hat{g}_1 \mathcal{O}_1^{\{s'\}}(t) + \hat{g}_2 \mathcal{O}_2^{\{s', s'\}}(t) \right) \xrightarrow{\text{IR}} S_{int} = -g \int dt \sum_i \Phi_i(t, 0) F[\phi(t)], \quad (24)$$

with

$$F[\phi(t)] = J \left[e^{\phi(t)/2} - \frac{g'}{g} e^{\phi(t)} \right]. \quad (25)$$

With this the full action reads

$$S = \underbrace{\frac{N\alpha_s}{J} \int dt \left(\frac{\dot{\phi}^2}{2} - 2J^2 e^{\phi} \right)}_{S_0} - \underbrace{g \int dt F[\phi(t)] \sum_{i=1}^{N_f} \Phi_i(t, 0)}_{S_{int}} + \underbrace{\frac{1}{2} \sum_{i=1}^{N_f} \int dt \int_0^\infty dx (\partial \Phi_i)^2}_{S_{bath}}. \quad (26)$$

We have already introduced S_0 ((9)). As mentioned earlier, our auxiliary bath system consist of N_f free, massless scalars Φ_i on the half-line and its action is S_{bath} in (26). The interaction between the bath and SYK is turned on at $t = 0$ (see Figure 1) and the interaction is localized at the boundary ($x = 0$).

We will consider two sub-cases of S_{int} in (26) depending on whether \hat{g}_2 is zero or not:

- (Model a) Only a relevant coupling (see (18))

$$F(\phi(t))/J = \exp[\phi(t)/2], \quad g = \frac{\hat{g}_1}{\sqrt{4\pi}} \cos \theta. \quad (27)$$

- (Model b) A mixture of relevant and marginal coupling (see (20))

$$F(\phi(t))/J = \exp[\phi(t)/2] - \frac{g'}{g} \exp[\phi(t)], \quad g = \frac{\hat{g}_1}{\sqrt{4\pi}} \cos \theta, \quad g' = -\frac{\hat{g}_2}{4\pi} \cos^2 \theta. \quad (28)$$

The black hole evaporation that we study in this paper occurs in a certain range of the parameters g and g' (see Figure 16 and Section 4.3 for more details). One can make sure that g and g' are in this range by tuning \hat{g} and \hat{g}' . The relative minus sign between the two couplings would be crucial to achieve complete black hole evaporation. In Model (b) we consider g and g' to be constant initially and to have a slow fall-off in time at late stages (see Section 4.2). Note that $e^{\phi/2}$ is a relevant operator and e^ϕ is a marginal operator – see comments below equation (14).

Large N limit The SYK action is order N , the interaction term and the bath action both are order N_f . We would take a large N limit along with a large N_f limit in such a way that

$$n_f = N_f/N \quad (29)$$

is held fixed and small. This ensures that all the terms in equation 26 are comparable, of $O(N)$ and one can use the saddle point method. This scaling also ensures that the fraction of energy lost by the black hole

due to evaporation is of the same order (in terms of N) as the initial energy, as we will see explicitly later in Section 4. This feature is necessary to observe a time-dependent geometry due to backreaction from the radiation appropriate for an evaporating black hole.

We note here that the limit $n_f \rightarrow 0$ is interesting to study. One would expect to recover the usual quasi-static approximation of black hole radiation in this limit. It would be interesting to see if the energy flux in the bath discussed in Section 7.3 becomes a thermal flux in that limit. We wish to come back to this issue in the future.¹⁷

3.1 Schwinger-Keldysh Formalism and the Effective Action

Our primary aim is to obtain an evaporating black hole solution in terms of the Liouville mode $\phi(t)$. In the limits considered in (29), the action is proportional to N and the path integral can be computed by a saddle point approximation. To extract this solution which saturates the integral in real time, it is instructive to consider the expectation value of some operator \mathcal{O} in the SYK theory at some arbitrary real time $t = T$ (see Figure 2). These operators are order 1 in N scaling and won't change the solution of the Liouville mode which saturates the path integral. The expectation value is given by

$$\langle \mathcal{O}(T) \rangle = \text{Tr} [(\hat{\rho}_{Sch} \otimes \hat{\rho}_{bath}) \mathcal{O}(T)] = \langle B_s(l) \otimes \Psi_0(L) | e^{iHT} \mathcal{O} e^{-iHT} | B_s(l) \otimes \Psi_0(L) \rangle, \quad (30)$$

here H is the full Hamiltonian of SYK plus scalar field bath including the interaction. The initial state is taken to be a tensor product of¹⁸

$$\hat{\rho}_{sch} = |B_s(l)\rangle \langle B_s(l)| \quad \text{and} \quad \hat{\rho}_{bath} = |\Psi_0(L)\rangle \langle \Psi_0(L)|. \quad (31)$$

Note that the Euclidean evolution in the preparation of the state (22) (and (31)) is with the uncoupled Hamiltonian as opposed to the real time evolution which is with the full interacting Hamiltonian H . It is well-known (see [60] etc.) that expectation values such as (30) involve contours which run back and forth in Lorentzian time, in addition to Euclidean parts for the specific pure states we mentioned above. Such contours are called Schwinger-Keldysh (SK) contours; they are depicted in Figure 2.

As we presently consider operators that have support only on the SYK Hilbert space, we might as well work with the reduced density matrix RDM which can be obtained by taking a trace over the bath Hilbert space (see Figure 3):

$$\hat{\rho}(T) = \text{Tr}_{Bath} [e^{-iHT} \hat{\rho}_{Sch} \otimes \hat{\rho}_{bath} e^{iHT}], \quad (32)$$

and the expectation value of the SYK operator can also be computed from the RDM

$$\langle \mathcal{O}(T) \rangle = \text{Tr} [\hat{\rho}(T) \mathcal{O}]. \quad (33)$$

As indicated earlier, our primary aim is to get the evaporating black hole solution in terms of the Liouville mode $\phi(t)$. We would like to write down a path integral expression for (32) or (33). The action for this

¹⁷We thank Shiraz Minwalla for making this suggestion.

¹⁸We can also consider the bath in a thermal state (see Appendix B.5).

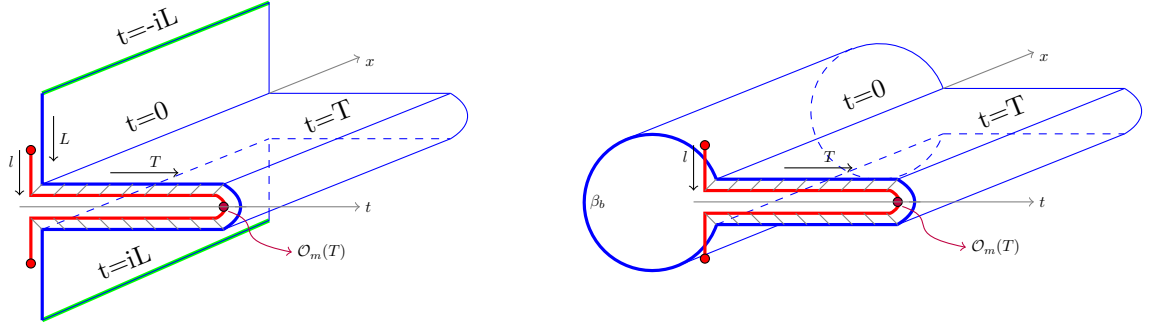


Figure 2: Schwinger-Keldysh contours: The horizontal direction is the real time and the transverse direction is the spatial extent of the bath theory. In the figure on the left, the vertical direction is the imaginary time direction. The bath (indicated by blue contours) is prepared in the Calabrese-Cardy state at $t = 0$. It is prepared by a time evolution along the imaginary time, starting from $t = -iL$, indicated by the vertical blue lines. The green lines at $t = \pm iL$ are depicting the $|Bd\rangle$ ($\langle Bd|$) state. The blue contours are joined up smoothly at the right end (at Lorentzian time $t = T$) as the operator which we have inserted there has support only on the SYK Hilbert space. The SYK contours (red) are similar, except for the insertion of an operator \mathcal{O}_m at the right end ($t = T$), indicated by the purple dot. The figure on the right is similar to the left figure, except that the bath is in a thermal state at $t = 0$ and we have depicted it by a closed circle of length β_b in the imaginary time. In both the figures, gray lines between red and blue contours are indicating the interaction between the two systems and as depicted it is only present along the real time.

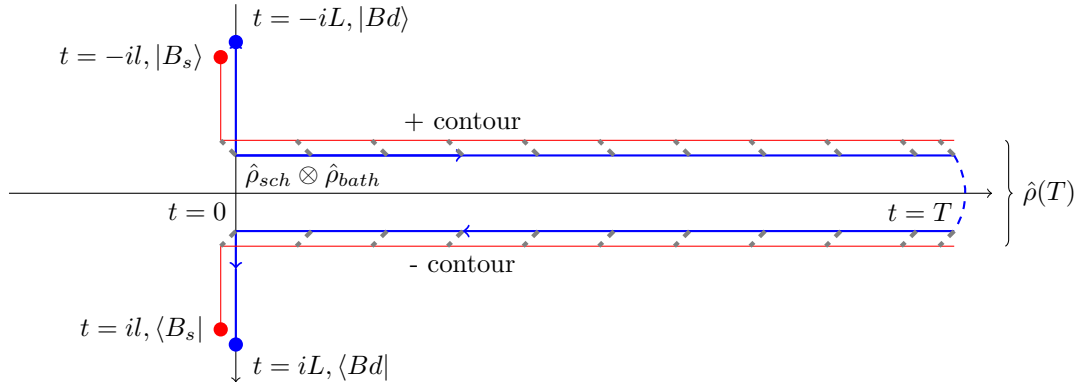


Figure 3: This is the same diagram as Figure 2 with the x direction suppressed. The bath contour is depicted in blue and the SYK path is depicted by red. The blue and red dots on the top depict the kets $|Bd\rangle$ and $|B_s\rangle$ respectively and on the bottom depicts the bras $\langle Bd|$ and $\langle B_s|$ respectively. The state at $t = 0$ is $\hat{\rho}_{sch} \otimes \hat{\rho}_{bath}$ and the state at $t = T$ is the reduced density matrix defined as $\hat{\rho}(T) = \text{Tr}_{bath} [e^{-iHT} \hat{\rho}_{sch} \otimes \hat{\rho}_{bath} e^{iHT}]$. The tracing out of the bath fields is depicted by the blue dashed line connected the upper and lower bath contour. The '+' (upper) contour and the '-' (lower) contour are at $\text{Im}(t) = 0$, the gap in the above figure is only shown for better presentation, the value of real time along both contours is also the same. Hence, to distinguish fields on the upper contour from the fields on the lower contour we add a \pm subscript.

path integral would be (26) with the path integral contour described in Figure 2. The SYK action in (26) is already projected onto the low energy sector and the physics is described by the Liouville mode. We will also integrate out the bath fields from the path integral and obtain an effective action in which the Liouville mode will be the only dynamical variable. The details of the computation described above are presented in Appendix B. The final result is

$$\begin{aligned} \langle \mathcal{O} \rangle &= \int d\phi_T^+ d\phi_T^- \mathcal{O}(\phi_T^+, \phi_T^-) \int_{\phi_0}^{\phi_T^+} D\phi^+ \int_{\phi_0}^{\phi_T^-} D\phi^- e^{iS_{SYK}[\phi^+] - iS_{SYK}[\phi^-]} e^{N_f W[F(\phi^+), F(\phi^-)]} \\ &= \int d\phi_T^+ d\phi_T^- \mathcal{O}(\phi_T^+, \phi_T^-) \int_{\phi_0}^{\phi_T^+} D\phi^+ \int_{\phi_0}^{\phi_T^-} D\phi^- e^{iS_{SK}[\phi^+, \phi^-]} \end{aligned} \quad (34)$$

where S_{SK} is given in (36) and the Feynman-Vernon influence functional $W[F(\phi^+), F(\phi^-)]$ appears as a result of integrating out the bath fields and is given by

$$\begin{aligned} W[F(\phi^+), F(\phi^-)] &= g^2 \left[\int_0^T dt dt' F(\phi^+(t)) \kappa_{++}(t, t') F(\phi^+(t')) + \int_0^T dt dt' F(\phi^-(t)) \kappa_{--}(t, t') F(\phi^-(t')) \right. \\ &\quad \left. + 2 \int_0^T dt dt' F(\phi^+(t)) \kappa_{+-}(t, t') F(\phi^-(t')) \right]. \end{aligned} \quad (35)$$

The explicit form of the kernels is given in equation (185) for the pure CC state and in equation (191) for the thermal state. The contour for the path integral is given in Figure 3. The field $\phi^+(\phi^-)$ lives on the ‘+’ (‘-’) contour.

The first thing to note is that the influence functional is non-local. The kernel κ_{++} gives bilocal interactions on the ‘+’ contour, κ_{--} gives bilocal interactions on the ‘-’ contour while κ_{+-} leads to interactions with one leg each on the ‘+’ and ‘-’ contours. This structure can be simply understood as arising after integrating a quadratic field leading to the standard functional form $e^{J \cdot \Delta \cdot J}$ for the ‘source’ $J = F(\phi)$, which lives on both + and - contours. Details of this calculation are provided in Appendix B.3. In (34), $\mathcal{O}(\phi_T^+, \phi_T^-) = \langle \phi_T^+ | O_{\text{SYK}} | \phi_T^- \rangle$, representing the operator insertion at time $t = T$ (see Fig 2).

Together with the Influence functional, the effective Schwarzian action on the Schwinger-Keldysh contour reads

$$\begin{aligned} S_{SK}[\phi^+, \phi^-] &= S_{Sch}[\phi^+] - S_{Sch}[\phi^-] - iN_f W[F(\phi^+), F(\phi^-)] \\ &= N \left\{ \frac{\alpha_s}{J} \int_0^T dt \left[\frac{1}{2} \dot{\phi}^{+2} - V(\phi^+) \right] - \frac{\alpha_s}{J} \int_0^T dt \left[\frac{1}{2} \dot{\phi}^{-2} - V(\phi^-) \right] - in_f W[F(\phi^+), F(\phi^-)] \right\}, \end{aligned} \quad (36)$$

with

$$V(\phi) = 2J^2 \exp(\phi). \quad (37)$$

Note that in (34), the Influence functional W comes with a prefactor N_F , the number of scalar fields. Therefore the effective action, with the scaling given in (29) has an overall factor of N and hence the path integral will be saturated by the large N solution of the Liouville mode. The insertion of the operator \mathcal{O}

will have no effect on the large N solution of the Liouville mode as long as it is order 1 in the N scaling, which is the case we consider.

The variation of S_{SK} with respect to the Liouville fields $\phi^+(t)$ and $\phi^-(t)$ lead to the following equations of motion for $\phi^+(t)$ and $\phi^-(t)$ respectively:

$$\frac{\alpha_s}{J} \left[\ddot{\phi}^+(t) + V'(\phi^+(t)) \right] + in_f g^2 \left[F'(\phi^+(t)) \int_0^T dt' \kappa_{++}^S(t, t') F(\phi^+(t')) + 2F'(\phi^+(t)) \int_0^T dt' \kappa_{+-}(t, t') F(\phi^-(t')) \right] = 0, \quad (38)$$

$$\frac{\alpha_s}{J} \left[\ddot{\phi}^-(t) + V'(\phi^-(t)) \right] - in_f g^2 \left[F'(\phi^-(t)) \int_0^T dt' \kappa_{--}^S(t, t') F(\phi^-(t')) + 2F'(\phi^-(t)) \int_0^T dt' F(\phi^+(t')) \kappa_{+-}(t', t) \right] = 0. \quad (39)$$

Notice that only the symmetric kernels

$$\kappa_{++}^S(t, t') = \kappa_{++}(t, t') + \kappa_{++}(t', t); \quad \kappa_{--}^S(t, t') = \kappa_{--}(t, t') + \kappa_{--}(t', t) \quad (40)$$

appear in the equation of motion.

Some properties of the kernels

$$\begin{aligned} \text{Re} [\kappa_{++}(t, t') + \kappa_{+-}(t, t')] &= 0, \\ \text{Im} [\kappa_{++}^S(t, t') + 2\kappa_{+-}(t, t')] &= [1 + \text{sgn}(t - t')]/2 = \theta(t - t'), \\ 2\text{Re} [\kappa_{++}(t, t') - \kappa_{+-}(t, t')] &= K(t, t'), \end{aligned} \quad (41)$$

where the kernel $K(t, t')$ depends on whether the bath initially is in a pure state or in a thermal state. In case of the pure state,

$$\begin{aligned} K(t, t') &= -\frac{2}{\pi} \int_0^\infty \frac{dk}{k} [\cos(kt) \cos(kt') \tanh(kL) + \sin(kt) \sin(kt') \coth(kL)] \\ &= -\frac{1}{2L} (t + t' - |t - t'|) - \frac{2}{\pi} \log \left[\frac{1 + e^{-\pi|t+t'|/(2L)}}{1 - e^{-\pi|t-t'|/(2L)}} \right]. \end{aligned} \quad (42)$$

It is easy to verify that this kernel is negative definite. Similarly when the bath is initially prepared in thermal state at inverse temperature β_b ,

$$\begin{aligned} K(t, t') &= -\frac{2}{\pi} \int_0^\infty \frac{dk}{k} \cos[k(t - t')] \coth \left(\frac{k\beta_b}{2} \right) \\ &= \frac{2}{\beta_b} |t - t'| + \frac{2}{\pi} \log \left[1 - e^{-2\pi|t-t'|/\beta_b} \right] \equiv K_{\beta_b}(t - t'). \end{aligned} \quad (43)$$

The kernels have the usual UV divergence for coincident points which goes like $\log |t - t'|$ in 2 dimensions¹⁹. It is worth noting that the $t - t'$ dependent part of the kernel in the Calabrese-Cardy state is the same as in the thermal state with the identification $\beta_b = 4L$ ²⁰.

Note here that $\log |t - t'|$ behaviour of the above kernel is attained in the large β_b limit, whereas in the opposite limit of small β_b , one obtains the linear term proportional to $|t - t'|$ — this is the one-dimensional Green's function, as one would expect in a Kaluza-Klein reduction in the presence of a thermal circle.

¹⁹At finite UV cutoff, this divergence is regulated. See appendix B.4 for details.

²⁰This is known from previous studies of correlation functions in (generalized)-Calabrese-Cardy states, see e.g. [58].

Keldysh rotation

We have obtained the effective action (36) on the Schwinger-Keldysh contour Figure 3 only in terms of Schwarzian mode. We can now study its dynamics more systematically. It is convenient to switch to following variables²¹

$$\phi_c(t) = \frac{1}{2} [\phi^+(t) + \phi^-(t)], \quad \phi_q(t) = \frac{1}{2} [\phi^+(t) - \phi^-(t)], \quad (44)$$

in terms of which our effective action reads

$$S_{SK} = N \left\{ \frac{\alpha_s}{J} \int_0^T dt \left\{ 2\dot{\phi}_c \dot{\phi}_q - V(\phi_c + \phi_q) + V(\phi_c - \phi_q) \right\} - in_f W[F(\phi_c + \phi_q), F(\phi_c - \phi_q)] \right\}. \quad (45)$$

We can compute the two equations of motion of this action and verify that

$$\phi_q(t) = 0, \quad (46)$$

$$\frac{\alpha_s}{J} \left[\ddot{\phi}_c(t) + V'(\phi_c(t)) \right] - n_f g^2 F'(\phi_c(t)) \int_0^t dt' F(\phi_c(t')) = 0, \quad (47)$$

constitute exact solutions of the above system (45) to all orders in ϕ_q . In terms of the \pm variables, (46) is simply $\phi^+(t) = \phi^-(t)$. With this, the two equations (38) and (39) reduce to (47) above with $\phi^+ = \phi^- = \phi_c$.

3.2 Fluctuations and a Langevin equation

Let us now look at the fluctuation

$$\phi_q(t) = \phi_q^0(t) + \frac{1}{\sqrt{N}} \delta\phi_q(t) + O\left(\frac{1}{N}\right) \quad (48)$$

around the solution $\phi_q^0 = 0$. In this case, with the use of explicit relations involving the kernels (41), the action can be rearranged in powers of N as follows

$$S_{SK} = -2\sqrt{N} \int_0^T dt \delta\phi_q(t) \left[\frac{\alpha_s}{J} \left(\ddot{\phi}_c(t) + V'(\phi_c(t)) \right) - n_f g^2 F'(\phi_c(t)) \int_0^T dt' \theta(t-t') F(\phi_c(t')) \right] \\ + \frac{i}{2} \int_0^T dt \int_0^T dt' \delta\phi_q(t) \tilde{K}(t, t') \delta\phi_q(t') + O\left(\frac{1}{\sqrt{N}}\right), \quad (49)$$

where

$$\tilde{K}(t, t') = -2n_f g^2 F'(\phi_c(t)) K(t, t') F'(\phi_c(t')). \quad (50)$$

Therefore up to this order, we have quadratic action for the fluctuations $\delta\phi_q(t')$ and the factors of N are organized such that $\langle \delta\phi_q(t') \delta\phi_q(t) \rangle \sim \tilde{K}^{-1} \sim O(1)$ in N scaling.

We will now replace the quadratic term in $\delta\phi_q$ using an auxiliary variable η and the following identity

$$\exp \left[-\frac{1}{2} \int_0^T dt dt' \delta\phi_q(t) \tilde{K}(t, t') \delta\phi_q(t') \right] = \mathcal{N} \int [D\eta] \exp \left[-\frac{1}{2} \int_0^T dt dt' \eta(t) \tilde{K}^{-1}(t, t') \eta(t') + i \int_0^T dt \eta(t) \delta\phi_q(t) \right]. \quad (51)$$

²¹Sometimes these are called classical-quantum variables [60] or the average-difference variables [61]. However the name classical-quantum is misleading since ϕ_c can also have fluctuations.

With this new variable η , the action is now linear in $\delta\phi_q$,

$$S_{SK} = -2\sqrt{N} \int_0^T dt \delta\phi_q(t) \left[\frac{\alpha_s}{J} \left(\ddot{\phi}_c(t) + V'(\phi_c(t)) \right) - g^2 F'(\phi_c(t)) \int_0^T dt' \theta(t-t') F(\phi_c(t')) - \frac{1}{2} \frac{\eta(t)}{\sqrt{N}} \right] + \frac{i}{2} \int_0^T dt dt' \eta(t) \tilde{K}^{-1}(t, t') \eta(t') + O(N^{-1/2}). \quad (52)$$

Now variation with respect to $\delta\phi_q$ leads us to a Langevin-type equation

$$\frac{\alpha_s}{J} \left(\ddot{\phi}_c(t) + V'(\phi_c(t)) \right) - n_f g^2 F'(\phi_c(t)) \int_0^t dt' F(\phi_c(t')) = \frac{1}{2} \frac{\eta(t)}{\sqrt{N}}, \quad (53)$$

with the following ‘noise’ correlation

$$\langle \eta(t) \eta(t') \rangle = \tilde{K}(t, t') = -2n_f g^2 F'(\phi_c(t)) K(t, t') F'(\phi_c(t')). \quad (54)$$

This Langevin equation is complicated for two reasons. Firstly, the left hand side has an integral which reflects that the equation is non-Markovian and has memory of the dynamics from time 0 to t . Secondly, the Gaussian noise is correlated in a non-local way. It is of great interest to calculate correlation functions of this model and also the time dependence of the probability distribution of the stochastic variable $\phi_c(t)$. The asymptotic behaviour of the correlation functions and the distribution function will not necessarily be thermal like standard Brownian motion (as we will see in Section 6.2) and will carry information about the initial micro-state in terms of the scalar products of the spin of the micro-state $|B_s\rangle$ with the spins of the operators (13) that are coupled to the bath.

In Section 6.1 we will present a calculation of the equal time correlation function of fluctuations around the two specific solutions of the Langevin equation that correspond, at large times, to a) a black hole at a lower temperature where we verify the Einstein-Smoluchowski relation, and b) to a spacetime without a horizon (complete evaporation) where the large time behaviour is oscillatory (see Figure 17, Section 6.2) and characteristic of Brownian motion in a bounded potential.

To tackle the problem of finding an analogue of the Kolmogorov-Fokker-Planck (KFP) equation for the probability distribution it seems best to recast the second order equation (53) into a local third order equation in time.

$$\begin{aligned} \frac{\alpha_s}{J} \left[F'[\phi_c] \ddot{\phi}_c - F''[\phi_c] \dot{\phi}_c \dot{\phi}_c + \{ F'[\phi_c] V''(\phi_c) - F''[\phi_c] V'(\phi_c) \} \dot{\phi}_c \right] - n_f g^2 (F'[\phi_c])^2 F[\phi_c] \\ = \frac{1}{2\sqrt{N}} \left(F'[\phi_c] \dot{\eta} - F''[\phi_c] \dot{\phi}_c \eta \right). \end{aligned} \quad (55)$$

The proof of the equivalence of the two equations (53) and (55) is done separately for the cases when $F'[\phi_c] \neq 0$ and $F'[\phi_c] = 0$. This third order differential equation is supplied by the two initial conditions $\phi_c(0)$, $\dot{\phi}_c(0)$ and the third initial condition $\ddot{\phi}_c(0)$ is determined in terms of $\phi_c(0)$ and $\dot{\phi}_c(0)$ using (53). Recasting the third order equation into three first order equations for the ‘position’ $x \equiv \phi_c$, velocity v , and acceleration a , we can write

$$\begin{aligned} \dot{x} = v, \quad \dot{v} = a \quad \text{and} \\ \dot{a} - \frac{F''[x]}{F'[x]} a v - \left\{ V''(x) - \frac{F''[x]}{F'[x]} V'(x) \right\} v - \frac{J}{\alpha_s} n_f g^2 F'[x] F[x] = \frac{J}{2\alpha_s \sqrt{N}} \left(\dot{\eta} - \frac{F''[x]}{F'[x]} v \eta \right). \end{aligned} \quad (56)$$

This can be useful in establishing a KFP type equation for the probability function $P(x, v, a, t)$. Integrating $P(x, v, a, t)$ over v and a will give the probability distribution of $x = \phi_c$.

It must be noted that for a generalized KFP equation with greater than two (but finite) number of derivatives, the distribution function ceases to be positive definite. This is known as Pawula's theorem [62]²². However as suggested in [63], from a practical viewpoint it is still sometimes useful to work with a finite number of derivatives.

3.3 Solving the Langevin equation in a perturbative expansion in $1/\sqrt{N}$

At large N , the RHS of equation (53) vanishes. The effect of the noise field $\eta(t)$ can only be felt by the fluctuations in $\phi_c(t)$

$$\phi_c(t) = \phi(t) + \frac{1}{\sqrt{N}} \delta\phi_c(t) + O\left(\frac{1}{N}\right). \quad (57)$$

Equation (53) then leads to the following two equations

$$\frac{\alpha_s}{J} \left(\ddot{\phi}(t) + V'(\phi(t)) \right) - n_f g^2 F'(\phi(t)) \int_0^t dt' F(\phi(t')) = 0, \quad (58)$$

$$\begin{aligned} \frac{\alpha_s}{J} \left(\delta\ddot{\phi}_c(t) + V''(\phi(t))\delta\phi_c(t) \right) \\ - n_f g^2 \left\{ F''(\phi(t))\delta\phi_c(t) \int_0^t dt' F(\phi(t')) + F'(\phi(t)) \int_0^t dt' F'(\phi(t')) \delta\phi_c(t') \right\} = \frac{1}{2}\eta(t). \end{aligned} \quad (59)$$

$\phi(t)$ is the solution at strictly large N without any noise and will be studied in detail in the next Section 4. The two-point function of $\delta\phi_c(t)$ will be studied in Section 6 in the background of the solutions of (58).

4 Schwarzian + bath dynamics to leading order in large N : description and results

In this section, we solve the leading large- N equation (58), which we reproduce here

$$\frac{\alpha_s}{J} \left(\ddot{\phi}(t) + V'(\phi(t)) \right) - n_f g^2 F'(\phi(t)) \int_0^t dt' F(\phi(t')) = 0. \quad (60)$$

Here F is given by (25); we will treat the two cases of only the relevant coupling (27) in Model (a) and the mixed coupling (28) in Model (b) separately below. The potential V is given by (37). As explained in [43], (see Appendix C for more details) we take the initial conditions as

$$\phi(0) = \ln\left(\frac{\pi}{\beta J}\right)^2, \quad \dot{\phi}(0) = 0. \quad (61)$$

As explained in the previous section we can get rid of the integral in (60) by taking one more time derivative, which leads to the third order differential equation at leading order in N

$$F'[\phi(t)] \ddot{\dot{\phi}} - F''[\phi(t)] \dot{\phi} \dot{\phi} + \{F'[\phi(t)]V''(\phi(t)) - F''[\phi(t)]V'(\phi(t))\} \dot{\phi} - \frac{J}{\alpha_s} n_f g^2 (F'[\phi(t)])^2 F[\phi(t)] = 0. \quad (62)$$

²²We thank Neha Wadia for pointing this out to us.

We can now solve this differential equation by using the initial conditions (61) and $\ddot{\phi}(0) = -2J^2 e^{\phi(0)}$. Note that even though this is a third order differential equation, only two sets of initial data are needed for the time evolution of our system and is therefore a causal equation²³. This is because $\phi(0)$ and $\dot{\phi}(0)$ are the only two independent initial conditions, while $\ddot{\phi}(0)$ is determined in terms of $\phi(0)$ by putting $t = 0$ in (60). The (inverse) temperature of the black hole β^{-1} enters through the initial condition.

Energy

The dynamics (60) is clearly not invariant under time translation, and hence does not have a conserved energy (signifying energy transfer to the bath). As is conventional in treatments of systems coupled to a bath, one can continue to describe the original expression of the energy (before the coupling) as a ‘time-dependent energy’ of the system, which, in our case, is given by the Schwarzian

$$E_{sch} = N \frac{\alpha_s}{J} \left[\frac{1}{2} \dot{\phi}^2 + 2J^2 e^{\phi} \right]. \quad (63)$$

Note that the Schwarzian is $SL(2, R)$ gauge-independent quantity. It is also important to note that the Schwarzian equals the ADM mass of the black hole [5]. In the rest of the paper, we will present details of the time dependence of this energy.

A second notion of energy can be obtained as follows: let us rewrite equation (62) as

$$\frac{d}{dt} E_{\Delta}(t) = -N_f g^2 F[\phi(t)]^2, \quad (64)$$

where we have defined

$$E_{\Delta}(t) = N \frac{\alpha_s}{J} \left[\frac{1}{2} \dot{\phi}^2 + 2J^2 e^{\phi} \right] - N_f g^2 F[\phi(t)] \int_0^t dt' F[\phi(t')]. \quad (65)$$

The quantity $E_{\Delta}(t)$ can be interpreted as a time dependent energy of our system. Then the equation (64) tells us that this energy can only dissipate with time since the right-hand side is non-positive. A justification for $E_{\Delta}(t)$ to be a good notion of energy is as follows. We eliminate the non-locality in the equation of motion (60) by introducing a new variable $\mathcal{E}(t) = g \int_0^t dt' F(\phi(t'))$,

$$\ddot{\phi}(t) + 2J^2 e^{\phi(t)} - \frac{n_f g J}{\alpha_s} \mathcal{E}(t) F'(\phi(t)) = 0, \quad \dot{\mathcal{E}}(t) = g F(\phi(t)). \quad (66)$$

For constant $\mathcal{E}(t) = \epsilon$, we have $E_{\Delta} = \frac{1}{2} \dot{\phi}^2 + 2J^2 e^{\phi} - \frac{n_f g J}{\alpha_s} \epsilon F(\phi)$. In fact for $F(\phi) = J e^{\phi/2}$, this is exactly the same as the Kourkoulou-Maldacena deformation [43]. For time-dependent $\mathcal{E}(t)$, $E_{\Delta}(t)$ is therefore an appropriate generalization of energy in presence of a bath.

In JT gravity, complete evaporation of black hole has a simple diagnostic – whether the boundary curve (e^{ϕ}) hits a zero or not. This is explained in detail in Section 7.2 and Appendix G. The absence or presence of horizon is a gauge-invariant statement and therefore this is a smoking gun test of whether the bulk geometry contains a horizon or not.

²³Generically 3rd order equations can have solution which are acausal. The Abraham-Lorentz equation, which describes the non-relativistic motion of an accelerating charge particle, is a well-known third order equation in electrodynamics (see for example [64]). It is known to have pathological solutions in which the particle accelerates before any force is even applied.

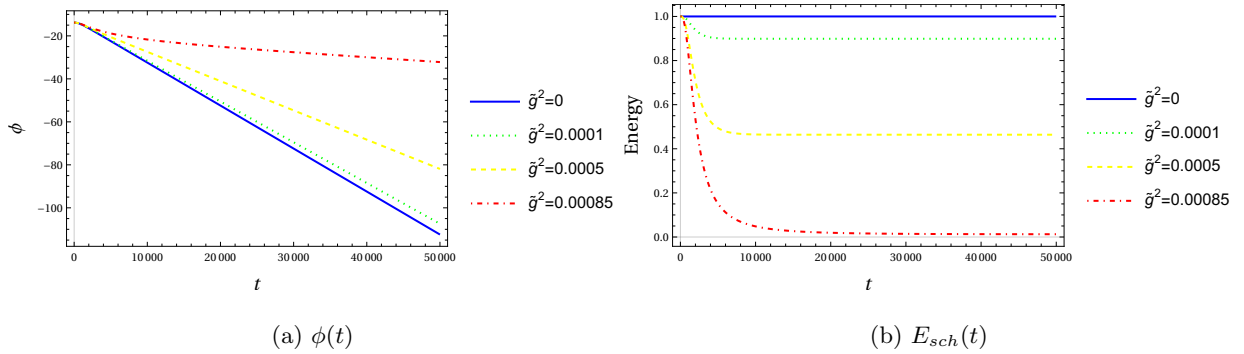


Figure 4: Plot of $\phi(t)$ and energy (estimated by the Schwarzian) for various values of the coupling. Note that the energy loss is greater for stronger coupling. Numerics done for $\beta = 1000\pi$ with $J = 1$.

The solution we will find, up to some strength of coupling, corresponds to cooling of the SYK system, which can be interpreted as black hole losing energy to the bath, in other words, black hole evaporation. This can be qualitatively compared with part of the results of [38, 39], except that while they describe the time evolution in terms of the (G, Σ) variables, we are able to describe the entire time evolution in terms of the Schwarzian model, thus allowing a gravity interpretation all the way.

Now we turn to solving the equation (60) (or equivalently (62)) for different types of couplings((27) and (28)) mentioned in Section 3.

4.1 Model (a): Interaction with just the relevant operator ($\Delta = 1/2$)

We start with only the relevant interaction (see (27)), i.e. we specialize to

$$F(\phi) = J e^{\phi/2}. \quad (67)$$

4.1.1 Numerical solution

We simply solve the 3rd order equation (62). For the above interaction it reads (after setting $J = 1$ – this can be regarded as a choice of units, and can be reinserted simply by replacing $\beta \rightarrow \beta J, t \rightarrow tJ$, etc.)

$$\ddot{\phi} - \frac{1}{2}\ddot{\phi}\dot{\phi} + e^{\phi}\dot{\phi} - \tilde{g}^2 e^{\phi} = 0, \quad \tilde{g}^2 \equiv \frac{n_f g^2}{2\alpha_s}. \quad (68)$$

Following the comments below (62), we impose the initial conditions:

$$\phi(0) = 2 \ln \left(\frac{\pi}{\beta} \right), \quad \dot{\phi}(0) = 0, \quad \ddot{\phi}(0) = -2 \left(\frac{\pi}{\beta} \right)^2 \quad (69)$$

The solution for $\phi(t)$ as well as the energy (estimated by the Schwarzian) for various values of the coupling \tilde{g}^2 is shown in figures 4a and 4b. Comparison between the two energies 63 and 65 is also displayed in Figure 5. The solutions ($\dot{\phi}$ and energy) reach an equilibrium and the final energy can be read-off from the slope at late times which can be determined numerically. At late times, $\phi = -at + \dots$, the asymptotic energy is

$$E_{Sch} = E_{\Delta} = N \frac{\alpha_s}{J} \frac{a^2}{2}. \quad (70)$$

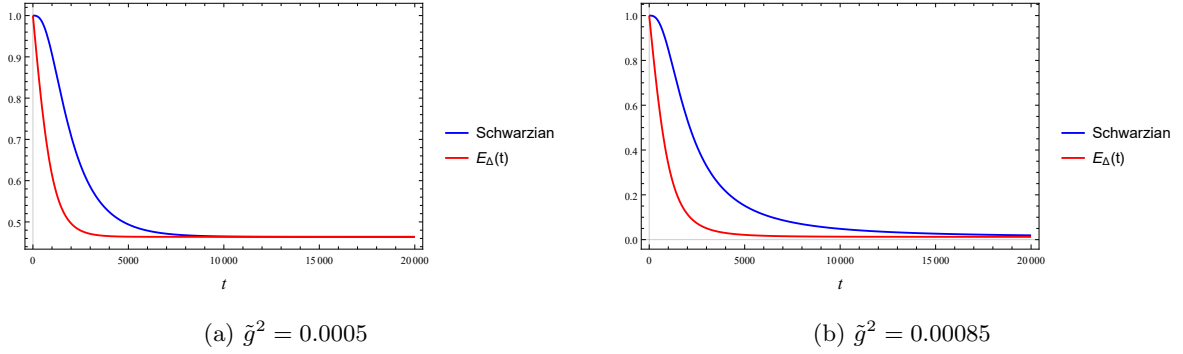


Figure 5: The energy as a fraction of the initial value at $t = 0$. The blue curve is the Schwarzian while the red curve is E_Δ . The two definitions of energy disagree at intermediate times but they agree at late times. Stronger coupling leads to greater energy loss. Numerics done for $\beta = 1000\pi$ with $J = 1$.

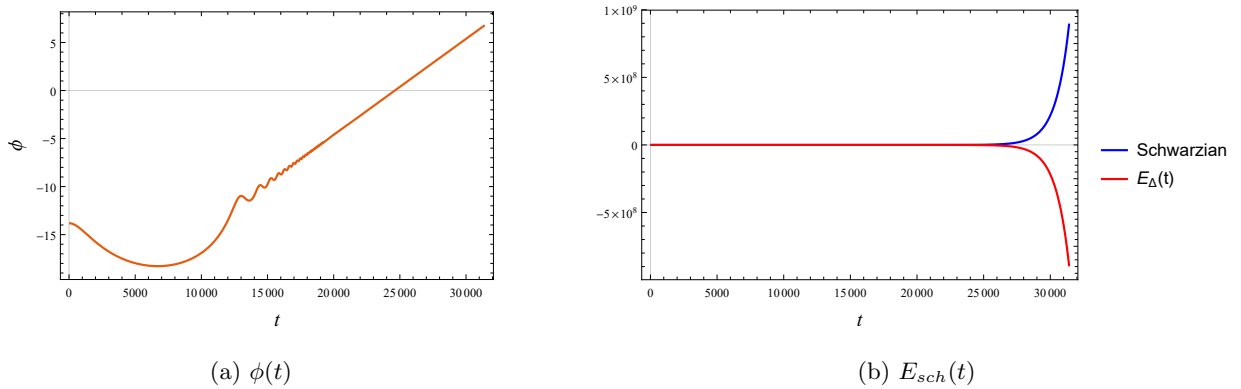


Figure 6: Plot of $\phi(t)$ and energies above critical coupling (71). Here $\tilde{g}^2 = 0.001$, $\beta = 1000\pi$ and $J = 1$.

It may appear surprising at the first sight that the equilibrium configuration of the system is independent of the bath temperature. However it is a familiar phenomenon in usual system-bath models of equilibration. For example, for a pendulum oscillating in a hot viscous medium, the classical motion comes to a stop whose position has nothing to do with the temperature of the medium. However the mean square fluctuations around the classical motion do indeed see the bath temperature. Although our coupling to the bath is more complicated, we find a similar phenomenon. A crucial difference from the pendulum example is that because our coupling is non-linear and non-local in time, the effective friction decreases exponentially in time so that the equilibrium configuration remembers about the coupling strength.

Above a certain value of the coupling \tilde{g} , given by

$$\tilde{g}_* \approx 0.65 \sqrt{\frac{2\pi}{\beta J}}, \quad (71)$$

the solution $\phi(t)$, instead of decreasing, grows linearly at late times. This is shown below in Figure 6a. Note that the third order equation (68) possesses an exact, linearly growing, solution

$$\phi(t) = \tilde{g}^2 t. \quad (72)$$

Although this solution does not satisfy the initial conditions (69), one finds numerically that, the actual

solution of (68), with the correct initial conditions, coincides with (72) at late times. Additionally, as shown in Figure 6b, both the energies E_{sch} and E_{Δ} , grow unbounded in magnitude. There are a number of ways that one can see that the solution, beyond the critical coupling (71), is unphysical; see Section 4.1.4.

4.1.2 Analytic solution

After setting $F(\phi) = e^{\phi/2}$, the equation (60) becomes (after setting $J = 1$)

$$\left(\ddot{\phi}(t) + 2e^{\phi(t)}\right) - \tilde{g}^2 e^{\phi(t)/2} \int_0^t e^{\phi(t')/2} dt' = 0, \quad \tilde{g}^2 = \frac{n_f g^2}{2\alpha_s}. \quad (73)$$

This equation can be solved analytically in a perturbation theory in \tilde{g}^2 at least to leading order in this coupling; the answer is

$$\phi(t) = \phi_0(t) + \tilde{g}^2 \phi_1(t) + O(\tilde{g}^4), \quad (74)$$

$$\phi_0(t) = \log \left(\frac{\pi^2}{\beta^2} \operatorname{sech}^2 \frac{\pi t}{\beta} \right),$$

$$\phi_1(t) = -\frac{1}{\pi} \operatorname{sech} \left(\frac{\pi t}{\beta} \right) \left\{ \sinh \left(\frac{\pi t}{\beta} \right) \left[\beta + \beta \log 2 - \beta \log \left(e^{\frac{2\pi t}{\beta}} + 1 \right) + \pi t \right] - \beta \cot^{-1} \left[\operatorname{csch} \left(\frac{\pi t}{\beta} \right) \right] \right\}. \quad (75)$$

At large t , the behaviour of the solution can be found from the asymptotic expression

$$\phi(t) = \left(\tilde{g}^2 - \frac{2\pi}{\beta} \right) t - 2 \left[\log \frac{\beta}{2\pi} + \tilde{g}^2 \frac{\beta}{2\pi} (1 + \log 2) \right] + O(\exp[-\pi t/\beta]). \quad (76)$$

At large t , the term linear in t dominates, leading to

$$\phi(t) \rightarrow -at, \quad a = \left(\frac{2\pi}{\beta} - \tilde{g}^2 \right), \quad \tilde{g}^2 = \frac{n_f g^2}{2\alpha_s}. \quad (77)$$

It is easy to see that, for

$$\tilde{g} \geq \tilde{g}_*^A \equiv \sqrt{\frac{2\pi}{\beta J}}, \quad (78)$$

$a < 0$ and the solution $\dot{f}(t) = e^{\phi(t)}$ grows linearly without bound, thus indicating breakdown of perturbation theory in \tilde{g}^2 . We found the same phenomenon in the numerical solutions also (see (71)) for a slightly different critical value. We compare the analytic and numerical solutions below (see Section 4.1.3).

In the region (78), one can estimate the time t_* beyond which the solution shows a runaway behaviour. In (76), for short enough times the constant term dominates, but the linearly diverging term dominates from $t \gtrsim t_*$ where

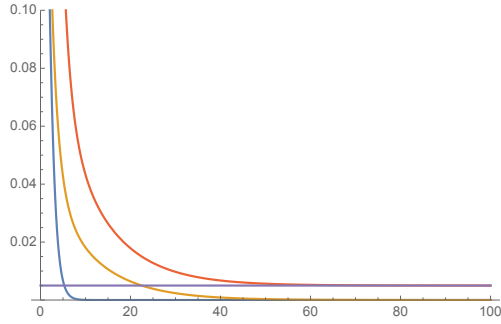
$$t_* = \frac{2 \left[\log \frac{\beta}{2\pi} + \tilde{g}^2 \frac{\beta}{2\pi} (1 + \log 2) \right]}{\left(\tilde{g}^2 - \frac{2\pi}{\beta} \right)}.$$

Asymptotics: A sensible asymptotic solution (77) is found for couplings in the range $\tilde{g} < \tilde{g}_*$:

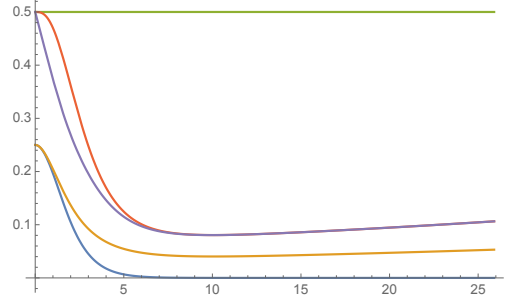
$$\phi(t \rightarrow \infty) \rightarrow -t((\tilde{g}_*^A)^2 - \tilde{g}^2), \text{ hence } \dot{f}(t) \rightarrow 0, \quad (79)$$

$$E_{sch}(t \rightarrow \infty) = E_{\Delta}(t \rightarrow \infty) \equiv E_{\infty} \equiv N\alpha_s J \frac{1}{2} ((\tilde{g}_*^A)^2 - \tilde{g}^2)^2 = N\alpha_s J \frac{1}{2} \left(\frac{2\pi}{\beta J} - \tilde{g}^2 \right)^2. \quad (80)$$

In Section 7, we will interpret this classical solution as representing a final black hole solution at a smaller energy compared to the initial black hole, obtained as a result of interaction with the bath.

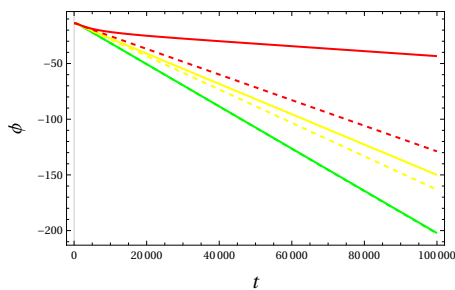


(a) $\tilde{g}^2 = 0.9$. Red= E_{sch} , purple= E_{Δ} , brown= E_{∞} , blue= e^{ϕ_0} , orange= e^{ϕ} .

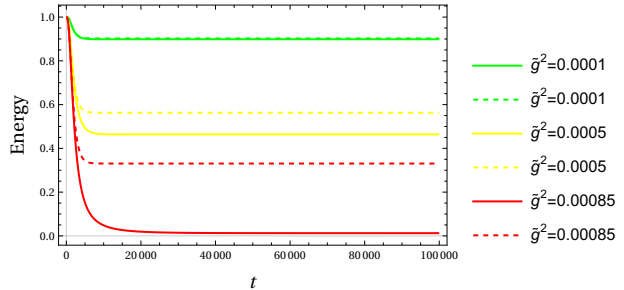


(b) $\tilde{g}^2 = 1.02$. Red= E_{sch} , purple= E_{Δ} , green= E_0 , blue= e^{ϕ_0} , orange= e^{ϕ} .

Figure 7: In both figures, $\beta J = 2\pi$, so that $\tilde{g}_*^A = 1$. The left panel, where $\tilde{g} < \tilde{g}_*^A$, shows approach to an asymptotic value for energy as well as $\exp[\phi]$. In the right panel, energy as well as $\exp[\phi]$ show unbounded growth.



(a) $\phi(t)$



(b) $E_{Sch}(t)$

Figure 8: Comparison between numerical (solid lines) and analytical perturbative solutions (dashed lines) for various strengths of the coupling. They match at small couplings but begin to differ at larger couplings.

4.1.3 Comparison of numerical and analytical solutions

We find above that both the numerical and the perturbative analytical methods predict a sensible asymptotic classical solution if the coupling strength \tilde{g}^2 is small enough (with critical coupling dictated by the initial energy of the $|B_s(l)\rangle$ state). The small difference between the numerical and analytical values of the critical coupling (see (71), (78)) may arise from the fact that (78) is obtained from first order perturbation theory in \tilde{g}^2 which may not be valid near criticality.²⁴ From the explicit solutions in Figure 8, one can see that the numerical and analytical solution match well at small couplings but begin to differ at larger couplings as one approaches near criticality.

²⁴This is to be expected if the actual solution is non-analytic in $(g_*^2 - \tilde{g}^2)$, in which case the radius of convergence in an expansion in \tilde{g}^2 will be g_*^2 , signaling a breakdown of perturbation theory near criticality. Note that in [47] we found a branch cut singularity in the solution as a function of the KM-coupling. Note also that in a first order \tilde{g}^2 expansion, a non-analytic function like $(1 - \frac{\tilde{g}^2}{g_*^2})^p$ will behave like $(1 - p\frac{\tilde{g}^2}{g_*^2} + \dots)$, thus appearing to shift the critical point to $\tilde{g}^2 = pg_*^2$ at first order.

4.1.4 Unphysical solutions in Model (a)

We found above the existence of diverging solutions beyond the critical coupling (71). There are a number of ways that one can see that these solutions are unphysical:

1. The unbounded energy E_{sch} soon exceeds the scale J , which signals breakdown of the low energy approximation under which the analysis of the model in terms of the Schwarzian is based.
2. As we will describe below in more detail for Model (b), coupling to a bath can be roughly regarded as assigning a time-dependence to the coupling constant(s). This can be seen from rewriting the equation of motion as eq. 66 in terms of the time dependent coupling $\mathcal{E}(t)$. With the unbounded solution under discussion here, $\mathcal{E}(t)$ diverges exponentially in time, thus taking the relevant coupling beyond the regime of conformal perturbation theory around the SYK fixed point.
3. **Anti-dissipation:** The unbounded energy E_{sch} is unphysical simply because it represents absorption of energy by the SYK system from the bath which is effectively colder. This indicates anti-dissipation, or negative friction. In the perturbative solution (76), one can explicitly see the transition from dissipative behaviour to anti-dissipative behaviour ($\dot{f}(t)$ changes from exponentially decaying to exponentially growing), as the coupling constant crosses the critical value (78).²⁵ Note that anti-dissipative behaviour is not visible in the standard system-bath models like the Caldeira-Leggett model [65] which has linear couplings to an Ohmic bath.

It is important to note that the unphysical solutions we find here are not related to the well-known runaway solutions of third order differential equations, e.g. in the radiation reaction problem of electrodynamics.

We will come back to the issue of the unphysical solutions in more details and more generally in Section 4.3.

4.2 Model (b): Complete Evaporation: Relevant + marginal interaction

First we argue that it is not possible to achieve complete black hole evaporation with a single coupling $F(\phi) = e^{\Delta\phi}$, with $\Delta = 1/2$ for relevant and $\Delta = 1$ for marginal coupling (we have put $J = 1$). It is easy to see that a bounded solution of equation (60) is simply not possible! Let us assume that there exists a solution such that

$$\phi_{max} > \phi(t \rightarrow \infty) > \phi_{min} \tag{81}$$

i.e. it is bounded both above and below. The lower bound is required for disappearance of the horizon while the upper bound is imposed such that the boundary curve does not venture far into the bulk as $\hat{z} \propto \dot{f} = \exp(\phi)$ (see Section 7.2 and Appendix G for a detailed discussion). The bound implies that $e^{\Delta\phi_{max}} t > \int_0^t e^{\Delta\phi(t')} dt' > e^{\Delta\phi_{min}} t$ and therefore the integral grows linearly with time. At sufficiently late

²⁵The difference of this from (71) has been discussed above.

times the integral term overtakes the potential term $2e^\phi$ and the equation of motion (60) reads

$$\ddot{\phi}(t) \approx \frac{n_f g^2 A^2 \Delta}{\alpha_s} t,$$

where $A = \exp(\Delta\phi(t \rightarrow \infty))$ is the asymptotic value that is bounded $\exp(\Delta\phi_{min}) < A < \exp(\Delta\phi_{max})$. The solution

$$\phi(t) \approx \frac{n_f g^2 A^2 \Delta}{6\alpha_s} t^3$$

is unbounded as it keeps growing with time, in contradiction with our assumption (81). This implies that either $\exp(\phi) \rightarrow 0$ as $t \rightarrow \infty$ and we remain in the black hole phase, or $\exp(\phi) \rightarrow \infty$ as $t \rightarrow \infty$ and the low-energy Schwarzsian description breaks down.

Now we will overcome this by turning on more than one interaction term simultaneously and achieve complete black hole evaporation. There is another way to achieve complete black hole evaporation if we allow a fixed KM potential term which we briefly mention in appendix D.2.

We choose the function F to have both relevant and marginal coupling

$$gF(\phi) = gJ e^{\phi/2} - g' J e^\phi. \quad (82)$$

The equation of motion (60) in this case reads (after setting $J = 1$, which can be reinserted simply by replacing $\beta \rightarrow \beta J, t \rightarrow tJ$, etc.)

$$\left(\ddot{\phi}(t) + 2e^{\phi(t)} \right) - \frac{n_f}{\alpha_s} \left(\frac{1}{2} g e^{\phi(t)/2} - g' e^{\phi(t)} \right) \int_0^t dt' \left(g e^{\phi(t')/2} - g' e^{\phi(t')} \right) = 0. \quad (83)$$

It is important to have a relative minus sign between the two couplings. This allows the solution for ϕ to approach a finite value. This is achieved if in (83) either the integrand vanishes at late times or the pre-factor multiplying the integral effectively goes to zero at late times. Numerical solutions suggest that for generic values of the coupling parameters (see Figure 16), it is actually the latter. In Figure 9 we present the numerical solution where ϕ remains bounded at arbitrary large times. This indicates that the bulk geometry is horizonless and therefore the black hole is gone. Without the relative minus sign, the solution $\phi(t) \rightarrow -\infty$ as $t \rightarrow \infty$, which remains a black hole (see Figure 16) just as in Model (a).

Since ϕ approaches $\phi_{eq} \equiv 2 \log\left(\frac{g}{2g'}\right)$ at late times, the integral

$$\mathcal{E}(t) \equiv \int_0^t dt' g \left(e^{\phi(t')/2} - \frac{g'}{g} e^{\phi(t')} \right) \approx \int_0^t dt' \frac{g^2}{4g'} = \frac{g^2}{4g'} t \quad (84)$$

grows linearly with time. We have also verified this numerically for various values of g and g' . It is important that $\phi(t \rightarrow \infty)$ is not exactly $\phi_{eq} = 2 \log\left(\frac{g}{2g'}\right)$, but remains very close to it. Otherwise the effect of the coupling would simply vanish. To understand this ‘attractive’ nature of the solution it is useful to consider a time-dependent potential²⁶

$$V_{eff}(\phi(t)) = 2e^{\phi(t)} - \frac{n_f}{\alpha_s} g \left(e^{\phi(t)/2} - \frac{g'}{g} e^{\phi(t)} \right) \mathcal{E}(t). \quad (85)$$

²⁶We note that this problem is not adiabatic by any means and we will not use the time-dependent potential do calculations. Nevertheless we find it useful in the present context.

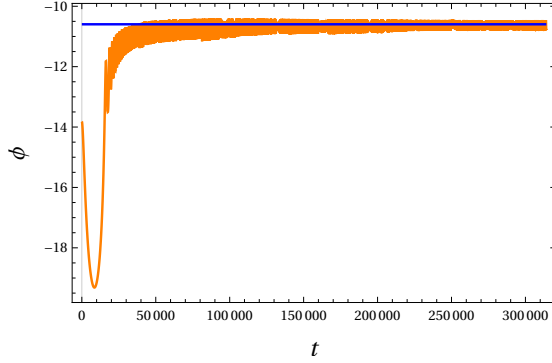


Figure 9: The solution for ϕ with both relevant and marginal coupling remains bounded at late times. Numerics done for $\beta = 1000\pi$, $J = 1$, $n_f = 0.01$, $g = 0.04$ and $g' = 4$. At late times, ϕ seems to approach the value $\phi_{eq} = 2 \log\left(\frac{g}{2g'}\right) \approx -10.6$ shown by the blue line.

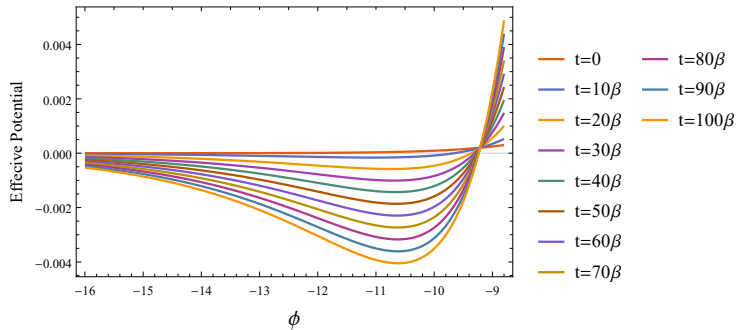


Figure 10: The effective potential (85) becomes deeper and deeper as time increases. This is because the integral increases linearly with time. Here $\beta = 1000\pi$ is the initial inverse temperature of the black hole. Further we chose $n_f = 0.01$, $g = 0.04$ and $g' = 4$.

Since the integral grows linearly, at late times the potential also scales linearly with time

$$V_{eff}(\phi) \approx \frac{n_f}{4\alpha_s} g^2 \left(e^\phi - \frac{g}{g'} e^{\phi/2} \right) t \quad (86)$$

and therefore becomes deeper and deeper by stretching along the y-axis linearly with time (see Figure 10). Then effectively we have a dynamics of a particle trapped in such a well whose depth increases linearly with time. This also explains why the motion is bounded.

The energies ((63) and (65)) for the bounded solution of (83) however also keep increasing with time, see Figure 11.

4.2.1 Analytic solution at large times in terms of Airy functions

From the numerical solution we saw that at late times ϕ approaches a fixed value $\phi_{eq} = 2 \log\left(\frac{g}{2g'}\right)$. This suggests that we separate

$$\phi(t) = \phi_{eq} + \psi(t). \quad (87)$$

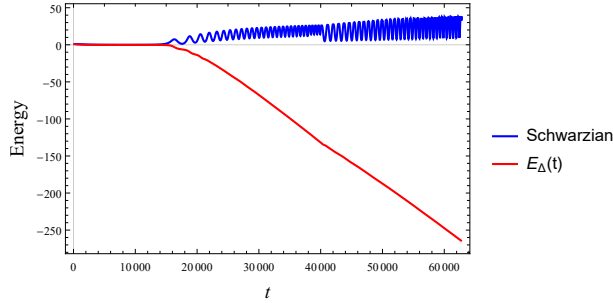


Figure 11: Energies as a function of time. Here $\beta = 1000\pi$, $n_f = 0.01$, $g = 0.04$ and $g' = 4$.

Note that this is outside the validity of perturbation theory in small coupling. The equation of motion to leading order in small ψ reads (setting $J = 1$)

$$\ddot{\psi}(t) + 2e^{\phi_{eq}}(1 + \psi(t)) + \frac{n_f g^2}{32\alpha_s} \left(\frac{g}{g'}\right)^2 t \psi(t) = 0. \quad (88)$$

The last term comes from the integral in (83) and grows linearly as we saw in (84). At very late times it will overtake the potential $e^{\phi_{eq}}$, which is just a constant²⁷. The equation then becomes of the Airy form

$$\ddot{\psi}(t) + \frac{n_f g^2}{32\alpha_s} \left(\frac{g}{g'}\right)^2 t \psi(t) = 0, \quad (89)$$

with the solution

$$\begin{aligned} \psi(t) &= c_1 Ai(-ct) + c_2 Bi(-ct), \\ c &= \frac{c'}{2 \cdot 2^{2/3}} (-c')^{-2/3}, \quad c' = \frac{n_f g^4}{\alpha_s g'^2}. \end{aligned} \quad (90)$$

The asymptotic form reads

$$\phi(t) = \phi_{eq} + c_1 \frac{\sin\left(\frac{2}{3}(ct)^{3/2} + \frac{\pi}{4}\right)}{\sqrt{\pi}(ct)^{1/4}} + c_2 \frac{\cos\left(\frac{2}{3}(ct)^{3/2} + \frac{\pi}{4}\right)}{\sqrt{\pi}(ct)^{1/4}} + O(t^{-7/4}). \quad (91)$$

Thus the solution approaches the constant value ϕ_{eq} slowly as a power law modulated by oscillations whose frequency increases with time.

Note that the above solution is not valid for arbitrarily small values of the coupling as discussed above (see Figure 16).

4.2.2 Quench and stabilizing the effective potential

For the solution of (83), as we saw above both the energies and the effective potential kept increasing without bound. This means that sooner or later the Schwarzian approximation we are working with will break down. More precisely, the low-energy approximation that we have used to locate the IR fixed point is $\omega \ll J$. Applying the same principle to the linearized Airy equation (89), the time-dependent frequency should satisfy

$$\omega(t) = \left(\frac{n_f g^4}{32\alpha_s g'^2} t\right)^{1/2} \ll 1. \quad (92)$$

²⁷One can also solve the equation with the constant term present but we omit it here as it is not particularly illuminating.

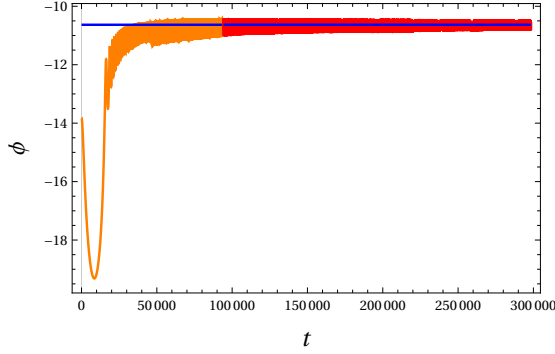


Figure 12: The solution for ϕ with both relevant and marginal coupling remains bounded even while quenching the parameters as in (94). The orange curve is before the quench, which is initiated at $t = t_{max} = 30\beta$. After that the solution shown in red, remains finite and bounded at all times. In fact ϕ approaches the value $2 \log\left(\frac{g}{2g'}\right) - \frac{8\alpha_s}{8\alpha_s + n_f t_{max} g^2} \approx -10.63$ shown by the blue line. Here $J = 1, \beta = 1000\pi, n_f = 0.01, g = 0.04, g' = 4$.

This gives us a time-scale t_*

$$t_* = \frac{32\alpha_s g'^2}{n_f g^4} \quad (93)$$

at which our solution breaks down. In other words we can only trust our solution for times $t \ll t_*$.

Now we quench the coupling parameters in such a way that the potential and energies stabilize at late times. We are allowed to this because the couplings are by themselves not dynamical variables of the system and thus can be tuned. By quench we mean that both g and g' are made explicit functions of time. Note that it is really the UV couplings \hat{g}_1, \hat{g}_2 that are being quenched and the effect carries over to g, g' as they are linearly related (28). We choose the following quench protocol.

$$\begin{aligned} g(t) &= g [\Theta(t) - \Theta(t - t_{max})] + g \Theta(t - t_{max}) \sqrt{\frac{t_{max}}{t}}, \\ g'(t) &= g' [\Theta(t) - \Theta(t - t_{max})] + g' \Theta(t - t_{max}) \sqrt{\frac{t_{max}}{t}}, \end{aligned} \quad (94)$$

i.e. after $t = t_{max}$, the couplings go down in strength as $t^{-1/2}$. This time must satisfy $t_{max} \ll t_*$. Note that the ratio $g'(t)/g(t)$ remains constant. For time-dependent parameters the equation of motion (83) is modified to

$$\left(\ddot{\phi}(t) + 2e^{\phi(t)}\right) - \frac{n_f}{\alpha_s} g(t) \left(\frac{1}{2}e^{\phi(t)/2} - \frac{g'}{g}e^{\phi(t)}\right) \int_0^t dt' g(t') \left(e^{\phi(t')/2} - \frac{g'}{g}e^{\phi(t')}\right) = 0. \quad (95)$$

We solve this modified equation with the quench protocol (94) and find that even now ϕ approaches $\phi_{eq} = 2 \log \frac{g}{2g'}$ and therefore is still finite and bounded as shown in Figure 12. In Figure 13 and Figure 14 we plot the effective potential and the energies (both (63) and (65)) respectively. After $t = t_{max}$ we see that all of them are bounded unlike without the quench. For the specific values of parameters, namely $n_f = 0.01, g = 0.04, g' = 4$ and $\alpha_s \approx 0.007$, for which we present the plots, we choose t_{max} , such that $t_{max} \approx 10^5 \ll t_* \approx 10^8$.

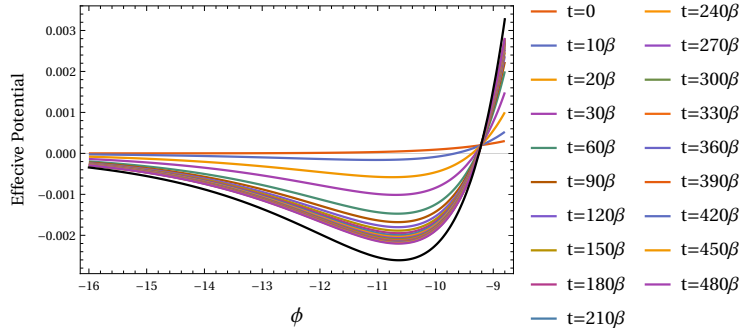


Figure 13: We plot the effective potential (85) while quenching the parameters g and g' as in equation (94). The black curve is the asymptotic value ($t \rightarrow \infty$) of the effective potential (101). The post-quench solution stabilizes and seems to slowly approach the black curve asymptotically. Also compare with the previous case in Figure 10, where the potential kept on increasing. We quench both the coupling parameters g and g' at $t = t_{max} = 30\beta$. Here $J = 1, \beta = 1000\pi, n_f = 0.01, g = 0.04, g' = 4$.

Long times after quench: Since the solution remains finite and bounded at all times, we can do a similar analysis that led us to the Airy equation before. Writing

$$\phi(t) = \phi_{eq} + \psi(t), \quad (96)$$

the equation of motion to leading order in small ψ at long times after the quench ($t \gg t_{max}$) reads

$$\ddot{\psi}(t) + 2e^{\phi_{eq}}(1 + \psi(t)) + \frac{n_f t_{max} g^2}{16\alpha_s} \left(\frac{g}{g'}\right)^2 \psi(t) = 0. \quad (97)$$

We have set $J = 1$. Compared to equation 88, the last term does not grow linearly with time. We can solve this equation, the solution is simple

$$\psi(t) = -\frac{8\alpha_s}{8\alpha_s + n_f t_{max} g^2} + c_1 \sin(\Omega t) + c_2 \cos(\Omega t), \quad \Omega = \left(\frac{8\alpha_s g^2 + n_f t_{max} g^4}{16\alpha_s g'^2}\right)^{1/2}. \quad (98)$$

Therefore we find that at late times the solution oscillates with constant frequency Ω around the value

$$\tilde{\phi}_{eq} = \phi_{eq} - \frac{8\alpha_s}{8\alpha_s + n_f t_{max} g^2} = 2 \log\left(\frac{g}{2g'}\right) - \frac{8\alpha_s}{8\alpha_s + n_f t_{max} g^2}. \quad (99)$$

For the parameter values $n_f = 0.01, g = 0.04, g' = 4, \alpha_s \approx 0.007$ used in Figure 12, $\tilde{\phi}_{eq} \approx -10.63$ and the frequency $\Omega \approx 0.037$. There is a simple way to understand (98). At long times ($t \gg t_{max}$), we find that the integral in equation of motion (95) stabilizes, and we can rewrite the equation simply as

$$\ddot{\phi} + V'_{eff}(\phi) = 0, \quad (100)$$

with the asymptotic value of the effective potential (we have reinstated J)

$$V_{eff}(\phi) = 2J^2 e^\phi + \frac{J t_{max}}{2\alpha_s} n_f g^2 J^2 \left(e^\phi - \frac{g}{g'} e^{\phi/2}\right), \quad (101)$$

which is time-independent²⁸. This is also shown in Figure 13 for comparison. In a similar spirit, one can show that the energy E_Δ (65), asymptotically corresponds to particle motion in the above asymptotic

²⁸In arriving at this expression we have dropped terms that are power law suppressed as $1/\sqrt{t}$.

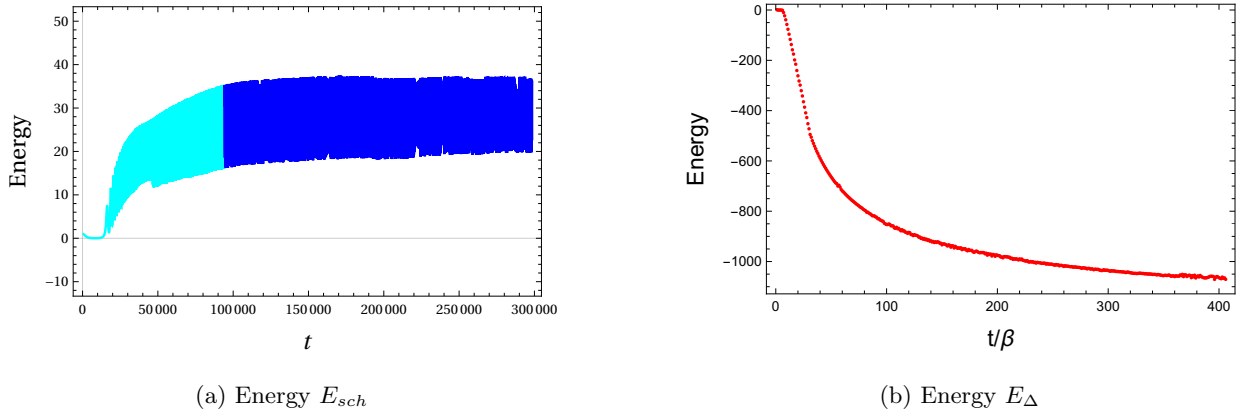


Figure 14: We plot the energies, namely Schwarzschild (63) (left) and E_{Δ} (65) (right). We quench the parameters g and g' as in eq. (94) with $t_{max} = 30\beta \approx 94000$. Before t_{max} (shown in light blue) the amplitude of the Schwarzschild keeps on increasing, however after t_{max} (shown in dark blue) the amplitude growth stops, but it keeps on oscillating. For E_{Δ} , the linear growth stops at $t = t_{max} = 30\beta$. Both the energies are shown in units of the initial energy. Here $J = 1, \beta = 1000\pi, n_f = 0.01, g = 0.04, g' = 4$.

potential (101) (we have reinstated J):

$$E_{\Delta}(t \rightarrow \infty) = N \frac{\alpha_s}{J} \left[\frac{1}{2} \dot{\phi}^2 + 2J^2 e^{\phi} + \frac{J t_{max}}{2\alpha_s} n_f g^2 J^2 \left(e^{\phi} - \frac{g}{g'} e^{\phi/2} \right) \right] = N \frac{\alpha_s}{J} \left[\frac{1}{2} \dot{\phi}^2 + V_{eff}(\phi) \right]. \quad (102)$$

Note that E_{sch} , which has only the term $2J^2 e^{\phi}$ of the potential, misses coupling term. Thus, E_{Δ} is the more appropriate definition of energy here than E_{sch} ²⁹

4.3 Nature of solutions and admissible domain of the g - g' plane

Note first of all that Model (a) can be regarded as a special case of Model (a), i.e. Model (a) is obtained by putting $g' = 0$ in Model (b). As we saw above in this section, the nature of the solutions strongly depends on the couplings g and g' . From our numerical analysis, we were able to chart out various solutions in the g - g' plane which is shown in Figure 15.

Broadly we found three types of solutions, (i) well-behaved solutions, $\phi(t \rightarrow \infty) \rightarrow -\infty$, that correspond to black hole geometries (shown in red), (ii) bounded solutions that oscillates around a fixed value ϕ_{eq} with a diminishing amplitude (shown in green), and (iii) runaway solutions $\phi(t \rightarrow \infty) \rightarrow \infty$, which we disregarded (shown in blue). Based on this, a schematic cartoon of the solution space is constructed and is shown in Figure 16. While we have not marked the full plane, the entire region ‘outside’ corresponds to runaway (blue) solutions.

We note that near the origin, the solutions are always (smaller) black holes. However there is a finite region in g - g' plane for which the solutions as well as energies at late times remain finite and bounded, after using the quench protocol (94). They correspond to horizonless geometries, as shown in Figure 9 and

²⁹It is important to realize that although it appears that the coupling g goes to zero as a power law, it is not enough to decouple the system from the bath; as a result the two notions of energy remain different even asymptotically.

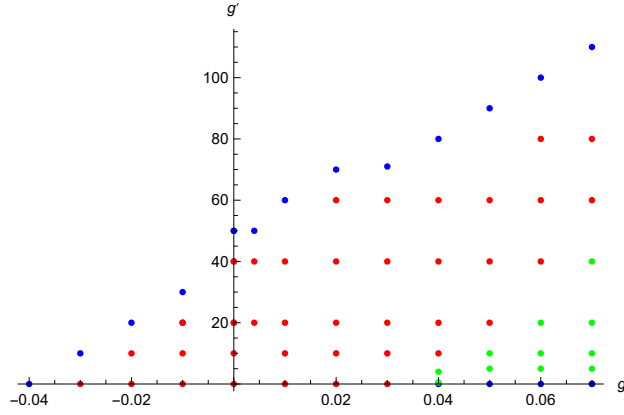


Figure 15: The various solutions in the g - g' plane: (i) well-behaved solutions, $\phi(t \rightarrow \infty) \rightarrow -\infty$, that correspond to black hole geometries (shown in red), (ii) bounded solutions that oscillates around a fixed value ϕ_{eq} with a diminishing amplitude (shown in green), and (iii) runaway solutions $\phi(t \rightarrow \infty) \rightarrow \infty$, which we disregard (shown in blue). Models represented by green dots lead to horizonless geometries after one turns on a quench protocol (94).

are shown as green dots and regions in Figures 15 and 16. This means that horizonless geometries cannot be obtained in perturbation theory in couplings, as we already found.

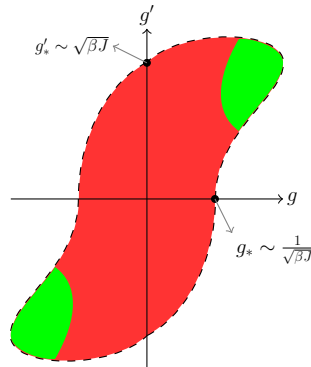


Figure 16: The ‘phase-diagram’ in the g - g' plane. This is a cartoon based on our numerical investigation (see Figure 15) and is not drawn to scale. This diagram has used the fact that the allowed domain has a reflection symmetry in the origin of the $g - g'$ plane. The color coding is the same as Figure 15, except now the blue dots populate the white region outside the black dashed curve. We note that the place where this curve intersects the g axis is $g_* \sim O(1/\sqrt{\beta J})$, and the place where it intersects the g' axis is $g'_* \sim O(\sqrt{\beta J})$ which is very large. In principle some part of the green region can extend to infinity.

Whenever the solution $\phi(t)$ grows unbounded, the Schwarzian E_{sch} also grows without bound (due to the exponential potential $2e^{\phi(t)}$). Therefore outside the red region, there is anti-dissipation and the system takes in energy from the (colder) bath. This kind of behaviour is unphysical, and is a generalization of such behaviour in the special case of Model (a) ($g' = 0$) as elaborated in Section 4.1.4. In the green region too, the energy increases, but it does so in a much milder, power law, fashion. With an appropriate

time-dependent coupling as in (94), one obtains in this case finite energy solutions that remain bounded and correspond to horizonless geometry.

Lastly, we note that in order to generate Figure 15, we solved the third order equation (62) and not the second order equation 60. One might worry that the runaway solutions are pathologies of the 3rd order equation, similar to the radiation reaction problem in electrodynamics³⁰. However we numerically verify that the solutions we find satisfy the original 2nd order equation, so that the runaway solutions are indeed pathologies of the 2nd order equation.

5 Information recovery

We would like to determine our black hole microstate from the asymptotic measurements. In other words, we would like to determine the spin vector s of the SYK pure state $|B_s(l)\rangle$.

To do this we imagine doing the following “experiment”. At time $t = 0$ we couple the SYK system to a bath using a certain coupling of our choice. In the previous section, in both models (a) and (b), we found that in a certain range of the coupling parameters there exist asymptotic solutions and that they carry an imprint of the spin vector s . In the following we will investigate whether this imprint is enough to determine the spin vector s entirely. We will consider models (a) and (b) in turn.

5.1 Model (a): partial evaporation

In this case the SYK system is coupled to the bath through the operator $\hat{g}_1 \mathcal{O}_1^{\{s'\}}$. We will consider \hat{g}_1 and spin s' as the coupling parameters, which we imagine being able to choose freely.³¹

We first show that the existence of a well defined asymptotic solution is ensured if we fix \hat{g}_1 as follows

$$\hat{g}_1 = c_1 \frac{1}{\sqrt{\beta J}}, \quad (103)$$

where c_1 is any fixed number satisfying

$$c_1 \ll 4\pi \sqrt{\frac{\alpha_s}{n_f}}. \quad (104)$$

Proof: To show this, note that the effective IR coupling, g or \tilde{g} , is given in terms of the coupling parameters \hat{g}_1 and s' by (see (11), (27) and (68))

$$\tilde{g} = g \sqrt{\frac{n_f}{2\alpha_s}}, \quad g = \frac{\hat{g}_1}{\sqrt{4\pi}} \cos \theta, \quad \cos \theta = s' \cdot s \equiv \frac{1}{N/2} \sum_{i=1}^{N/2} s'_i s_i \quad (105)$$

(103) implies that

$$\frac{\tilde{g}^2}{2\pi/(\beta J)} = \left(\frac{c_1}{4\pi \sqrt{\alpha_s/n_f}} \right)^2 \cos^2 \theta \ll \cos^2 \theta \ll 1 \quad (106)$$

³⁰We are grateful to R. Loganayagam and Suvrat Raju for raising this point.

³¹We will come back to this point shortly. See Section 5.3.

where in the penultimate step we have used (104). The final inequality ensures that bounds such as (71) or (78) are satisfied which ensures the existence of a well-defined asymptotic solution. Note that it is enough to fix \hat{g}_1 as above; the bound (106) is satisfied irrespective of what s' is. [QED]

Once the existence of a well-defined asymptotic solution is ensured in this way, we would like to ask whether the asymptotic solution retains some information about the original black hole microstate $|B_s(l)\rangle$. It is easy to see that the asymptotic energy (80), given by

$$E_\infty = N\alpha_s J \frac{1}{2} \left(\frac{2\pi}{\beta J} - \tilde{g}^2 \right)^2 \quad (107)$$

does retain such information, since by measuring it, we can determine $(\tilde{g})^2$ and running through the maps in (105) and using the fixed value of \hat{g}_1 in (103) and (104), we can determine square of the inner product $(s' \cdot s)^2$. We have imagined here that the spin s' is part of the preparation of the experiment, which we know and can tune (see Section 5.3). For any given choice of s' , the quantity $(s' \cdot s)^2$ carries a rather small amount of information about the spin vector s , which we are interested in. However by repeating the experiment for $\binom{N/2}{2}$ distinct choices of the spin vector s' , say, $s' = s^{(\alpha)}$, $\alpha = 1, 2, \dots, \binom{N/2}{2}$, then one can determine the spin s up to a sign. This is explained in detail in Appendix E.

We now turn to Model (b). We will see here that we can determine the spin vector s uniquely.

5.2 Model (b): complete evaporation

Recall that in this model we use the mixed coupling

$$\hat{g}_1 \mathcal{O}_1^{\{s'\}} + \hat{g}_2 \mathcal{O}_2^{\{s', s'\}}, \quad (108)$$

which is characterized by the data $\{\hat{g}_1, \hat{g}_2, s'\}$. The relation to the IR data is given by

$$g = \hat{g}_1 \frac{\cos \theta}{\sqrt{4\pi}}, \quad g' = -\hat{g}_2 \left(\frac{\cos \theta}{\sqrt{4\pi}} \right)^2, \quad \cos \theta = s' \cdot s \quad (109)$$

As in the previous subsection, we begin by examining the constraint on the couplings coming from the requirement of existence of a well-defined asymptotic solution. In model (a), it was given by an upper bound on g or \tilde{g} . In model (b), it is given by the coloured region of the $g - g'$ plane, as explained in Figure 16. The algorithm here is divided into two steps: 1) finding the spin s up to overall sign and 2) then fixing the sign.

Keeping in mind the different scaling of the two axes with respect to $\sqrt{\beta J}$ we fix the UV parameters as

$$\hat{g}_1 = \frac{c_1}{\sqrt{\beta J}}, \quad \hat{g}_2 = c_2 \sqrt{\beta J} \quad (110)$$

where c_1, c_2 are $O(1)$ numbers ensuring that g, g' always remain within the red region near the origin in Figure 16. The solution in the red region remains a black hole and the asymptotic energy (Schwarzian) is a function of g and g' . From the energy one can recover the inner product $(s \cdot s')^2$ numerically or analytically in perturbation theory using³²

$$E_{sch} = N \frac{\alpha_s}{J} \frac{a^2}{2}, \quad a = \left(\frac{2\pi}{\beta} - \tilde{g}^2 - \frac{\pi^2}{3\beta^2} \tilde{g}'^2 \right). \quad (111)$$

³²This expression for a can be easily derived by combining the results of equations (77) and (200).

Repeating the experiment for $\binom{N/2}{2}$ distinct choices of the spin vector s' , just as in Model (a), we can recover the initial spin s up to a sign³³. This completes the first step.

In the 2nd step, we fix c_1 and c_2 such that if $\cos\theta = 1$, then the point (g, g') would lie in the green region. Here we will choose the values

$$g = 0.04, g' = 4 \implies c_1 = 0.04\sqrt{4\pi\beta J}, c_2 = -\frac{16\pi}{\sqrt{\beta J}} \quad (112)$$

which we know lie in the green region. Now we take either of 2 possible signs ($s' = \pm s$) and run our experiment with the above values of the UV parameters. If the late time solution oscillates around $\phi_{eq} = 2\log\left(\frac{g}{2g'}\right)$, then we know that it is the correct sign. If on the other hand we find some other behaviour, then we know that the other sign is the correct one. Thus we have determined the spin s completely. Therefore we can determine the spin s completely by doing $O(N^2)$ experiments. The polynomial dependence in N has already been remarked on in point 3 of Section 1.

5.3 Choice of s'

As we explained above, the low energy experiments performed at asymptotic times can measure the IR couplings g and g' . In the protocol described above, we have assumed that we can freely choose the UV data, in particular we can choose the spin s' characterizing the SYK operators which couple to the bath at $t = 0$. It is important to note that this requires access to microscopic physics which goes beyond the low energy approximation. This should be contrasted with the asymptotic measurement of the energy (for Model (a)) or the frequency of the stable oscillation (for Model (b)) which can be expressed in terms of the Schwarzian mode. The important point is that the distinction between different $|B_s(t)\rangle$ states cannot be made by operators built out of the Schwarzian mode, *i.e.* the “boundary graviton”. In our construction of the SYK-bath coupling, we have crucially used the KM operator $\mathcal{O}_1^{s'}$ which can make such a distinction among the various black hole microstates. As has been discussed in the literature, such operators cannot be described purely in terms of the boundary graviton, but possibly requires non-local constructions in the bulk (see, e.g. [66, 67], [43, 55, 68]). Our ability to choose such couplings to the bath is to be understood in terms of some such bulk construction; we hope to come back to this important issue in detail in the future.

6 Two-point function of fluctuations

Until now, we have only focused on the leading large- N solution. Now we also look at the two-point function $\langle\delta\phi_c(t)\delta\phi_c(t')\rangle$, which are suppressed in N . Formally one can rewrite (59) as

$$\mathcal{D}_t \cdot \delta\phi_c = \frac{1}{2}\eta(t),$$

where \mathcal{D} is the integro-differential operator in (59). To find the two-point function of $\delta\phi_c$, one needs to invert this operator

$$\langle\delta\phi_c(t)\delta\phi_c(t')\rangle = \frac{1}{4}\mathcal{D}_t^{-1}\mathcal{D}_{t'}^{-1}\langle\eta(t)\eta(t')\rangle. \quad (113)$$

³³Note that we did not really need Model (b), for this Model (a) was sufficient.

In general this is hard because of two complications – firstly it involves an integral and secondly it is a function of both $t - t'$ and $t + t'$. Since the classical solution in the two models 4.1 and 4.2 are starkly different, we compute the 2-point functions in these models separately.

6.1 Model (a)

In model (a) 4.1, the classical solution reaches another equilibrium corresponding to a smaller black hole. At late times the solution behaves as $\phi(t) = -at + \dots$, which allows us to self-consistently drop the integrals in the Langevin equation (59). Therefore at late times, equation (59) essentially becomes

$$\frac{\alpha_s}{J} \delta \ddot{\phi}_c(t) = \frac{1}{2} \eta(t),$$

or equivalently the differential operator simply reads

$$\mathcal{D}_t = \frac{\alpha_s}{J} \partial_t^2.$$

Now inversion is achieved trivially by integrating twice with respect to t and t' . The two-point function at late times ($t \gg a^{-1}$) is given in terms of an integral

$$\begin{aligned} \langle \delta \phi_c(t) \delta \phi_c(t') \rangle = e^{-a(t+t')/2} & \left\{ -\frac{2C}{\pi} \int_{-\Lambda}^{\Lambda} \frac{dk e^{ik(t-t')}}{k(k^2 + a^2/4)^2} \coth(2kL) \right. \\ & \left. + \frac{C}{4\pi} \int_{-\Lambda}^{\Lambda} \frac{dk e^{ik(t+t')}}{k(k^2 + a^2/4)^4} \left[\frac{a^4}{2} - 12a^2k^2 + 8k^4 - i(16ak^3 - 4a^3k) \right] \operatorname{csch}(2kL) \right\}, \end{aligned} \quad (114)$$

where $C = 2n_f g^2 \left(\frac{J^2}{2\alpha_s} \right)^2$. This is UV finite unlike the noise correlator (54) and therefore we can take the cutoff $\Lambda \rightarrow \infty$. Then one can evaluate this integral and the full form of the 2-point function is given by (207) in the appendix F. In particular the equal-time correlator ($t = t' \gg a^{-1}$) reads

$$\langle \delta \phi_c(t) \delta \phi_c(t) \rangle = e^{-at} \left[\frac{16C}{a^4 L} t + \text{constant} + O(e^{-\pi t/L}) + O(e^{-at}) \right]. \quad (115)$$

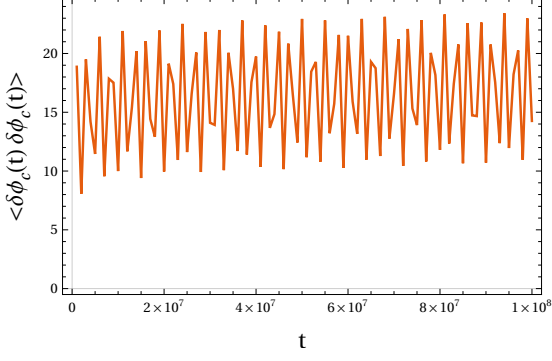
The diffusion constant appears in the Einstein-Smoluchowski form (see [69] for example) in terms of the effective³⁴ bath temperature $(4L)^{-1}$. In a similar fashion one can also evaluate the 2-point function for the energy E_{Δ} defined in (65).

6.2 Model (b)

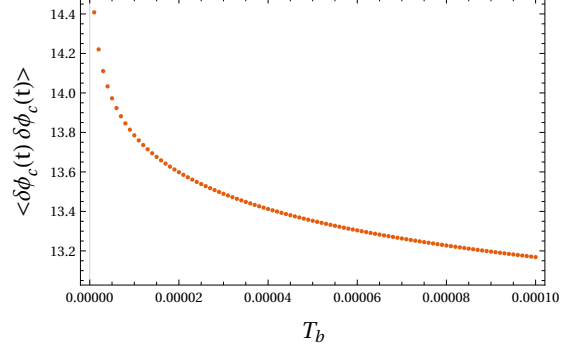
In model (b) 4.2, the final geometry is horizonless. To get rid of the integral involving fluctuation $\delta \phi_c$ in (59), we take one time more derivative. The third order equation with time-dependent coupling reads

$$\begin{aligned} \delta \ddot{\phi}_c(t) - \delta \ddot{\phi}_c(t) & \left\{ \frac{F''(\phi(t))}{F'(\phi(t))} \dot{\phi}(t) + \frac{\dot{g}(t)}{g(t)} \right\} + \left\{ V''(\phi(t)) - \frac{Jn_f}{\alpha_s} g(t) F''(\phi(t)) \int_0^t dt' g(t') F(\phi(t')) \right\} \delta \dot{\phi}_c(t) \\ + \left[V'''(\phi(t)) \dot{\phi}(t) - \left\{ \frac{F''(\phi(t))}{F'(\phi(t))} \dot{\phi}(t) + \frac{\dot{g}(t)}{g(t)} \right\} V''(\phi(t)) - \frac{Jn_f}{\alpha_s} g(t) \right. & \left. \left\{ F'''(\phi(t)) \dot{\phi}(t) \int_0^t dt' g(t') F(\phi(t')) \right\} \right] \end{aligned}$$

³⁴We use the term “effective” temperature because the bath is in a pure state in which the late time correlators behave as thermal correlators at this temperature.



(a) Fixed bath temperature $T_b = 2.5 \times 10^{-6}$



(b) Fixed time $t = 10^8$

Figure 17: We plot the equal-time 2-point function $\langle \delta\phi_c(t)\delta\phi_c(t) \rangle$ by evaluating (123) numerically. In the left panel we plot it as a function of time t at fixed effective bath temperature $T_b = (4L)^{-1} = 2.5 \times 10^{-6}$. In the right panel we plot it as a function of effective bath temperature T_b at time $t = 10^8 \gg t_{max} \approx 10^5$. The temperature dependence is clearly not linear as in the Einstein-Smoluchowski relation. Here $J = 1, \beta = 1000\pi, n_f = 0.01, g = 0.04, g' = 4$ and $t_{max} = 30\beta \approx 10^5$.

$$\begin{aligned}
& +F''(\phi(t))g(t)F(\phi(t)) + g(t)(F'(\phi(t)))^2 - \frac{(F''(\phi(t)))^2}{F'(\phi(t))}\dot{\phi}(t) \int_0^t dt' g(t')F(\phi(t')) \Big\} \delta\phi_c(t) \\
& = \frac{J}{2\alpha_s}\dot{\eta}(t) - \frac{J}{2\alpha_s} \left\{ \frac{F''(\phi(t))}{F'(\phi(t))}\dot{\phi}(t) + \frac{\dot{g}(t)}{g(t)} \right\} \eta(t). \tag{116}
\end{aligned}$$

Now we make a technical simplification, namely that the classical solution at late times after quench sits at the bottom of the potential (101), which we call ϕ_m . This is equivalent to putting $c_1 = c_2 = 0$ in (98) and therefore $\dot{\phi}_m = 0$. Plugging in this solution at late times after quench (94), the 3rd order equation reads

$$\begin{aligned}
& \delta\ddot{\phi}_c(t) + \frac{1}{2t}\delta\ddot{\phi}_c(t) + \left\{ V''(\phi_m) - \frac{2}{\alpha_s}\eta_f g^2 J t_{max} F''(\phi_m)F(\phi_m) \right\} \delta\dot{\phi}_c(t) \\
& - \frac{1}{t} \left[\frac{n_f}{\alpha_s} g^2 J t_{max} \left\{ F''(\phi_m)F(\phi_m) + (F'(\phi_m))^2 \right\} - \frac{1}{2}V''(\phi(t)) \right] \delta\phi_c(t) = \frac{J}{\alpha_s} \left\{ \frac{1}{2}\dot{\eta}(t) + \frac{1}{4t}\eta(t) \right\}. \tag{117}
\end{aligned}$$

At very late times we can further drop the $1/t$ terms, then we are only left with

$$\delta\ddot{\phi}_c + \omega^2 \delta\phi_c = \frac{J}{2\alpha_s} \dot{\eta} \quad \xrightarrow{\text{integrate}} \quad \delta\dot{\phi}_c + \omega^2 \delta\phi_c = \frac{J}{2\alpha_s} \eta, \tag{118}$$

$$\omega^2 = V''(\phi_m) - \frac{2}{\alpha_s}\eta_f g^2 J t_{max} F''(\phi_m)F(\phi_m). \tag{119}$$

The fluctuation correlation can now be calculated in terms of the noise correlation as

$$\begin{aligned}
\langle \delta\phi_c(t)\delta\phi_c(t') \rangle & = \left(\frac{J}{2\alpha_s} \right)^2 \int_0^\infty dt_1 \int_0^\infty dt_2 G_R(t, t_1) G_R(t', t_2) \langle \eta(t_1) \eta(t_2) \rangle \\
& = \left(\frac{J}{2\alpha_s \omega} \right)^2 \int_0^t dt_1 \int_0^{t'} dt_2 \sin[\omega(t-t_1)] \sin[\omega(t'-t_2)] \langle \eta(t_1) \eta(t_2) \rangle,
\end{aligned} \tag{120}$$

where we have used the retarded Green's function

$$G_R(t-t') = \theta(t-t') \frac{\sin[\omega(t-t')]}{\omega}. \tag{121}$$

We already know the noise 2-point function (54)

$$\langle \eta(t_1) \eta(t_2) \rangle = -2 n_f g(t_1) F'(\phi(t_1)) K(t_1, t_2) g(t_2) F'(\phi(t_2)) \approx -2 \frac{n_f g^2 t_{max}}{\sqrt{t_1} \sqrt{t_2}} F'(\phi_{min})^2 K(t_1, t_2), \quad (122)$$

where in the right most expression we have put the classical solution $\phi = \phi_{min}$ at late times. Using the integral form of the kernel (42), this allows us to express the 2-point function as the following integral

$$\langle \delta\phi_c(t) \delta\phi_c(t') \rangle = \frac{n_f t_{max}}{\pi} \left(\frac{JgF'(\phi_m)}{\alpha_s \omega} \right)^2 \int_0^\Lambda \frac{dk}{k} \left\{ f_c(k, t) f_c(k, t') \tanh(kL) + f_s(k, t) f_s(k, t') \coth(kL) \right\}, \quad (123)$$

where

$$f_s(k, t) = \int_0^t dt' \sin[\omega(t-t')] \frac{\sin(kt')}{\sqrt{t'}} = \sqrt{\frac{\pi}{2}} \frac{\sin(\omega t) S\left(\sqrt{\frac{2}{\pi}} \sqrt{t(k+\omega)}\right) + \cos(\omega t) C\left(\sqrt{\frac{2}{\pi}} \sqrt{t(k+\omega)}\right)}{\sqrt{k+\omega}} + \sqrt{\frac{\pi}{2}} \frac{\sin(\omega t) S\left(\sqrt{\frac{2}{\pi}} \sqrt{t(k-\omega)}\right) - \cos(\omega t) C\left(\sqrt{\frac{2}{\pi}} \sqrt{t(k-\omega)}\right)}{\sqrt{k-\omega}}, \quad (124)$$

$$f_c(k, t) = \int_0^t dt' \sin[\omega(t-t')] \frac{\cos(kt')}{\sqrt{t'}} = \sqrt{\frac{\pi}{2}} \frac{\sin(\omega t) C\left(\sqrt{\frac{2}{\pi}} \sqrt{t(k+\omega)}\right) - \cos(\omega t) S\left(\sqrt{\frac{2}{\pi}} \sqrt{t(k+\omega)}\right)}{\sqrt{k+\omega}} + \sqrt{\frac{\pi}{2}} \frac{\sin(\omega t) C\left(\sqrt{\frac{2}{\pi}} \sqrt{t(k-\omega)}\right) + \cos(\omega t) S\left(\sqrt{\frac{2}{\pi}} \sqrt{t(k-\omega)}\right)}{\sqrt{k-\omega}}, \quad (125)$$

with the Fresnel integrals defined as

$$S(z) = \int_0^z \sin(\pi x^2/2) dx, \quad C(z) = \int_0^z \cos(\pi x^2/2) dx. \quad (126)$$

This is UV finite unlike the noise correlator (54) and therefore we can take the cutoff $\Lambda \rightarrow \infty$ in (123).

In Figure 17 we plot the equal-time correlation function $\langle \delta\phi_c(t) \delta\phi_c(t) \rangle$, both as a function of time at fixed L and also a function of L at fixed time. For this we have to evaluate the integral (123) numerically. As is evident from the graph 17b, the temperature dependence here is not linear as in the Einstein-Smoluchowski relation. Further the time-dependence has oscillatory behaviour as is characteristic of Brownian motion in a bounded potential (see Figure 13). For Brownian motion in a harmonic potential, which is exactly soluble, the time dependence of equal time 2-point function is oscillatory [70].

7 Diagnostics of black hole evaporation

Since our discussion of the SYK model coupled to the bath is always in a regime described by the Schwarzian mode, there is a direct correspondence between the SYK dynamics and black hole dynamics. In Model (a) (Section 4.1), the solutions which at late times behave as $\phi(t) = -at + \dots$, correspond to black hole geometries with a smaller mass. Model (b) (Section 4.2) consists of solution in which $\dot{f}(t) = e^{\phi(t)}$ remains finite and bounded at all times and they correspond to non-black hole geometries. In this section we make these statements a bit more precise. We can explicitly see the phenomenon of black hole evaporation, in various ways:

7.1 Energy loss

In Model (a) we are able to explicitly calculate the Schwarzian (63) and E_Δ (65). In Figure 5 we plotted both Schwarzian and E_Δ as a function of time and found that they decrease with time. While the two energies disagree at intermediate times they agree at late times, when equilibrium is reached. The total loss of energy depends on the coupling g^2 . Note that by tuning g^2 to be arbitrarily close to its critical value, we can have an asymptotic black hole solution which is arbitrarily small; thus, using our set-up we can potentially explore questions related to information loss, while always remaining within weak coupling.

In Model (b), we found for the fixed coupling parameters g and g' , the energies ((63) or (65)) keep growing in magnitude Figure 11, and our solution breaks down at a timescale t_* given by (93). For this reason we did a quench (94), after which both the energies are bounded (see Figure 14). In particular E_Δ , which is the more appropriate energy in this scenario, has a well-defined asymptotic form (102) at late times which is smaller than the initial energy, as is evident from Figure 14b.

7.2 Existence and location of the horizon

In this subsection, we determine whether the solutions we found in Models (a) and (b) correspond to geometries with a horizon or not. The details of how to do it are discussed in Appendix G.1, where we find that for a (future) horizon to exist, in the limit $t \rightarrow \infty$, we must have that $\dot{f}(t) \rightarrow 0$ and that $f(t)$ reaches a finite value \hat{t}_H , which demarcates the point where the horizon meets the boundary $\hat{z} = 0$.

As noted in that Appendix, the above condition is invariant under an $SL(2, R)$ transformation of $f(t)$. We can therefore determine the above condition in any given $SL(2, R)$ gauge, in particular, the one we already used in fixing one of the initial conditions $\dot{\phi}(0) = 0 = \ddot{f}(0)$ for solving the classical equation (60) and choice of the Lagrange multiplier (see footnote 14) in arriving to the Liouville action (9), together with $f(0) = 0$. We determine $f(t)$ from a solution for $\phi(t)$ as follows

$$\dot{f}(t) = e^{\phi(t)}, \quad f(t) = \int_0^t dt' e^{\phi(t')}. \quad (127)$$

Model (a) Analytic solution In (75), (77), an analytic solution is presented in a perturbation theory in the coupling g . It is easy to see from there that the condition for existence of a future horizon is satisfied since

$$\begin{aligned} \dot{f} &= \exp[\phi(t)] \xrightarrow{t \rightarrow \infty} \exp[-at] \rightarrow 0, \quad a = \left(\frac{2\pi}{\beta J} - \tilde{g}^2 \right) \\ \hat{t}_H = f(t) &\xrightarrow{t \rightarrow \infty} \int_0^\infty dt' e^{-at} = \frac{1}{\frac{2\pi}{\beta J} - \tilde{g}^2} < \infty. \end{aligned} \quad (128)$$

Note that the second line evaluates the coordinate of the endpoint of the horizon $\hat{t}_H = f(\infty)$ (which is the same as the endpoint of the boundary curve, see the detailed discussion in Appendix G.1). Note that as \tilde{g} increases, the location of the endpoint of the horizon rises, that is, the horizon shifts to the future. The perturbative result indicates that $\hat{t}_H \rightarrow \infty$, i.e. the horizon disappears when $\tilde{g}^2 = \frac{2\pi}{\beta J}$.

Numerical solution The analytic solutions are perturbative. In Section 4.1.1, we discussed numerical solutions which do not take recourse to perturbation theory. Based on the results there, we present in

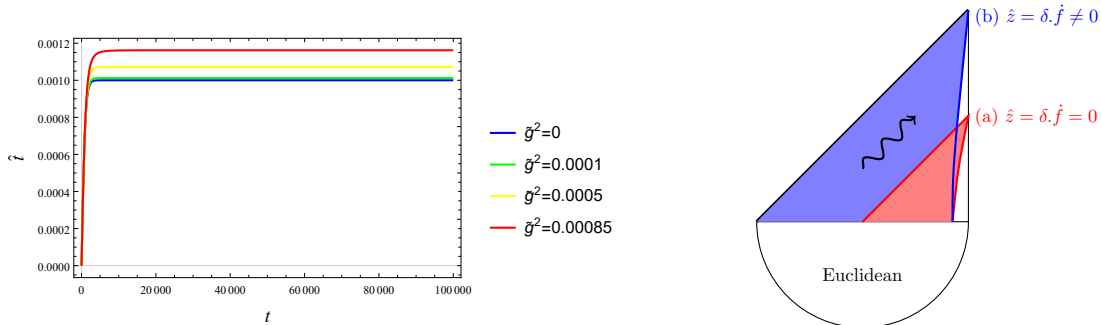


Figure 18: (Left) Bulk time $\hat{t} = f(t)$ for various strengths of single relevant interaction in model (a). Note that this comparison makes sense only in a fixed gauge. Numerics done for $\beta = 1000\pi, J = 1$. (Right) The top half portrays Poincare patch for $\hat{t} \geq 0$. In model (a), the red curve hits $\hat{z} = 0$ at a finite bulk time, so any signal after that will not be received by the boundary observer. On the other hand in model (b) the blue curve never hits $\hat{z} = 0$ and therefore covers the full Poincare patch. This corresponds to no horizon.

Figure 18 the result for $f(t)$. We find that the results (shown in from Figure 18) are in agreement with the analytic findings, namely that $\hat{t}_H = f(t)$ asymptotes to a finite value, and that as we increase the coupling \tilde{g}^2 , the horizon meets the boundary at larger and larger times \hat{t} , i.e. the horizon shifts to the future. We stress again that this comparison makes sense only in a given fixed gauge.

The spacetime diagram for Model (a) is presented on the right panel of Figure 18, which falls in the ($t > 0$ portion of) class (B) of the diagrams Figure 25 and Figure 26.

This model, therefore, represents a final black hole of lower energy (80) than the initial energy of the microstate. We will say more on the final state in Section 8.3.2.

Model (b) Analytic solution The late time (post-quench) analytic solution in this case is given by (96), (98). Clearly $\dot{f}(t) \not\rightarrow \infty$, as $t \rightarrow \infty$. Hence the solution corresponds to a geometry without a horizon. The same result is supported by the numerical calculations (see Section 4.2.2).

The spacetime diagram for Model (b) is presented on the right panel of Figure 18, which falls in the ($t > 0$ portion of) class (A) of the diagrams Figure 25 and Figure 26.

The final geometry (208), for both Models (a) and (b), is presented in Section 8.3.

7.3 Radiation into the bath

In the first scenario, as shown above in Section 7.1, the system energy decreases. Since the total energy of the system and bath is constant, it can be inferred that the energy has gone into the bath. In our description of the dynamics (see (34), (36)) since the bath degrees of freedom have been integrated, the above inference is indirect. In order to directly compute the radiation into the bath, one can compute the expectation value of the energy flux $T_{xt}^{\text{bath}}(x, t) = \sum_{i=1}^{N_f} \frac{1}{2} \partial_x \Phi_i \partial_t \Phi_i(x, t)$ at an interior point $x > 0$ of the bath at time t . This can be done by inserting the operator T_{xt}^{bath} , instead of the system operator $O(t)$, in (30). It is easy to see that this quantity is zero in the decoupled case; once the coupling is switched on,

it can be seen from perturbative calculations, that the energy flux turns non-zero and it moves towards $x \rightarrow \infty$ with the speed of light; in other words, the system emits a radiation of energy into the bath. More generally, it would be interesting to understand the time dependence of bath correlation functions and entanglement properties by treating the bath as the open system obtained after tracing over the SYK.

8 Discussion

8.1 Comments on thermalization and comparison with other works

As mentioned earlier, the issue of thermalization in the SYK + bath model has been discussed before, in particular in [38] and [39]. In these papers, the analysis is at large N , but not restricted to large J , which necessitates the use of the bilocal variable $G(t_1, t_2)$ (the description in terms of the Schwarzian or the Liouville mode $\phi(t)$ is available only at large J) It is argued in these papers that the SYK + bath system asymptotically thermalizes to the bath temperature. The argument is that the bilocal variable G is essentially the two-point of the fermions; thus, the classical evolution of G represents the large N time-evolution of the two-point function. Assuming that the two-point function satisfies the fluctuation-dissipation theorem, applying it to its asymptotic form of G one can determine the asymptotic temperature, which is found equal to the bath temperature.

In our paper, we find something ostensibly different; the classical equation of motion of the Liouville field $\phi(t)$ is independent of the bath ‘temperature’³⁵ $T_b = \frac{1}{4L}$, so the asymptotic solution for $\phi(t)$ does not see the bath temperature at all (this is true in both of our Models (a) and (b)). The difference is not unwarranted, however. As already mentioned, the classical quantity of interest in [38, 39], is itself a *two-point* function. It is well-known, e.g. from the Caldeira-Leggett model of an oscillator (the “system”) + bath (see [60, 65]), that the classical motion of the system, in particular its equilibrium position, is independent of the bath temperature. It is the equilibrium *two-point function* of the system which gives the bath temperature. This turns out to be true in our work as well. Both in Models (a) and (b), although the classical motion of the Liouville field, given by $\phi_c(t)$, does not see the bath temperature, two point function described in Section 6, are sensitive to the bath temperature. In Model (a) the two-point function actually satisfies a version of the Einstein-Smoluchowski relation, which can be used to identify the equilibrium temperature with the bath temperature. Model (b) is more non-trivial, however. Here the two-point function is not proportional to the bath temperature. This can perhaps be attributed to the fact that the solution investigated in this model is non-perturbative in the coupling (see Figure 16 and Section 4.3), and is outside of the linear response regime, which is necessary for the naive version of the fluctuation-dissipation theorem.³⁶

³⁵see comments below (23)

³⁶We do not rule out some modified FDT relation using which one can still read off the equilibrium temperature from the two-point function; this is an interesting issue which we wish to come back to.

8.2 Some comments on black hole entropy

We might wonder what the dynamical solutions computed in this paper imply for the time evolution of entanglement entropy (EE). This question can be addressed by considering the so-called purity of the time-evolved state. Let us start from the factorized state

$$|\chi_0\rangle = |\widetilde{B_s(l)}\rangle \otimes |\widetilde{\Psi_0(L)}\rangle \quad (129)$$

which is the normalized version of (22)³⁷ The Hamiltonian of the full system is of the form

$$H = H_{SYK} + H_{bath} + gH_{int} \quad (130)$$

which can be read off from the total action (26). The time-evolved state, at time T , is given by

$$|\chi_T\rangle = \exp[-iHT] |\chi_0\rangle. \quad (131)$$

Whether the SYK system is entangled with the bath in this state can be found by defining the reduced density matrix³⁸

$$\rho_{SYK}(T) = \text{Tr}_{bath} |\chi_T\rangle \langle \chi_T|, \quad (132)$$

which is the same as (32) except that (132) is correctly normalized with unit trace. As is well known, if the final state of the full system, (131), is factorizable between the SYK system and the bath, then (132) is a pure state density matrix (with only one nonzero eigenvalue $\lambda_1 = 1$ and the rest are zero), which implies that the purity $\gamma \equiv \text{Tr}(\rho_{SYK}(T)^2) = 1$. On the other hand, it is a straightforward exercise in time-dependent perturbation theory to show that, with H_{int} of the form $\mathcal{O}_{SYK} \otimes \mathcal{O}_{bath}$ the factorizable initial state turns non-factorizable. The interaction Hamiltonian causes simultaneous transition to orthogonal states both in the SYK Hilbert space as well as in the bath Hilbert space. Thus, e.g., to first order in g , and for sufficiently short time, the final state is a linear combination of orthogonal factorized states, which itself is not factorizable.³⁹ One can generalize to any order of perturbation theory to show that the final state is not factorizable. This is equivalent to saying that $\rho_{SYK}(T)$ must have multiple non-zero eigenvalues $\lambda_i < 1$, so that the purity is

$$\gamma \equiv \text{Tr}(\rho_{Sch}(T)^2) < 1. \quad (133)$$

Note that this strict inequality is valid at large N since the transition amplitudes discussed above are caused by H_{int} which is proportional to N .

The computation of purity corresponds to computing a path integral along a contour described in Figure 19. At leading order in N , the path integral in the above figure can be computed by solving the

³⁷Note that the norm of $|B_s(l)\rangle$ is $\sqrt{Z_{SYK}(2l)}$. Similarly the norm of $|\Psi_0(L)\rangle$ is $\sqrt{Z_{bath}(4L)}$.

³⁸One could alternatively define a reduced density matrix for the bath $\rho_{bath}(t)$, as in [25], which gives an equivalent measure of entanglement (e.g. the same Renyi entropies) as long as the total state of the system and bath is a pure state.

³⁹One can verify these statements in a simple toy model consisting of two qubits, each with energy levels $\pm E_1, \pm E_2$. Start with a product state e.g. $|++\rangle$ and some interaction Hamiltonian of the form $H_{int} = g\sigma_{X,1}\sigma_{X,2}$. For small g , the state immediately becomes mixed, although after a sufficiently long time T , depending on the value of g , it comes back to a product state and the process repeats in a periodic fashion.

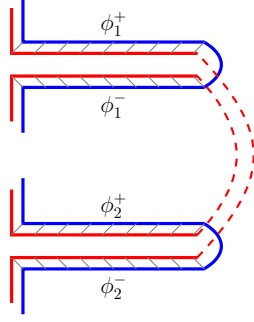


Figure 19: The path integral contour to calculate purity (133). There are two copies of the Schwinger-Keldysh contour (we omit the space direction), denoted by the upper and lower parts of the figure, each of which corresponds to SYK+bath system as in Figure 3. The blue contours refer to the bath which are joined within each copy, representing the partial trace over the bath Hilbert space. The two replicas are joined by the identification (136) shown by the dashed red lines. The fields ϕ_r^\pm , $r = 1, 2$, denote the Schwarzian path integral variables over the two replica copies.

saddle-point equations (cf. (38), (39))

$$\frac{\alpha_s}{J} \left[\ddot{\phi}_r^+(t) + V'(\phi_r^+(t)) \right] + in_f g^2 \left[F'(\phi_r^+(t)) \int_0^T dt' \kappa_{++}^S(t, t') F(\phi_r^+(t')) + 2F'(\phi_r^+(t)) \int_0^T dt' \kappa_{+-}(t, t') F(\phi_r^-(t')) \right] = 0, \quad (134)$$

$$\frac{\alpha_s}{J} \left[\ddot{\phi}_r^-(t) + V'(\phi_r^-(t)) \right] - in_f g^2 \left[F'(\phi_r^-(t)) \int_0^T dt' \kappa_{--}^S(t, t') F(\phi_r^-(t')) + 2F'(\phi_r^-(t)) \int_0^T dt' F(\phi_r^+(t')) \kappa_{+-}(t', t) \right] = 0, \quad (135)$$

which are to be solved subject to the identification

$$\phi_1^+(T) = \phi_2^-(T), \quad \phi_1^-(T) = \phi_2^+(T). \quad (136)$$

Trivial saddle point: Note that there is a trivial saddle point solution

$$\phi_1^+(t) = \phi_1^-(t) = \phi_2^+(t) = \phi_2^-(t), \quad (137)$$

all equal to the solution $\phi_c(t)$ which satisfies (47). It is easy to see that this solution corresponds to the large N path integral for the disconnected diagram $(\text{Tr } \rho_{\text{SYK}}(T))^2$ which is $1^2 = 1$ ⁴⁰. Thus, if the above saddle point were the only one, we would get the purity $\gamma = 1$.

Nontrivial saddle point: Since we found in (133) that the strict inequality $\gamma < 1$ must be valid at large N , there must be at least one non-trivial saddle point solution besides (137). Such a solution must connect the two replica copies non-trivially, making use of the twisted identifications (136). In the Keldysh notation $\phi_{r,\pm}(t) = \phi_{r,c}(t) \pm \phi_{r,q}(t)$, (136) reads

$$\phi_{1,c}(T) + \phi_{1,q}(T) = \phi_{2,c}(T) - \phi_{2,q}(T), \quad \phi_{1,c}(T) - \phi_{1,q}(T) = \phi_{2,c}(T) + \phi_{2,q}(T). \quad (138)$$

⁴⁰Note that besides the twisted identification (136), the solution (137) also satisfies $\phi_1^+(T) = \phi_1^-(T)$, $\phi_2^+(T) = \phi_2^-(T)$ appropriate to tracing over the system Hilbert space in each replica copy.

If we choose $\phi_{r,q} = 0$, we are immediately forced to the trivial solution (137). For a non-trivial solution, we must have non-zero $\phi_{r,q}$, which cannot be obtained from (45) perturbatively in $\phi_{r,q}$; hence it has to be a non-perturbative solution. Contribution from the non-trivial saddle point to the path integral in Fig 19 will have to be negative, to reduce the purity from 1 which is obtained from the trivial saddle point (137). We hope to come back to this issue in the future.

8.3 The final state

8.3.1 Model (b): the evaporation model

We will first consider model (b) which exhibits complete evaporation.

By the final state, we will imply here the RDM (reduced density matrix) (32) as $T \rightarrow \infty$. In case we are interested in computing expectation values of low energy SYK operators \mathcal{O} which are diagonal in the ϕ -representation, such as ϕ itself, the expectation value (33) involves only diagonal elements of ρ , namely $\langle \phi^+ | \rho | \phi^- \rangle$, with $\phi^+ = \phi^-$. Such diagonal elements are obtained by saddle point solutions ϕ_c of (47), which are described in detail in Section 4. By using large N factorization, expectation values of any function $F[\phi]$ are also given by $F[\phi_c]$. e.g. we can find the asymptotic value of $\dot{f}(t) = \exp[\phi(t)]$ using this argument.

Using the above arguments, the asymptotic form of the Schwarzian mode $f(t)$ for Model (b) is given by (96) and (98):

$$\dot{f} = \exp\{\phi\}, \quad \phi = \text{constant} + c_1 \sin \Omega t + c_2 \cos \Omega t, \quad \Omega = \left(\frac{8\alpha_s g^2 + n_f t_{max} g^4}{16\alpha_s g^2} \right)^{1/2}. \quad (139)$$

In the boundary dual, $f(t)$ represents a Diff/SL(2,R) transformation U_f of the ground state of the approximately conformal SYK theory⁴¹. Hence $|\text{final}_{\text{SYK}}\rangle = U_f |0\rangle$.⁴² It is possible to write the unitary transformation U_f explicitly, however, it is more useful to characterize the state $U_f |0\rangle$ in terms of expectation values of various operators. Thus, the fermion two-point function in such a state will be given by

$$G(t_1, t_2) = \langle 0 | U_f^\dagger \psi_i(t_1) \psi_i(t_2) U_f | 0 \rangle = C \frac{(f'(t_1) f'(t_2))^\Delta}{(f(t_1) - f(t_2))^{2\Delta}} \quad (140)$$

where the last equality follows by applying the conformal transformation $f(t)$ to $\langle 0 | \psi_i(t_1) \psi_i(t_2) | 0 \rangle = C/(t_1 - t_2)^{2\Delta}$. (140) can be explicitly evaluated by using the expression for $f(t)$ from (139).

The final geometry after evaporation

As we discussed in Section 7.2, the geometry in this case does not have a horizon. The explicit geometry (208), at large times, can be obtained from (139) which gives $\dot{f}(t) = e^{\phi(t)}$:

$$ds^2 = \frac{dz^2}{z^2} - \frac{dt^2}{z^2} \left(1 + \frac{z^2}{2} g(t) \right)^2,$$

⁴¹These statements are the two-dimensional counterparts of a Brown-Henneaux diffeomorphism of AdS₃ which correspond to a conformal transformation of the vacuum of the dual CFT₂. The difference in the lower dimensional case is that the IR fixed point at $1/J = 0$ is singular, hence one works with small but non-zero $1/J$.

⁴²Note that the initial SYK state, in a low energy projection, is given by, $|B_s(l)\rangle \approx U_{f_0} |0\rangle$, where $f_0(t) = \pi/\beta \tanh(\pi t/\beta)$ is the Diff element corresponding to a thermal transformation.

$$g(t) = \{f(t), t\} = -\frac{1}{2}(c_1\Omega \cos(\Omega t) - c_2\Omega \sin(\Omega t))^2 - c_1\Omega^2 \sin(\Omega t) - c_2\Omega^2 \cos(\Omega t). \quad (141)$$

Note that if the assumption about the final state being a product state is not true, then the final state of the SYK will be described as an RDM as in the above discussion and the asymptotic form of $f(t)$ should be interpreted as in Model (a) (see below).

8.3.2 Model (a): incomplete evaporation

As described in Section 7.2, in this model the final geometry has a horizon, whose location (in a fixed gauge) is given by (128). It represents a black hole with a lower mass.

In the quantum theory, the thermal microstate $|B_s(l)\rangle$, after coupling to the bath, becomes entangled with the bath. Since the final configuration is a black hole, the state is expected to be an entangled state between the bath and the system; for system observables, the state can be represented as a RDM (reduced density matrix) $\rho_{\text{SYK}}(\text{final})$ with nontrivial von Neumann entropy. The final energy (80) as well as the asymptotic form of $f(t) = \int_0^t \exp[\phi(t)]$ obtainable from (79) should be interpreted as the expected values of the corresponding operators, in this RDM $\rho_{\text{SYK}}(\text{final})$.

The fermion two-point function is given by the conformal transformation from (140) where $f(t)$ for Model (a) is to be read off from (128). The final geometry (208) is given by

$$ds^2 = \frac{dz^2}{z^2} - \frac{dt^2}{z^2} \left(1 - \frac{z^2 a^2}{4}\right)^2. \quad (142)$$

The horizon is the null surface $z = 2/a$ which translates to $\hat{t} + \hat{z} = f(\infty) = 0$ (in accordance with Appendix G.1).

Acknowledgements

We would like to thank Soumyadeep Chaudhuri, R Loganayagam, Juan Maldacena, Shiraz Minwalla, Kyriakos Papadodimas, Onkar Parrikar, Suvrat Raju, Subir Sachdev, Ashoke Sen, Ritam Sinha, Nilakash Sorokhaibam, Sandip Trivedi and Neha Wadia for discussions and comments during the course of this work. S.R.W. would like to thank the support of the Infosys Foundation Homi Bhabha Chair at ICTS-TIFR. A.K. and G.M. acknowledge support from the Quantum Space-Time Endowment of the Infosys Science Foundation.

A SYK Operators in the IR

In this section, we will compute the expectation value of the operator

$$\mathcal{O}_m(t) = (-1)^{m+1} J \prod_{j=1}^m \left(\frac{i}{N} \sum_{k=1}^{N/2} s_k^j \psi_{2k-1}(t) \psi_{2k}(t) \right), \quad (143)$$

in a thermal microstate $|B_s(l)\rangle$.

$$\frac{1}{Z} \langle B_s(l) | \mathcal{O}_m(t) | B_s(l) \rangle = (-1)^{m+1} \left(\frac{i}{N} \right)^m J \left(\frac{1}{Z} \langle B_s(l) | \prod_{j=1}^m s_k^j \psi_{2k-1}(t) \psi_{2k}(t) | B_s(l) \rangle \right). \quad (144)$$

Here index k is summed over $k = 1, \dots, N/2$. Let us define $\hat{S}_k = 2i\psi_{2k-1}\psi_{2k}$, such that $\hat{S}_k |B_s\rangle = s_k |B_s\rangle$ where s_k is the k th component of the spin vector s . It is also clear that $\hat{S}_k^2 = \mathbb{I}$. With this

$$\begin{aligned} \frac{1}{Z} \langle B_s(l) | \prod_{j=1}^m s_k^j \psi_{2k-1}(t) \psi_{2k}(t) | B_s(l) \rangle &= \frac{1}{Z} \langle B_s | e^{-lH_0} \prod_{j=1}^m \left(\sum_{k=1}^{N/2} s_k^j \psi_{2k-1}(t) \psi_{2k}(t) e^{-lH_0} \hat{S}_k^2 \right) | B_s \rangle \\ &= \frac{1}{Z} \langle B_s(l) | \prod_{j=1}^m \left(\sum_{k=1}^{N/2} s_k^j s_k \psi_{2k-1}(t) \psi_{2k}(t) \hat{S}_k(il) \right) | B_s(l) \rangle \\ &= (2i)^m \frac{1}{Z} \langle B_s(l) | \prod_{j=1}^m \left(\sum_{k=1}^{N/2} s_k^j s_k \psi_{2k-1}(t) \psi_{2k}(t) \psi_{2k-1}(il) \psi_{2k}(il) \right) | B_s(l) \rangle \\ &= \prod_{j=1}^m \left(2i \sum_{k=1}^{N/2} s_k^j s_k \right) G_\beta(t-il)^2. \end{aligned} \quad (145)$$

The last expression is obtained at large N after the disorder average. With the above result we get

$$\begin{aligned} \frac{1}{Z} \langle B_s(l) | \mathcal{O}_m(t) | B_s(l) \rangle &= -J G_\beta(t-il)^{2m} \prod_{j=1}^m \left(\frac{2}{N} \sum_{k=1}^{N/2} s_k^j s_k \right) \\ &= -J \left(\prod_{j=1}^m \cos(\theta_j) \right) G_\beta(t-il)^{2m}, \end{aligned} \quad (146)$$

where we have defined $\cos(\theta_j) = \frac{2}{N} \sum_{k=1}^{N/2} s_k^j s_k$.

B Effective Action and Feynman-Vernon phase

In this section, we will derive the effective action along the real time piece of the Schwinger-Keldysh contour given in Figure 2, starting from (26) and integrating out the bath fields. The interaction term in the (26) is such that each bath field can be dealt with separately. The effective action for N_f fields can be obtained by multiplying the effective action of one field (obtained by integrating out that one field), by a factor of N_f .

Our model is described by the action (26) on the contour in the Figure 20. The interaction term, coupling the two theories is non-vanishing only along the real time part of the contour. In the euclidean part of the contour, both the theories evolve with their free Hamiltonians. Let us describe the Euclidean part of the contour given in Figure 20, and we will only show the construction of a ket, the construction of the bra follows similarly. In App B.1 we will construct the state at $t = 0$ with Euclidean time evolution from $|B_s\rangle \otimes |B_d\rangle$, in App B.2 we will evolve this state with interactions in real time and in App B.3, we will construct the density matrix $e^{-iHT} \hat{\rho}_{sch} \otimes \hat{\rho}_{bath} e^{iHT}$ and integrate out the bath fields. In AppB.4 we will comment on the UV nature of the effective Feynman-Vernon influence functional and in App B.5 we will discuss the effective Feynman-Vernon influence functional with the bath in a thermal state.

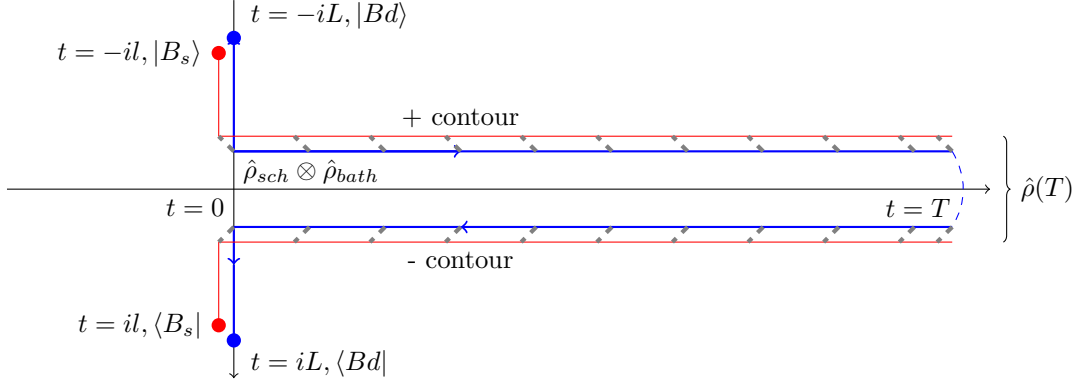


Figure 20: This is the same diagram as Figure 2 with the x direction suppressed. The bath contour is depicted in blue and the SYK path is depicted by red. The blue and red dots on the top depict the kets $|Bd\rangle$ and $|B_s\rangle$ respectively and on the bottom depicts the bras $\langle Bd|$ and $\langle B_s|$ respectively. The state at $t = 0$ is $\hat{\rho}_{sch} \otimes \hat{\rho}_{bath}$ and the state at $t = T$ is the reduced density matrix defined as $\hat{\rho}(T) = \text{Tr}_{bath} [e^{-iHT} \hat{\rho}_{sch} \otimes \hat{\rho}_{bath} e^{iHT}]$. The tracing out of the bath fields is depicted by the blue dashed line connected the upper and lower bath contour. The + (upper) contour and the - (lower) contour are exactly at $\text{Im}(t) = 0$, the gap in the above figure is only shown for better presentation, the value of real time along both contours is also the same. Hence, to distinguish fields on the upper contour from the fields on the lower contour we add a \pm subscripts on them.

B.1 Euclidean evolution and the initial bath wavefunctional

As stated in the text, the initial bath state is the CC state [45,53] which is obtained by Euclidean evolution of a pure boundary state

$$|\Psi_0(L)\rangle = e^{-LH_{bath}}|Bd\rangle, \quad (147)$$

with the boundary state defined by $\Phi|Bd\rangle = 0$. We will use the convention that the boundary state $|Bd\rangle$ is at the time $t = i\tau = -iL$. The bath state at time $t = 0$ can be formally given by

$$|\Psi_0(L)\rangle = \int D\Phi \Psi_0[\Phi(x)] |\Phi(x)\rangle, \quad (148)$$

with the wavefunctional $\Psi_0[\Phi(x)]$ defined as follows

$$\Psi_0[\Phi(x)] = \int_{\Phi(\tau=-L,x)=0}^{\Phi(\tau=0,x)=\Phi(x)} D\Phi e^{-\int_{-L}^0 d\tau \int_0^\infty dx L_{bath}^E[\Phi(\tau,x)]} = \langle \Phi(x) | \Psi_0(L) \rangle. \quad (149)$$

We can evaluate this path-integral with a saddle point approximation at large N . The bath field lives on a semi-infinite line. Variation of the action leads to the equation of motion $\partial^2\Phi = 0$ with a boundary term $\int d\tau \partial_x\Phi \delta\Phi(\tau,x)|_{x=0}$ at $x = 0$, where we impose Neumann boundary condition $\partial_x\Phi(\tau,x)|_{x=0} = 0$. The expansion of the bath field in momentum modes is

$$\Phi(\tau, x) = \frac{2}{\pi} \int_0^\infty dk \alpha_k(t) \cos(kx). \quad (150)$$

The equation of motion reads

$$(\partial_\tau^2 + \partial_x^2)\Phi(x, \tau) = \frac{2}{\pi} \int_0^\infty dk \cos(kx) [\ddot{\alpha}_k(\tau) - k^2 \alpha_k(\tau)] = 0, \quad (151)$$

with the solution $\alpha_k(\tau) = a(k) \cosh(k\tau) + b(k) \sinh(k\tau)$. Imposing the boundary condition $\Phi(-L, x) = 0$ gives $b(k) = a(k) \coth(kL)$. The on-shell action simply reduces to

$$S = \frac{1}{2} \int_0^\infty dx \Phi(0, x) \dot{\Phi}(0, x) = \frac{1}{\pi} \int_0^\infty k dk \frac{a(k)^2}{\tanh(kL)}. \quad (152)$$

Putting this all together we finally obtain

$$\Psi_0[\Phi(x)] = \Psi_0[a(k)] = \mathcal{N} \exp \left[-\frac{1}{\pi} \int_0^\infty dk \frac{k a(k)^2}{\tanh(kL)} \right], \quad \text{where} \quad \Phi(x) = \frac{2}{\pi} \int_0^\infty dk a(k) \cos(kx). \quad (153)$$

The normalization is proportional to the determinant of quadratic fluctuations around this classical solution. For the corresponding density matrix in the thermal state see (190).

B.2 Real time evolution

At $t \geq 0$ we turn on interactions between the bath and the SYK model, which are in their respective specified initial states. Consider the Lorentzian evolution till time T with the interactions turned on,

$$|\Psi(T)\rangle = e^{-iHT} |B_s(l)\rangle \otimes |\Psi_0(L)\rangle = \int D\tilde{\Phi} d\phi_T \Psi_T[\tilde{\Phi}, \phi_T] |\phi_T, \tilde{\Phi}\rangle, \quad (154)$$

$$\Psi_T[\tilde{\Phi}, \phi_T] = \int_{\phi_0}^{\phi_T} D\phi e^{iS_{Sch}[\phi(t)]} \chi[\tilde{\Phi}(x), \phi(t)], \quad (155)$$

with

$$\chi[\tilde{\Phi}(x), \phi(t)] = \int_{\Phi(x)}^{\tilde{\Phi}(x)} D\Phi \Psi_0[a(k)] \exp \left[i \int_0^T dt \int_0^\infty dx \mathcal{L}_{bath}[\Phi(t, x)] + i \int_0^T dt \mathcal{L}_{int}[\Phi(t, x=0), F(\phi(t))] \right], \quad (156)$$

where the lower boundary condition is $\Phi(x) = 2 \int dk \cos(kx) a(k) / \pi$, $F(\phi(t))$ is defined in (??), and $\phi_0 = 2 \log(\pi/\beta J)$ [43]. Similar expression can be obtained for the bra part $\langle B_s(l) | \otimes \langle \Psi_0(\Phi) | e^{iHT}$.

Comment on coupling

From the point of view of the bath fields, $F(\phi)$ simply acts as an external source. As in the Euclidean evolution we also use saddle point approximation here we will now solve the equations of motion for the field in the presence of non-trivial sources. Here the choice of boundary condition for the bath field at $x = 0$ becomes important. To appreciate this, consider a free scalar field on half-line ($x \geq 0$), with a source localized at the boundary at $x = 0$

$$S_{half} = \int dt \int_{x \geq 0} dx \frac{1}{2} (\partial\Phi)^2 + \int dt J(t) \Phi(t, x=0). \quad (157)$$

Its variation leads to

$$\begin{aligned}\delta S_{half} &= \int_{x \geq 0} d^2x [-\partial^2 \Phi \delta \Phi + \partial_\mu (\partial^\mu \Phi \delta \Phi)] + \int dt J(t) \delta \Phi(x=0) \\ &= \int_{x \geq 0} d^2x (-\partial^2 \Phi) \delta \Phi + \int dt [J(t) + \partial_x \Phi] \delta \Phi(x=0).\end{aligned}\quad (158)$$

To minimize the action, together with the EOM $\partial^2 \Phi = 0$ [43], we impose Neumann boundary condition $J(t) + \partial_x \Phi(t, x=0) = 0$. Our problem is essentially the same with $J(t) = -F(\phi(t))$ but in our case it is no longer a classical source, it is dynamical. The choice of Neumann boundary condition allows for interesting interacting dynamics between $F(\phi(t))$ and the bath field. If we impose Dirichlet boundary condition $\delta \Phi(t, x)|_{x=0} = 0$. Then the bath can be integrated out trivially and is essentially decoupled from the Schwarzian theory. This is essentially driving the dynamics of the system mechanically through the boundary condition. The exchange of energy-momentum at $x = 0$ boundary is quantified by the stress-tensor

$$T_{tx}(t, 0) = \partial_t \Phi \partial_x \Phi(t, 0) = \dot{\Phi}(t, 0) F(t) \quad (\text{Neumann BC}). \quad (159)$$

The Neumann BC allows for exchange of energy-momentum which in general is non-zero. This exchange of energy is necessary for the black hole to evaporate.

Computation of $\chi[\tilde{\Phi}(x), \phi(t)]$ via saddle point

In this subsection, we will simply denote $gF(\phi(t))$ as $F(t)$ to reduce clutter. We will bring back the full notation in the next subsection B.3. To accommodate the modified Neumann boundary condition we have the following mode expansion

$$\Phi(x, t) = \frac{2}{\pi} \int_0^\infty dk \alpha(k, t) \cos(kx) + \frac{2}{\pi} \int_0^\infty dk s(k) F(t) \sin(kx), \quad (160)$$

such that

$$\partial_x \Phi(t, 0) = F(t) \frac{2}{\pi} \int_0^\infty dk k s(k) = s'(0) F(t) = F(t). \quad (161)$$

A function which satisfies this is

$$s(x) = x \exp(-ax^2), \quad a > 0. \quad (162)$$

We have in mind $a \rightarrow \infty$, such that it quickly decays for $x > 0$. For this choice of the shift function

$$s(k) = \int_0^\infty dk \sin(kx) s(x) = \sqrt{\frac{\pi}{2}} \frac{k}{a^{3/2}} e^{-k^2/2a}. \quad (163)$$

Now we evaluate

$$\chi[\tilde{\Phi}(x), \phi(t)] = \int_{\Phi(x)}^{\tilde{\Phi}(x)} D\Phi \Psi_0[a(k)] \exp \left[i \int_0^T dt \int_0^\infty dx \mathcal{L}_{bath}[\Phi(t, x)] + i \int_0^T dt \mathcal{L}_{int}[\Phi(t, x=0), F(t)] \right]. \quad (164)$$

As in the Euclidean part, we evaluate the on-shell action. Lets deal with each term separately. First, just the bath action

$$\int_0^\infty dx \dot{\Phi}^2(x, t) = \frac{2}{\pi} \int_0^\infty dk \left[\dot{\alpha}_k^2(t) + s_k^2 \dot{F}^2(t) + 2\dot{\alpha}_k(t) \dot{F}(t) \frac{1}{a} I(k/\sqrt{a}) \right], \quad (165)$$

where

$$\frac{1}{a} I(k/\sqrt{a}) \equiv \frac{2}{\pi} \int_0^\infty dq \frac{q}{q^2 - k^2} s_q = \frac{1}{a} (1 - 2D_F(k/\sqrt{2a})); \quad D_F(x) = e^{-x^2} \int_0^x dy e^{y^2}. \quad (166)$$

In obtaining this expression, we have used $\int_0^\infty dx \cos(kx) = \frac{1}{2} \text{Re} \int_0^\infty dx \exp(ikx) = \pi \delta(k)$ and $\int_0^\infty dx \sin(kx) = 1/k$. There is a similar expression for $\int_0^\infty dx \Phi'^2(x, t)$. Combining, we get

$$\begin{aligned} S_{bath} &= \frac{1}{2} \int_0^T dt \int_0^\infty dx \left(\dot{\Phi}^2(t, x) - \Phi'^2(t, x) \right) \\ &= \frac{1}{2} \int dt \frac{2}{\pi} \int_0^\infty dk \left[(\dot{\gamma}_k^2(t) - k^2 \gamma_k^2) + (\dot{F}^2(t) - k^2 F^2(t)) \left\{ s_k^2 - \left(\frac{1}{a} I(k/\sqrt{a}) \right)^2 \right\} \right], \end{aligned} \quad (167)$$

where we have completed squares in α_k and defined $\gamma_k = \alpha_k + F(t) \frac{1}{a} I(\frac{k}{\sqrt{a}})$. The interaction term is simple

$$\begin{aligned} S_{int} &= - \int dt \Phi(t, 0) F(t) = - \int dt \frac{2}{\pi} \int dk \alpha_k(t) F(t) \\ &= - \int dt \frac{2}{\pi} \int dk \left[\gamma_k(t) F(t) - \frac{1}{a} I(k/\sqrt{a}) F^2(t) \right] = - \int dt \frac{2}{\pi} \int dk \gamma_k(t) F(t). \end{aligned} \quad (168)$$

The last equality follows because $\int_0^\infty dk I(k/\sqrt{a}) = 0$. Together, we have

$$S_{bath} + S_{int} = \frac{1}{2} \int dt \frac{2}{\pi} \int_0^\infty dk \left[(\dot{\gamma}_k^2(t) - k^2 \gamma_k^2 - 2\gamma_k(t) F(t)) + (\dot{F}^2(t) - k^2 F^2(t)) \left\{ s_k^2 - \left(\frac{1}{a} I(k/\sqrt{a}) \right)^2 \right\} \right]. \quad (169)$$

The last term vanishes in the $a \rightarrow \infty$ limit. Numerical analysis shows that it vanishes even at finite a . Henceforth we will ignore this γ_k independent term. The variation leads to the following equation for the modes γ_k

$$\ddot{\gamma}_k(t) + k^2 \gamma_k + F(t) = 0, \quad (170)$$

with the solution

$$\gamma_k(t) = \gamma_k(0) \cos(kt) + \dot{\gamma}_k(0) \frac{\sin(kt)}{k} - \int_0^t dt' \frac{\sin[k(t-t')]}{k} F(t'). \quad (171)$$

This is better expressed in terms of the initial and final values of the modes $\gamma_k(0) = a_k$ and $\gamma_k(T) = c_k$

$$\begin{aligned} \gamma_k(t) &= a_k A(k, t) + B(k, t) + c_k C(k, t), \\ A(k, t) &= \frac{\sin[k(T-t)]}{\sin(kT)}, \quad C(k, t) = \frac{\sin(kt)}{\sin(kT)}, \\ B(k, t) &= C(k, t) \int_0^T dt' \frac{\sin[k(T-t')]}{k} F(t') - \int_0^t \frac{\sin[k(t-t')]}{k} F(t'). \end{aligned} \quad (172)$$

The on-shell value of the action evaluated on this solution is

$$(S_{bath} + S_{int}) \Big|_{on-shell} = \frac{1}{\pi} \int_0^\infty dk \{ \gamma_k(T) \dot{\gamma}_k(T) - \gamma_k(0) \dot{\gamma}_k(0) \} - \int dt F(t) \frac{1}{\pi} \int_0^\infty dk \gamma_k(t) \quad (173)$$

$$\begin{aligned}
&= \frac{1}{\pi} \int_0^\infty dk \left[-a_k^2 \dot{A}(k, t) + a_k \left\{ c_k \left(\dot{A}(k, t) - \dot{C}(k, t) \right) - \dot{B}(k, t) - \int_0^\infty dt A(k, t) F(t) \right\} \right. \\
&\quad \left. + c_k^2 \dot{C}(k, t) + c_k \left\{ \dot{B}(k, T) - \int_0^\infty dt C(k, t) F(t) \right\} - \int_0^\infty dt B(k, t) F(t) \right]. \quad (174)
\end{aligned}$$

Now integrating wrt to the initial bath wavefunctional $\Psi_0[a(k)]$ gives

$$\begin{aligned}
\chi[c_k, \phi(t)] &= \int \left(\prod_k da_k \right) \Psi_0[\{a_k\}] \int_{\{a_k\}} D\Phi \exp \left[i(S_{bath} + S_{int}) \Big|_{on-shell} \right] \quad (175) \\
&= \mathcal{N} \exp \left[- \int_0^\infty \frac{dk}{\pi} \kappa_1(k) c_k^2 + \int_0^T dt \int_0^\infty \frac{dk}{\pi} \kappa_2(k, t) F(t) c_k + \int_0^T dt \int_0^T dt' F(t) \kappa_3(t, t') F(t') \right],
\end{aligned}$$

where

$$\begin{aligned}
\kappa_1(k) &= k \coth[k(L + iT)], \quad (176) \\
\kappa_2(k, t) &= -2i \operatorname{csch}[k(L + iT)] \sinh[k(L + it)], \\
\kappa_3(t, t') &= \frac{i}{4} - \frac{i}{\pi} \int_0^\infty \frac{dk}{k} \sinh[k(L + it)] \operatorname{csch}[k(L + iT)] \sin[k(T - t')].
\end{aligned}$$

B.3 The Feynman-Vernon influence functional

Now that we have the state $|\Psi(T)\rangle = e^{-iHT} |B_s(l)\rangle \otimes |\Psi_0(L)\rangle$, it is easy to construct the state

$$e^{-iHT} \hat{\rho}_{sch} \otimes \hat{\rho}_{bath} e^{iHT} = \underbrace{|\Psi(T)\rangle}_{+contour} \underbrace{\langle \Psi(T) |}_{-contour}. \quad (177)$$

As indicated we differentiate the fields on the upper contour from those on the lower contour by adding a superscript \pm appropriately.

$$|\Psi(T)\rangle \langle \Psi(T)| = \int Dc_k^+ Dc_k^- d\phi_T^+ d\phi_T^- (\Psi_T[c_k^+, \phi_T^+] \Psi_T[c_k^-, \phi_T^-]^*) (|c_k^+, \phi_T^+\rangle \langle c_k^-, \phi_T^-|), \quad (178)$$

with

$$\Psi_T[c_k^+, \phi_T^+] \Psi_T[c_k^-, \phi_T^-]^* = \int_{\phi_0}^{\phi_T^-} D\phi^- \int_{\phi_0}^{\phi_T^+} D\phi^+ e^{iS_{Sch}[\phi^+(t)]} e^{-iS_{Sch}[\phi^-(t)]} \chi[c_k^+, \phi^+(t)] \chi[c_k^-, \phi^-(t)]^*. \quad (179)$$

Obtaining *RDM* from here is straight forward

$$\hat{\rho}(T) = \int Dc_k d\phi_T^+ d\phi_T^- (\Psi_T[c_k, \phi_T^+] \Psi_T[c_k, \phi_T^-]^*) (|\phi_T^+\rangle \langle \phi_T^-|). \quad (180)$$

Finally we identify the bath field modes on the + and - contours, and integrate.

$$\int Dc_k \Psi_T[c_k, \phi_T^+] \Psi_T[c_k, \phi_T^-]^* = \int_{\phi_0}^{\phi_T^-} D\phi^- \int_{\phi_0}^{\phi_T^+} D\phi^+ e^{iS_{Sch}[\phi^+(t)]} e^{-iS_{Sch}[\phi^-(t)]} \int Dc_k \chi[c_k, \phi^+(t)] \chi[c_k, \phi^-(t)]^*. \quad (181)$$

Let us focus on

$$\begin{aligned}
&\int Dc_k \chi[c_k, \phi^+(t)] \chi[c_k, \phi^-(t)]^* \\
&= |\mathcal{N}|^2 \int \left(\prod_k dc_k \right) \exp \left[- \int_0^\infty c_k^2 (\kappa_1(k) + \kappa_1^*(k)) + \int_0^\infty c_k g \left(\int_0^T dt \kappa_2(k, t) F(\phi^+(t)) + \int_0^T dt \kappa_2^*(k, t) F(\phi^-(t)) \right) \right]
\end{aligned}$$

$$+ g^2 \int_0^T dt \int_0^T dt' F(\phi^+(t)) \kappa_3(t, t') F(\phi^+(t')) + g^2 \int_0^T dt \int_0^T dt' F(\phi^-(t)) \kappa_3(t, t') F(\phi^-(t')) \Big]. \quad (182)$$

Similar to the a_k integral, this is also quadratic and is easily performed Let,

$$\int \left(\prod_k dc_k \right) \int Dc_k \chi[c_k, \phi^+(t)] \chi[c_k, \phi^-(t)]^* = \mathcal{N}' \exp(W[F(\phi^+), F(\phi^-)]) \quad (183)$$

$$W[F(\phi^+), F(\phi^-)] = g^2 \int_0^\infty \frac{dk}{4\pi} \frac{\left(\int_0^T dt \kappa_2(k, t) F(\phi^+(t)) + \int_0^T dt \kappa_2^*(k, t) F(\phi^-(t)) \right)^2}{\kappa_1(k) + \kappa_1^*(k)} + g^2 \int_0^T dt \int_0^T dt' F(\phi^+(t)) \kappa_3(t, t') F(\phi^+(t')) + g^2 \int_0^T dt \int_0^T dt' F(\phi^-(t)) \kappa_3^*(t, t') F(\phi^-(t')), \quad (184)$$

with following definitions

$$\kappa_{++}(t, t') = \kappa_{--}^*(t, t') = \kappa_3(t, t') + \int_0^\infty \frac{dk}{4\pi} \frac{\kappa_2(k, t) \kappa_2(k, t')}{\kappa_1(k) + \kappa_1^*(k)}, \quad (185)$$

$$\kappa_{+-}(t, t') = \kappa_{-+}^*(t, t') = \int_0^\infty \frac{dk}{4\pi} \frac{\kappa_2(k, t) \kappa_2^*(k, t')}{\kappa_1(k) + \kappa_1^*(k)}. \quad (186)$$

where κ_1, κ_1 and κ_3 were already defined in (176) above. We can rearrange above equation to obtain (35)

$$W[F(\phi^+), F(\phi^-)] = g^2 \left[\int_0^T dt dt' F(\phi^+(t)) \kappa_{++}(t, t') F(\phi^+(t')) + \int_0^T dt dt' F(\phi^-(t)) \kappa_{--}(t, t') F(\phi^-(t')) + 2 \int_0^T dt dt' F(\phi^+(t)) \kappa_{+-}(t, t') F(\phi^-(t')) \right]. \quad (187)$$

For the corresponding expressions of kernels where the bath is in a thermal state, see Appendix B.5.

Hence the final form of the *RDM* at time $t = T$ is

$$\hat{\rho}(T) = \mathcal{N}' \int d\phi_T^+ d\phi_T^- \left(\int_{\phi_0}^{\phi_T^-} D\phi^- \int_{\phi_0}^{\phi_T^+} D\phi^+ e^{iS_{Sch}[\phi^+(t)]} e^{-iS_{Sch}[\phi^-(t)]} e^{W[F(\phi^+(t)), F(\phi^-(t))]} \right) |\phi_T^+\rangle \langle \phi_T^-|. \quad (188)$$

B.4 Bath at a finite cutoff Λ

At finite cutoff Λ the kernel in last line of (41) is UV finite and reads

$$\begin{aligned} K(t, t') &= -\frac{2}{\pi L} \int_0^\Lambda dk \frac{\sin[kt] \sin[kt']}{k^2} - \frac{2L}{\pi} \sum_{n=1}^\infty \int_0^\Lambda dk \left\{ \frac{\cos[k(t-t')]}{n^2 \pi^2 + k^2 L^2} - \frac{\cos[k(t+t')]}{n^2 \pi^2 + k^2 L^2} \right\} \\ &\quad - \frac{2L}{\pi} \sum_{n=1}^\infty \int_0^\Lambda dk \left\{ \frac{\cos[k(t-t')]}{[(2n-1\pi/2)]^2 + k^2 L^2} + \frac{\cos[k(t+t')]}{[(2n-1\pi/2)]^2 + k^2 L^2} \right\} \\ &= \frac{2 \sin(\Lambda t) \sin(\Lambda t')}{\pi \Lambda L} + \frac{1}{L\pi} [(t-t') \text{Si}((t-t')\Lambda) + (t+t') \text{Si}((t+t')\Lambda)] \\ &\quad + \sum_{n=1}^\infty [\kappa_t(t-t') + \kappa_t(t+t') + \kappa_c(t-t') - \kappa_c(t+t')], \end{aligned} \quad (189)$$

where

$$\begin{aligned}\kappa_c(y) &= -\frac{2L}{\pi} \int_0^\Lambda dk \frac{\cos(ky)}{n^2\pi^2 + k^2L^2} \\ &= \frac{1}{\pi^2 n} \left\{ \cosh\left[\frac{\pi ny}{L}\right] \left[-i\text{Ci}\left(\left(\frac{i\pi n}{L} + \Lambda\right)y\right) + i\text{Ci}\left(\left(\Lambda - \frac{i\pi n}{L}\right)y\right) - \pi \right] \right. \\ &\quad \left. + \sinh\left[\frac{\pi ny}{L}\right] \left[\text{Si}\left(\left(\frac{i\pi n}{L} + \Lambda\right)y\right) + \text{Si}\left(\left(\Lambda - \frac{i\pi n}{L}\right)y\right) \right] \right\},\end{aligned}$$

and

$$\begin{aligned}\kappa_t(y) &= -\frac{2L}{\pi} \int_0^\Lambda dk \frac{\cos(ky)}{[(2n-1\pi/2)]^2 + k^2L^2} \\ &= \frac{1}{\pi^2(2n-1)} \left\{ 2 \sinh\left[\frac{\pi(2n-1)y}{2L}\right] \left[-i\text{Shi}\left(\frac{(2n-1)\pi y}{2L}\right) - i\text{Shi}\left(\frac{(1-2n)\pi y}{2L}\right) \right] \right. \\ &\quad \left. + \text{Si}\left(\Lambda y + \frac{i(2n-1)\pi y}{2L}\right) + \text{Si}\left(\Lambda y + \frac{i(1-2n)\pi y}{2L}\right) \right] \\ &\quad - 2i \cosh\left[\frac{\pi(2n-1)y}{2L}\right] \left[\text{Ci}\left(\Lambda y + \frac{i(2n-1)\pi y}{2L}\right) - \text{Ci}\left(\Lambda y + \frac{i(1-2n)\pi y}{2L}\right) \right] \\ &\quad \left. - \text{Ci}\left(\frac{i(2n-1)\pi y}{2L}\right) + \text{Ci}\left(\frac{i(1-2n)\pi y}{2L}\right) \right\}.\end{aligned}$$

Here Si and Ci sine-integral and cosine-integral functions respectively. We have also used

$$-\frac{2}{\pi L} \int_0^\Lambda dk \frac{\sin[kt] \sin[kt']}{k^2} = \frac{2 \sin(\Lambda t) \sin(\Lambda t')}{\pi \Lambda L} + \frac{1}{L\pi} [(t-t')\text{Si}((t-t')\Lambda) + (t+t')\text{Si}((t+t')\Lambda)].$$

B.5 Thermal bath

For the bath in a thermal state, the initial density matrix (at $t = 0$) reads

$$\rho_0[a_k, \bar{a}_k] = \mathcal{N} \exp \left[-\frac{1}{\pi} \int_0^\infty dk k \frac{(a_k^2 + \bar{a}_k^2) \cosh(k\beta) - 2a_k \bar{a}_k}{\sinh(kL)} \right]. \quad (190)$$

This is the analogue of the pure state (153). Following the same procedure as in the pure state, one can integrate out the bath field Φ to get the effective action. The structure is exactly the same as (35) in the main text except the kernels are different from (185)

$$\begin{aligned}\kappa_{++}(t, t') &= \kappa_{--}^*(t, t') = \kappa_{FF}(t, t') + \int_0^\infty \frac{dk}{4\pi} \frac{\kappa_F(k, t) \kappa_F(k, t')}{\kappa_\beta(k)}, \\ \kappa_{+-}(t, t') &= \frac{1}{2} \kappa_{F\bar{F}}(t, t') + \int_0^\infty \frac{dk}{4\pi} \frac{\kappa_F(k, t) \kappa_{\bar{F}}(k, t')}{\kappa_\beta(k)}, \\ \kappa_{FF}(t, t') &= \kappa_{\bar{F}\bar{F}}^*(t, t') = \frac{i}{4} - \int_0^\infty \frac{dk}{\pi k} \text{csch}(k\beta) \sin[k(T-t')] \sin[k(T-t-i\beta)], \\ \kappa_{F\bar{F}}(t, t') &= 2 \int_0^\infty \frac{dk}{\pi k} \text{csch}(k\beta) \sin[k(T-t)] \sin[k(T-t')], \\ \kappa_F(k, t) &= \kappa_{\bar{F}}^*(k, t) = -2i \cos[k(T-t+i\beta/2)] \text{sech}[k\beta/2], \\ \kappa_\beta(k) &= 2k \tanh[k\beta/2].\end{aligned} \quad (191)$$

C Initial conditions (61)

As explained in [43], for operators which are “flip-symmetric”, large N expectation values in a pure state $|B_s(l)\rangle$ become thermal expectation values corresponding to an inverse temperature $\beta = 2l$. The Z_2 symmetry of the original Euclidean configuration, $\tau \leftrightarrow -\tau$, is retained ($-l$ and l being identified). The consequence of this is as follows. Consider the Euclidean equation of motion on the thermal circle (with the marked point $\tau = 0$)

$$\ddot{\phi}(\tau) - V'(\phi(\tau)) = 0. \quad (192)$$

The solution is

$$\phi = \log \left(\frac{e_1}{4J^2} \sec^2 \left(\frac{\sqrt{e_1}}{2} (\tau + e_2) \right) \right).$$

Imposing

$$\phi(\tau) = \phi(-\tau), \phi(\tau) = \phi(\tau + \beta),$$

gives the initial condition; we get $e_1 = \frac{16\pi^2}{\beta^2}$, $e_2 = 0$, leading to

$$\phi(\tau) = \log \left(\frac{4\pi^2}{\beta^2 J^2} \sec^2 \left(\frac{2\pi}{\beta} \tau \right) \right). \quad (193)$$

This gives

$$\phi(0) = \log \left(\frac{4\pi^2}{\beta^2 J^2} \right) = \phi_0. \quad (194)$$

Let us now include the Lorentzian parts of the Schwinger-Keldysh contour. We imagine $\tau = 0$ to coincide with $t = 0$. Then (194) gives the first of the conditions in (61). [43] assumes that the initial time slice $t = 0$ is a moment of time reversal symmetry, which implies

$$\dot{\phi}(0) = 0.$$

In the full SK contour, this implies $\phi_{\pm}(0) = \phi_0$ and $\dot{\phi}_{\pm}(0) = 0$.

D Other bath couplings

D.1 Interaction with just the marginal operator ($\Delta = 1$)

Here we turn on only the marginal interaction ($O_{m=2}$ in the language of (13)), i.e. in (26) we specialize to

$$gF(\phi(t)) = g'J \exp[\phi(t)], \quad g' = -\frac{\hat{g}_2}{4\pi} \cos^2 \theta \quad (195)$$

D.1.1 Numerical solution

After setting $gF(\phi) = g'J e^{\phi}$, the 3rd order equation (62) now reads (after setting $J = 1$, which can be reinserted simply by replacing $\beta \rightarrow \beta J, t \rightarrow tJ$, etc.)

$$\ddot{\phi} - \ddot{\phi}\phi - \tilde{g}'^2 e^{2\phi} = 0, \quad \tilde{g}'^2 \equiv n_f g'^2 / \alpha_s \quad (196)$$

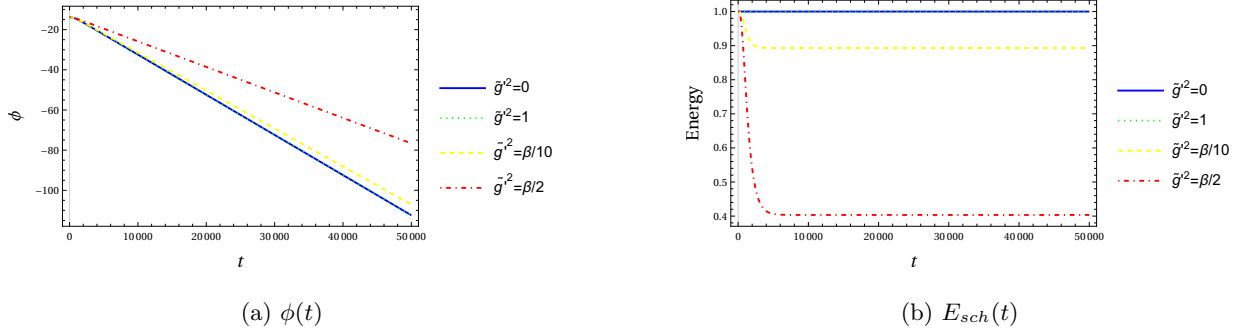


Figure 21: Plot of $\phi(t)$ and (Schwarzian) energy for various values of the marginal coupling \tilde{g}' . Note that here the coupling \tilde{g}'^2 has to be very large ($\sim \beta J$) for any significant evaporation. Numerics done for $\beta = 1000\pi$ with $J = 1$.

The solution ϕ and the (Schwarzian) energy are shown in figures 21a and 21b. Here the coupling \tilde{g}'^2 must be of the same order as $\beta J \gg 1$ for any significant evaporation to happen. This is evident from the plot of energy in Figure 21b.

Here also the solution shows a runaway behavior if the coupling is made very large. More precisely this happens at $\tilde{g}'_{\text{crit}} \approx 0.86 \sqrt{\beta J} \gg 1$. We will disregard these pathological solutions when the coupling g' exceeds the critical value \tilde{g}'_{crit} .

D.1.2 Analytic solution

After setting $gF(\phi) = g' J e^\phi$, the equation of motion (60) becomes (after setting $J = 1$)

$$\left(\ddot{\phi}(t) + 2e^{\phi(t)}\right) - \tilde{g}'^2 e^{\phi(t)} \int_0^t e^{\phi(t')} dt' = 0, \quad \tilde{g}'^2 = n_f g'^2 / \alpha_s \quad (197)$$

We can solve this equation perturbatively in \tilde{g}'^2 . We find

$$\phi(t) = \log \left(\frac{\pi^2}{\beta^2} \operatorname{sech}^2 \frac{\pi t}{\beta} \right) - \frac{\pi \tilde{g}'^2}{3\beta^2} \left[\beta \log 2 - \beta \log \left(e^{\frac{2\pi t}{\beta}} + 1 \right) + \pi t \right] \tanh \left(\frac{\pi t}{\beta} \right) + O(\tilde{g}'^4) \quad (198)$$

The long time solution is of the form

$$\phi(t) = \left(\frac{\pi^2}{3\beta^2} \tilde{g}'^2 - \frac{2\pi}{\beta} \right) t - 2 \left[\log \frac{\beta}{2\pi} + \frac{\pi}{6\beta} \tilde{g}'^2 \log 2 \right] + O(\exp[-\pi t / \beta]) \quad (199)$$

Clearly the dominant term is linear

$$\phi = -at + \dots, \quad a = \left(\frac{2\pi}{\beta} - \frac{\pi^2}{3\beta^2} \tilde{g}'^2 \right). \quad (200)$$

$a > 0$ gives a sensible solution for the original variable $\dot{f} = e^\phi$; this happens in the range $\tilde{g}' < \tilde{g}'_{\text{crit}}^A \equiv \sqrt{6\beta J / \pi}$. In this range $\dot{f} \rightarrow 0$, which signals an asymptotic solution which is a black hole, with asymptotic energy $E_{sch} = E_\Delta = N \frac{\alpha_s}{J} \frac{a^2}{2}$.

At the critical value, the solution for ϕ becomes asymptotically constant, and the energy becomes zero, which signals complete evaporation (zero temperature). Since this critical value is very large in the IR regime $\beta J \gg 1$, such an asymptotic solution is not accessible in perturbation theory.

This is what we also find in the numerical solutions except the critical value obtained numerically $\tilde{g}'_{\text{crit}} \approx 0.86 \sqrt{\beta J}$ is smaller than the analytical value $\tilde{g}'_{\text{crit}}^A = \sqrt{6\beta J / \pi} \approx 1.38 \sqrt{\beta J}$.

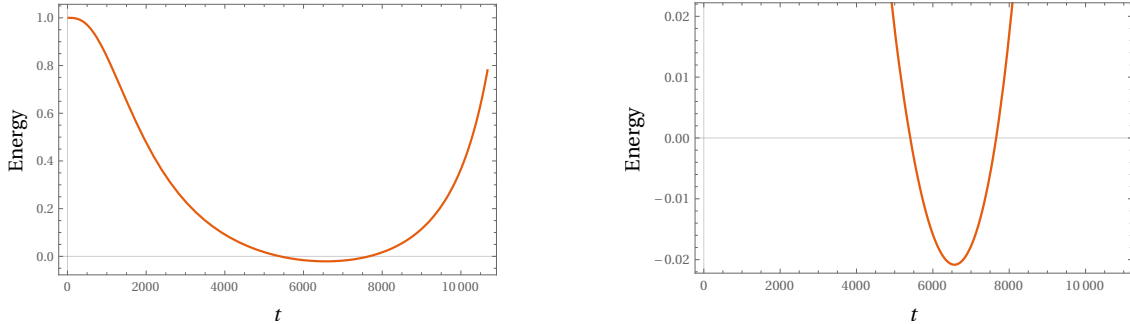


Figure 22: The (modified) Schwarzsian energy first decreases and then starts increasing. For a finite time window it is negative allowing us to decouple the bath and go to non black hole geometry. On the right we see the same energy zoomed to make this point clear. Here $J = 1, \beta = 1000\pi, \tilde{g}^2 = 0.00075, \hat{\epsilon} = \frac{1}{4}\hat{\epsilon}_{cr}$.

D.2 Relevant Interaction + KM term

Here to our model (26), we add the Kourkoulou-Maldacena term with a fixed (non-dynamical) coupling

$$S_{KM} = \frac{N\alpha_s}{J} \int dt \hat{\epsilon} J^2 e^{\phi/2}; \quad \hat{\epsilon} < \hat{\epsilon}_{cr} = \frac{2\pi}{\beta J} \quad (201)$$

It was shown in [KM] that for $\hat{\epsilon} > \hat{\epsilon}_{cr}$, the new geometry has no horizon. Therefore the condition $\hat{\epsilon} < \hat{\epsilon}_{cr}$ is imposed such that there is a black hole in absence of the bath. The (modified) Schwarzsian energy now includes the KM potential term

$$E = N \frac{\alpha_s}{J} \left[\frac{1}{2} \dot{\phi}^2 + 2J^2 e^{\phi} - \frac{\hat{\epsilon}}{2} J^2 e^{\phi/2} \right] \quad (202)$$

The equation of motion is modified to

$$\ddot{\phi}(t) + 2e^{\phi(t)} - \frac{\hat{\epsilon}}{2} e^{\phi(t)/2} - \tilde{g}^2 e^{\phi(t)/2} \int_0^t e^{\phi(t')/2} dt' = 0, \quad \tilde{g}^2 \equiv \frac{n_f g^2}{2\alpha_s} \quad (203)$$

where we have put $J = 1$. Now after coupling to the bath at $t = 0$, it is possible for the (modified) Schwarzsian energy, given by (202), to become negative for range of the coupling g . This however happens for $g \geq g_*$ ⁴³ when the solution shows a runaway behaviour as discussed in Section 4.1. There is however a window of time when the energy remains negative (see Figure 22), during which if we decouple the bath we get oscillating and bounded solution for ϕ . This means the horizon has disappeared and we are in a non-black hole phase. In Figure 23 the numerical solution⁴⁴ is shown where we achieve complete black hole evaporation. It was crucial for the coupling to be switched off at $O(\beta)$ time as one can see from the plot of the (modified) Schwarzsian energy as a function of time.

Note that even though we have added the KM term, without also coupling to the bath it was not possible to go to the non-BH geometry (see Figure 24), since $\hat{\epsilon} < \frac{2\pi}{\beta J}$. It is due to the fact that the BH dumps energy into the bath thereby effectively going to the bound state of the potential.

⁴³The critical coupling here is sensitive to the KM potential term and differs from (71).

⁴⁴In presence of the KM potential term, the initial condition for $\ddot{\phi}$ is modified to $\ddot{\phi}(0) = -J^2 \left(2e^{\phi(0)} - \frac{\hat{\epsilon}}{2} e^{\phi(0)/2} \right)$.

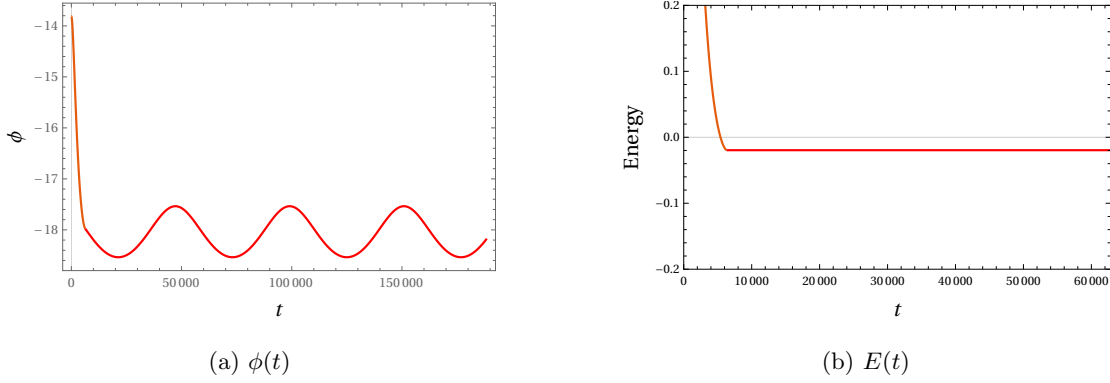


Figure 23: The coupling to the bath is switched off at $t = 2000\pi$. The solution after that (in red) is found by demanding continuity of ϕ and $\dot{\phi}$ and is shown on the left. The black hole loses energy initially but after it is decoupled, the energy is constant as seen on the right. Here $J = 1, \beta = 1000\pi, \tilde{g}^2 = 0.00075, \hat{\epsilon} = \frac{1}{4}\hat{\epsilon}_{cr}$.

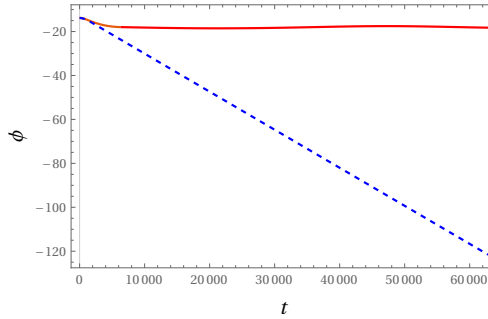


Figure 24: The blue dashed curve shows the effect of the KM term by itself without coupling to the bath. Clearly $\phi(t) \rightarrow -\infty$ as $t \rightarrow \infty$. For comparison the non-black hole solution obtained after coupling to bath is also shown in red. Here $J = 1, \beta = 1000\pi, \tilde{g}^2 = 0.00075, \hat{\epsilon} = \frac{1}{4}\hat{\epsilon}_{cr}$.

E Finding spin of the initial state in Model (a)

In this appendix we show that as claimed in Section 5.1, $\binom{N/2}{2}$ spins are enough to determine s up to a sign. Let us call the different trial spins as $s' = s^{(\alpha)}, \alpha = 1, 2, \dots, \binom{N/2}{2}$. They satisfy

$$(s^{(\alpha)} \cdot s)^2 = \left(\sum_{k=1}^{N/2} s_k^{(\alpha)} s_k \right)^2 = \left(\frac{N}{2} \cos \theta^{(\alpha)} \right)^2, \quad \alpha = 1, 2, \dots, \binom{N/2}{2} \quad (204)$$

where the value $(\cos \theta^{(\alpha)})^2$ for each choice of $s^{(\alpha)}$ is ‘experimentally determined’.

Since the above equations are difficult to work with, we proceed by linearizing this problem. The above set of equations can be rewritten as

$$\sum_{1 \leq i < j \leq N/2} s_i^{(\alpha)} s_j^{(\alpha)} s_i s_j = \frac{N}{4} \left[\frac{N}{2} (\cos \theta^{(\alpha)})^2 - 1 \right], \quad (205)$$

where we have used

$$(s^{(\alpha)} \cdot s)^2 = \sum_{k=1}^{N/2} (s_k^{(\alpha)})^2 s_k^2 + 2 \sum_{1 \leq i < j \leq N/2} s_i^{(\alpha)} s_j^{(\alpha)} s_i s_j = \frac{N}{2} + 2 \sum_{1 \leq i < j \leq N/2} s_i^{(\alpha)} s_j^{(\alpha)} s_i s_j, \quad (206)$$

and plugged this into the equation (204).

Now note that the equations (205) represents a system of linear equations in $s_i s_j$ as the variables which are $\binom{N/2}{2}$ in number since $1 \leq i < j \leq N/2$. These can be solved exactly provided the vectors $\left(s_1^{(\alpha)} s_2^{(\alpha)}, s_1^{(\alpha)} s_3^{(\alpha)}, \dots, s_{N/2-1}^{(\alpha)} s_{N/2}^{(\alpha)}\right)$ for $\alpha = 1, 2, \dots, \binom{N/2}{2}$, are linearly independent (as $\binom{N/2}{2}$ dimensional vectors). This can always be ensured by choosing $s^{(\alpha)}$'s to be the spins vectors with 2 minuses and $N/2 - 2$ pluses which are exactly $\binom{N/2}{2}$ in number. We have verified this explicitly in Mathematica up to $N = 100$. The fact that a choice of $\binom{N/2}{2}$ spins always exists is not surprising since the total number of all spins grows exponentially large with N .

Thus we can always determine the variables $s_i s_j, 1 \leq i < j \leq N/2$. Since this gives us $s_1 s_j$ for $j = 1, 2, \dots, N/2$, choosing $s_1 = \pm 1$ uniquely determines the spin s up to an overall sign.

F Two-point function in Model (a)

The integral on the RHS of equation (114) can be evaluated explicitly. For this we use the Mittag-Leffler pole expansions for coth and csch functions in the expression (114), perform the integral term by term and then sum them up to get

$$\begin{aligned} \langle \delta \hat{\phi}_c(t) \delta \hat{\phi}_c(t') \rangle &= \frac{16C}{a^4 L} |t^-| + \frac{8C}{a^4} e^{-\frac{1}{2}a|t^-|} [(a|t^-| + 4) \cot(aL) + 2aL \csc^2(aL)] \\ &+ \frac{16C}{\pi^2 a^4} e^{-\frac{\pi|t^-|}{2L}} \left[aL \left\{ \Phi_L \left(e^{-\frac{\pi|t^-|}{2L}}, 2, \frac{aL}{\pi} + 1 \right) - \Phi_{HL} \left(e^{-\frac{\pi|t^-|}{2L}}, 2, 1 - \frac{aL}{\pi} \right) \right\} \right. \\ &+ 2\pi \left\{ \Phi_{HL} \left(e^{-\frac{\pi|t^-|}{2L}}, 1, 1 - \frac{aL}{\pi} \right) + \Phi_L \left(e^{-\frac{\pi|t^-|}{2L}}, 1, \frac{aL}{\pi} + 1 \right) \right\} \left. + \frac{64C}{\pi a^4} \log \left(1 - e^{-\frac{\pi|t^-|}{2L}} \right) \right. \\ &- \frac{16C}{a^4 L} t^+ - \frac{2^7 C}{a^4 L} + \frac{64C}{\pi^4 a^4} \left[aL e^{-\frac{\pi t^+}{2L}} \left\{ aL \left[\pi \Phi_L \left(-e^{-\frac{\pi t^+}{2L}}, 3, \frac{aL}{\pi} + 1 \right) + aL \Phi_L \left(-e^{-\frac{\pi t^+}{2L}}, 4, \frac{aL}{\pi} + 1 \right) \right] \right. \right. \\ &\left. \left. + \pi^2 \Phi_L \left(-e^{-\frac{\pi t^+}{2L}}, 2, \frac{aL}{\pi} + 1 \right) \right\} - \pi^3 e^{\frac{1}{2}a(t^+ - 2iL)} B_{-e^{-\frac{\pi t^+}{2L}}} \left(\frac{aL}{\pi} + 1, 0 \right) - \pi^3 \log \left(e^{-\frac{\pi t^+}{2L}} + 1 \right) \right]. \end{aligned} \quad (207)$$

We have defined $\delta \hat{\phi}_c(t) = \delta \phi_c(t)/F'(\phi(t))$ and $t^\pm = t \pm t'$. The answer is expressed terms of the (Hurwitz)-Lerch transcendent $\Phi_{(H)L}$ and the incomplete beta function $B_z(a, b)$.

G A geometrical appendix

Solutions of JT gravity are completely specified by the Schwarzian mode. The metric can be described in two separate but equivalent ways.

In the first, the Schwarzian mode shows up as a large diffeomorphism of the AdS₂ metric. The metric has the following form [71]⁴⁵ in the Fefferman-Graham coordinates:

$$ds^2 = \frac{dz^2}{z^2} - \frac{dt^2}{z^2} \left(1 + \frac{z^2}{2} \{f(t), t\} \right)^2. \quad (208)$$

⁴⁵This form is the 2D counterpart of the Banados metric in 3D [72].

Since in the boundary theory, conformal symmetry is explicitly broken by choosing a large, but finite, value of the dimensionful parameter J , the bulk counterpart is to truncate the above geometry by a small, non-zero boundary $z = \delta$ or, more invariantly, by a choice of a boundary value of the dilaton $\Phi = \frac{a}{\delta}$ which is related to J .

In the second viewpoint [5], the metric is fixed to just AdS_2

$$ds^2 = \frac{-d\hat{t}^2 + d\hat{z}^2}{\hat{z}^2}. \quad (209)$$

The Schwarzian mode now shows up as a wiggle of the boundary curve which now reads, $(\hat{t}, \hat{z}) = (f(t), \delta\dot{f}(t))$ (see (210) for more detail) and the entire dynamics is then contained in the motion of the boundary curve.

The above two viewpoints are related to each other by a coordinate transformation

$$\begin{aligned} \hat{t} &= f(t) + \frac{2z^2 f'(t)^2 f''(t)}{\text{Denominator}}, \\ \hat{z} &= \frac{4z f'(t)^3}{\text{Denominator}}, \quad \text{Denominator} = 4f'(t)^2 - z^2 f''(t)^2. \end{aligned} \quad (210)$$

It is easy to check that the metric (209) transforms into (208) under (210), and that the boundary curves also transform into each other.

A topological remark: It is important to note that although $f(t)$ is a one-to-one diffeomorphism acting on the real line,⁴⁶ it need not be "onto", i.e. its image can be a proper (open) subset U of \mathbf{R} . In Figure 25, the case (A) represents $f : \mathbf{R} \rightarrow \mathbf{R}$, while in the other cases we have $f : \mathbf{R} \rightarrow U \subset \mathbf{R}$. In case (B), $U = (-\infty, \hat{t}_\infty)$, in case (C) $U = (-\hat{t}_{-\infty}, \infty)$, whereas in case (D), $U = (-\hat{t}_{-\infty}, \hat{t}_\infty)$. It is important to note that in order for $f(t)$ to asymptote to a finite value as $t \rightarrow \infty$, e.g. in (B), we must have $f'(t) \rightarrow 0$, as $t \rightarrow \infty$, i.e. $f'(\infty) = 0$. In (C), we will similarly have $f'(-\infty) = 0$ whereas in (D) we will have $f'(\infty) = 0, f'(-\infty) = 0$. In fact, the converse is also trivially true; if $f'(t) \rightarrow 0$ as t goes to ∞ and/or $-\infty$, the image of $f(t)$ will be an open subset.

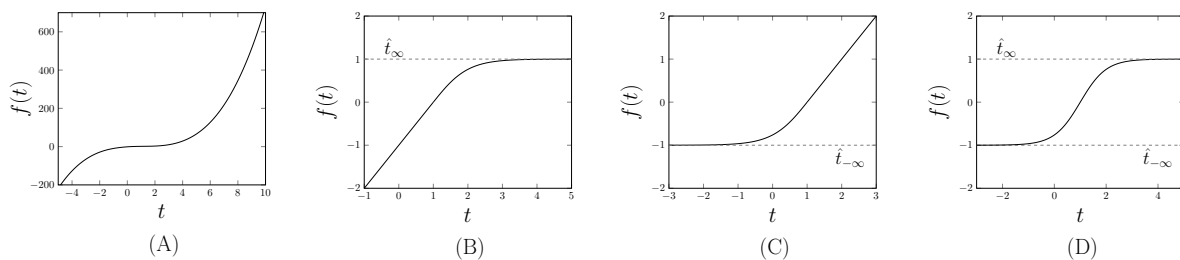


Figure 25: Various topological possibilities of $f(t)$. In panels (B,C,D) $f : \mathbf{R} \rightarrow U$ where U is a proper open subset of \mathbf{R} .

Examples of these classes:

(A) $f(t) = a(t - b)^{2n+1} + c \tanh(t)$, $n = 0, 1, 2, \dots$

(B) $f(t) = a(t - b)$, if $t \leq b$, $= \tanh(a(t - b))$ if $t > b$

⁴⁶We do not consider here the situation in which the *domain* of the map is a proper subset of the real line, reflecting the physics of the SYK model.

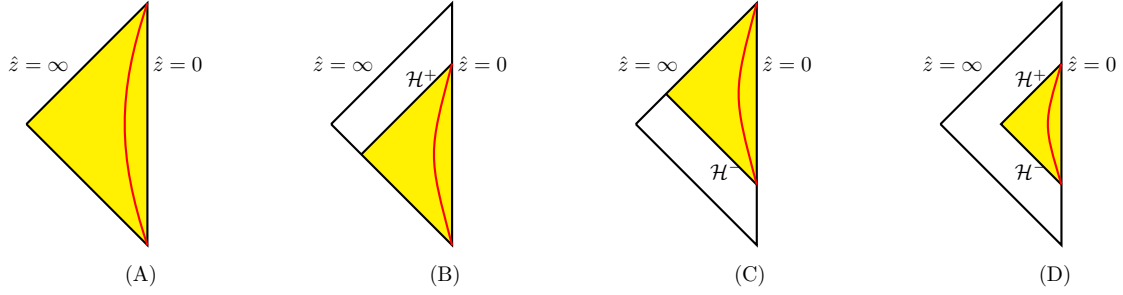


Figure 26: The yellow regions are the open subsets U_{bulk} , defined as the image of the map (210), in the four cases mentioned in Figure 25. The boundary curve $z = \delta$ is shown in the \hat{t}, \hat{z} coordinates in each case. The hallmark of appearance of a horizon is when the subset U_{bulk} is a **proper** subset. The null boundary/boundaries of U_{bulk} turn out to be horizons. The labels $\mathcal{H}^+, \mathcal{H}^-$ represent future and past horizons respectively.

(C) $f(t) = a(t - b)$, if $t > b$, $= \tanh(a(t - b))$ if $t \leq b$

(D) $f(t) = \tanh(a(t - b))$.

It is straightforward to argue, using these examples as well as generally,⁴⁷ that the image of the bulk diffeomorphism (210) is the full space $\mathbf{R}_+^2 = \{\hat{z} > 0, \hat{t} \in \mathbf{R}\}$ in case (A), where in the other cases, the image of the map is a proper open subset U_{bulk} (see Fig. 26).⁴⁸

G.1 Condition for existence of a horizon and how to locate it

The null lines in our geometry are obviously given by

$$\hat{t} \pm \hat{z} = c, \text{ or equivalently} \quad G_{\pm} = \frac{2z^2 f'(t)^2 f''(t)}{4f'(t)^2 - z^2 f''(t)^2} + f(t) \pm \frac{4z f'(t)^3}{4f'(t)^2 - z^2 f''(t)^2} - c = 0. \quad (211)$$

The top line is the obvious representation; the second line represents the same surfaces in the coordinates (t, z) , using (210). It can be explicitly verified that the null surface condition $(\partial_t G)^2 g^{tt} + 2\partial_t G \partial_z G g^{tz} + (\partial_z G)^2 g^{zz} = 0$ is satisfied for $G = G_{\pm}$, as it must.

It is easy to see that the boundaries of the subset U_{bulk} are null lines. In case (A), these are just the Poincaré horizons. In the other cases, when the subset U_{bulk} is a proper open subset, the boundaries involve horizons. E.g. in case (B), the upper boundary is the null line $\hat{t} + \hat{z} = c$, with $c = \hat{t}_{\infty} \equiv f(t = \infty)$; the value of c can be determined from the fact that this is the last line of U_{bulk} must meet the $z = 0$ line at the boundary value of the t -coordinate, i.e. $t = \infty$. It is obvious that this null line is the horizon

⁴⁷The general proof involves two steps: (i) to locate the null line (211) which ends up at $z = 0$ at $t = \infty$. It is of the form $\hat{t} + \hat{z} = c$. If $c = \infty$, the null line coincides with the Poincaré horizon. If $c < \infty$, it corresponds to the null line that last hits the boundary in terms of the t -clock. (ii) This null line is the boundary of the (z, t) coordinates, since the null line has a coordinate singularity where the Denominator in (210) vanishes. Note the similarity with the Schwarzschild geometry.

⁴⁸We should note that the *domain* of the map (210) may not be the full range $\mathbf{R}_+^2 = \{z > 0, t \in \mathbf{R}\}$ in situations where the Denominator in (210) vanishes. E.g. the map may have singularities. E.g. for $f(t) = t^3$, the map is well-defined for $0 < z < t$, demarcating a *domain* that ends at the horizon. See footnote 47.

\mathcal{H}_+ . To elaborate this, we note that the yellow regions in Fig. 26, covered by the (t, z) coordinates, are analogous to the region covered by the exterior Schwarzschild coordinates $(t, r > 2m)$ whose boundary $r = 2m$ corresponds to $t = \infty$. The white region in panel (B) cannot send signals into the yellow region; hence the boundary of the yellow region is the horizon. The horizon in this case is a “future” horizon (hence denoted as \mathcal{H}_+). By a similar reasoning, case (C) where $f(t)$ reaches a finite value as $t \rightarrow -\infty$ (ensured by $f'(-\infty) = 0$), has a horizon which is a past horizon (one cannot past evolve from the white region to the yellow region). In (D), we have both a future horizon and a past horizon.

An alternative way of constructing the horizon is the following (see [43] for a detailed discussion). Consider the behaviour of the boundary curve (image of $z = \delta$) in the (\hat{t}, \hat{z}) coordinates, namely

$$(\hat{t}(t), \hat{z}(t)) = (f(t), \delta f'(t)) \quad (212)$$

which can be obtained by plugging in $z = \delta$ for in (210) and taking δ small. The entire lifetime of the boundary observer $-\infty < t < \infty$ is represented by the full extent of this boundary curve. In the case (B) of Fig. 26, the condition that \hat{t} ends at a finite value \hat{t}_∞ as $t \rightarrow \infty$ is the same as $\dot{f}(\infty) = 0$ (see the analysis in Fig. 25) and the related comments). This is equivalent to saying that the the boundary curve (212) must asymptotically reach $\hat{z} = 0$.

Condition for existence of a horizon Thus, from both viewpoints the condition of existence of a future horizon is that in the limit $t \rightarrow \infty$, $f'(t) \rightarrow 0$, and $f(t)$ reaches a finite value. This is the condition we apply in Section 7.2.

Note that the above condition is gauge invariant, i.e it remains unchanged if one makes a transformation $f(t) \rightarrow \tilde{f}(t) = \frac{af(t)+b}{cf(t)+d}$, $ad - bc = 1$.

Equation of the horizon As explained above, the equation of the future horizon is $\hat{t} + \hat{z} = c$, with $c = \hat{t}_\infty \equiv f(t = \infty)$. Unlike the condition above, this equation depends on the $SL(2, \mathbb{R})$ gauge, since the value of $f(t = \infty)$ changes under the $SL(2, \mathbb{R})$ transformation mentioned above. In the language of the bulk, this $SL(2, \mathbb{R})$ transformation reflects the isometry of the Poincaré metric (209).

References

- [1] S. Sachdev and J.-w. Ye, *Gapless spin fluid ground state in a random, quantum Heisenberg magnet*, *Phys. Rev. Lett.* **70** (1993) 3339, [cond-mat/9212030].
- [2] A. Kitaev, ‘*A simple model of quantum holography*’, *Talks at KITP, April 7, and May 27, 2015*, .
- [3] J. Maldacena and D. Stanford, *Remarks on the Sachdev-Ye-Kitaev model*, *Phys. Rev. D* **94** (2016) 106002, [1604.07818].
- [4] S. Sachdev, *Bekenstein-Hawking Entropy and Strange Metals*, *Phys. Rev. X* **5** (2015) 041025, [1506.05111].

- [5] J. Maldacena, D. Stanford and Z. Yang, *Conformal symmetry and its breaking in two dimensional Nearly Anti-de-Sitter space*, *PTEP* **2016** (2016) 12C104, [1606.01857].
- [6] G. Sárosi, *AdS₂ holography and the SYK model*, *PoS Modave2017* (2018) 001, [1711.08482].
- [7] D. A. Trunin, *Pedagogical introduction to the Sachdev–Ye–Kitaev model and two-dimensional dilaton gravity*, *Usp. Fiz. Nauk* **191** (2021) 225–261, [2002.12187].
- [8] D. Stanford and E. Witten, *Fermionic Localization of the Schwarzian Theory*, *JHEP* **10** (2017) 008, [1703.04612].
- [9] L. V. Iliesiu and G. J. Turiaci, *The statistical mechanics of near-extremal black holes*, *JHEP* **05** (2021) 145, [2003.02860].
- [10] J. D. Bekenstein, *Black holes and the second law*, *Lett. Nuovo Cim.* **4** (1972) 737–740.
- [11] J. D. Bekenstein, *Black holes and entropy*, *Phys. Rev. D* **7** (1973) 2333–2346.
- [12] S. W. Hawking, *Black hole explosions*, *Nature* **248** (1974) 30–31.
- [13] S. W. Hawking, *Particle Creation by Black Holes*, *Commun. Math. Phys.* **43** (1975) 199–220.
- [14] A. Strominger and C. Vafa, *Microscopic origin of the Bekenstein-Hawking entropy*, *Phys. Lett. B* **379** (1996) 99–104, [hep-th/9601029].
- [15] J. R. David, G. Mandal and S. R. Wadia, *Microscopic formulation of black holes in string theory*, *Phys. Rept.* **369** (2002) 549–686, [hep-th/0203048].
- [16] J. M. Maldacena, *The Large N limit of superconformal field theories and supergravity*, *Adv. Theor. Math. Phys.* **2** (1998) 231–252, [hep-th/9711200].
- [17] S. S. Gubser, I. R. Klebanov and A. M. Polyakov, *Gauge theory correlators from noncritical string theory*, *Phys. Lett. B* **428** (1998) 105–114, [hep-th/9802109].
- [18] E. Witten, *Anti-de Sitter space and holography*, *Adv. Theor. Math. Phys.* **2** (1998) 253–291, [hep-th/9802150].
- [19] E. Witten, *Anti-de Sitter space, thermal phase transition, and confinement in gauge theories*, *Adv. Theor. Math. Phys.* **2** (1998) 505–532, [hep-th/9803131].
- [20] G. Penington, *Entanglement Wedge Reconstruction and the Information Paradox*, *JHEP* **09** (2020) 002, [1905.08255].
- [21] A. Almheiri, N. Engelhardt, D. Marolf and H. Maxfield, *The entropy of bulk quantum fields and the entanglement wedge of an evaporating black hole*, *JHEP* **12** (2019) 063, [1905.08762].
- [22] A. Almheiri, R. Mahajan, J. Maldacena and Y. Zhao, *The Page curve of Hawking radiation from semiclassical geometry*, *JHEP* **03** (2020) 149, [1908.10996].

- [23] A. Almheiri, R. Mahajan and J. Maldacena, *Islands outside the horizon*, 1910.11077.
- [24] M. Rozali, J. Sully, M. Van Raamsdonk, C. Waddell and D. Wakeham, *Information radiation in BCFT models of black holes*, *JHEP* **05** (2020) 004, [1910.12836].
- [25] G. Penington, S. H. Shenker, D. Stanford and Z. Yang, *Replica wormholes and the black hole interior*, 1911.11977.
- [26] A. Almheiri, T. Hartman, J. Maldacena, E. Shaghoulian and A. Tajdini, *Replica Wormholes and the Entropy of Hawking Radiation*, *JHEP* **05** (2020) 013, [1911.12333].
- [27] H. Z. Chen, Z. Fisher, J. Hernandez, R. C. Myers and S.-M. Ruan, *Evaporating Black Holes Coupled to a Thermal Bath*, *JHEP* **01** (2021) 065, [2007.11658].
- [28] A. Almheiri, T. Hartman, J. Maldacena, E. Shaghoulian and A. Tajdini, *The entropy of Hawking radiation*, *Rev. Mod. Phys.* **93** (2021) 035002, [2006.06872].
- [29] H. Geng and A. Karch, *Massive islands*, *JHEP* **09** (2020) 121, [2006.02438].
- [30] H. Geng, A. Karch, C. Perez-Pardavila, S. Raju, L. Randall, M. Riojas et al., *Inconsistency of islands in theories with long-range gravity*, *JHEP* **01** (2022) 182, [2107.03390].
- [31] C. Krishnan, *Critical Islands*, *JHEP* **01** (2021) 179, [2007.06551].
- [32] K. Ghosh and C. Krishnan, *Dirichlet baths and the not-so-fine-grained Page curve*, *JHEP* **08** (2021) 119, [2103.17253].
- [33] C. Krishnan, V. Patil and J. Pereira, *Page Curve and the Information Paradox in Flat Space*, 2005.02993.
- [34] C. Krishnan and V. Mohan, *Interpreting the Bulk Page Curve: A Vestige of Locality on Holographic Screens*, 2112.13783.
- [35] S. Raju, *Failure of the split property in gravity and the information paradox*, *Class. Quant. Grav.* **39** (2022) 064002, [2110.05470].
- [36] J. De Vuyst and T. G. Mertens, *Operational islands and black hole dissipation in JT gravity*, 2207.03351.
- [37] E. Bahiru, A. Belin, K. Papadodimas, G. Sarosi and N. Vardian, *State-dressed local operators in AdS/CFT*, 2209.06845.
- [38] A. Almheiri, A. Milekhin and B. Swingle, *Universal Constraints on Energy Flow and SYK Thermalization*, 1912.04912.
- [39] J. Maldacena and A. Milekhin, *SYK wormhole formation in real time*, *JHEP* **04** (2021) 258, [1912.03276].

- [40] Y. Chen, X.-L. Qi and P. Zhang, *Replica wormhole and information retrieval in the SYK model coupled to Majorana chains*, *JHEP* **06** (2020) 121, [2003.13147].
- [41] C. Teitelboim, *Gravitation and Hamiltonian Structure in Two Space-Time Dimensions*, *Phys. Lett.* **126B** (1983) 41–45.
- [42] R. Jackiw, *Lower Dimensional Gravity*, *Nucl. Phys.* **B252** (1985) 343–356.
- [43] I. Kourkoulou and J. Maldacena, *Pure states in the SYK model and nearly-AdS₂ gravity*, 1707.02325.
- [44] J. Engelsöy, T. G. Mertens and H. Verlinde, *An investigation of AdS₂ backreaction and holography*, *JHEP* **07** (2016) 139, [1606.03438].
- [45] P. Calabrese and J. Cardy, *Quantum Quenches in Extended Systems*, *J. Stat. Mech.* **0706** (2007) P06008, [0704.1880].
- [46] J. Cardy, *Thermalization and Revivals after a Quantum Quench in Conformal Field Theory*, *Phys. Rev. Lett.* **112** (2014) 220401, [1403.3040].
- [47] A. Dhar, A. Gaikwad, L. K. Joshi, G. Mandal and S. R. Wadia, *Gravitational collapse in SYK models and Choptuik-like phenomenon*, *JHEP* **11** (2019) 067, [1812.03979].
- [48] K. Papadodimas and S. Raju, *State-Dependent Bulk-Boundary Maps and Black Hole Complementarity*, *Phys. Rev. D* **89** (2014) 086010, [1310.6335].
- [49] K. Papadodimas and S. Raju, *Remarks on the necessity and implications of state-dependence in the black hole interior*, *Phys. Rev. D* **93** (2016) 084049, [1503.08825].
- [50] A. R. Brown, H. Gharibyan, G. Penington and L. Susskind, *The Python’s Lunch: geometric obstructions to decoding Hawking radiation*, *JHEP* **08** (2020) 121, [1912.00228].
- [51] G. Mandal and S. R. Wadia, *Black hole geometry around an elementary BPS string state*, *Phys. Lett. B* **372** (1996) 34–44, [hep-th/9511218].
- [52] A. Dhar, G. Mandal and S. R. Wadia, *Absorption versus decay of black holes in string theory and T symmetry*, *Phys. Lett. B* **388** (1996) 51–59, [hep-th/9605234].
- [53] P. Calabrese and J. L. Cardy, *Evolution of entanglement entropy in one-dimensional systems*, *J. Stat. Mech.* **0504** (2005) P04010, [cond-mat/0503393].
- [54] D. Bagrets, A. Altland and A. Kamenev, *Sachdev–Ye–Kitaev model as Liouville quantum mechanics*, *Nucl. Phys. B* **911** (2016) 191–205, [1607.00694].
- [55] A. Almheiri, A. Mousatov and M. Shyani, *Escaping the Interiors of Pure Boundary-State Black Holes*, 1803.04434.

- [56] G. Mandal, R. Sinha and N. Sorokhaibam, *Thermalization with chemical potentials, and higher spin black holes*, *JHEP* **08** (2015) 013, [1501.04580].
- [57] G. Mandal, S. Paranjape and N. Sorokhaibam, *Thermalization in 2D critical quench and UV/IR mixing*, *JHEP* **01** (2018) 027, [1512.02187].
- [58] P. Banerjee, A. Gaikwad, A. Kaushal and G. Mandal, *Quantum quench and thermalization to GGE in arbitrary dimensions and the odd-even effect*, *JHEP* **09** (2020) 027, [1910.02404].
- [59] J. V. Rocha, *Evaporation of large black holes in AdS: Coupling to the evaporon*, *JHEP* **08** (2008) 075, [0804.0055].
- [60] A. Kamenev, *Field theory of non-equilibrium systems*. Cambridge University Press, 2011.
- [61] F. M. Haehl, R. Loganayagam and M. Rangamani, *Schwinger-Keldysh formalism. Part I: BRST symmetries and superspace*, *JHEP* **06** (2017) 069, [1610.01940].
- [62] R. F. Pawula, *Generalizations and extensions of the fokker- planck-kolmogorov equations*, *IEEE Trans. Inf. Theory* **13** (1967) 33–41.
- [63] H. Risken and H. D. Vollmer, *On the application of truncated generalized fokker-planck equations*, *Zeitschrift für Physik B Condensed Matter* **35** (1979) 313–315.
- [64] J. Jackson, *Classical Electrodynamics*. Wiley, 2012.
- [65] A. O. Caldeira and A. J. Leggett, *Path integral approach to quantum Brownian motion*, *Physica A* **121** (1983) 587–616.
- [66] P. Gao, D. L. Jafferis and A. C. Wall, *Traversable Wormholes via a Double Trace Deformation*, *JHEP* **12** (2017) 151, [1608.05687].
- [67] J. Maldacena, D. Stanford and Z. Yang, *Diving into traversable wormholes*, *Fortsch. Phys.* **65** (2017) 1700034, [1704.05333].
- [68] J. Maldacena and X.-L. Qi, *Eternal traversable wormhole*, 1804.00491.
- [69] R. Pathria and P. Beale, *Statistical Mechanics*. Academic Press. Butterworth-Heinemann, 2011.
- [70] O. Contreras-Vergara, N. Lucero-Azuara, N. Sánchez-Salas and J. Jiménez-Aquino, *Harmonic oscillator brownian motion: Langevin approach revisited*, *Revista Mexicana de Física E* **18** (01, 2021) 97.
- [71] G. Mandal, P. Nayak and S. R. Wadia, *Coadjoint orbit action of Virasoro group and two-dimensional quantum gravity dual to SYK/tensor models*, *JHEP* **11** (2017) 046, [1702.04266].
- [72] M. Banados, *Three-dimensional quantum geometry and black holes*, *AIP Conf. Proc.* **484** (1999) 147–169, [hep-th/9901148].